4.10 U–Th–Pb Geochronology

Blair Schoene, Princeton University, Princeton, NJ, USA

4.10.1 Introduction

The year 2011 marked the one hundredth anniversary of what may be the first real geochronology paper, published by Arthur Holmes, entitled "The Association of Lead with Uranium in Rock-Minerals and Its Application to the Measurement of Geological Time" (Holmes, 1911). Holmes' early work was surprisingly accurate, even though it was carried out prior to the discovery of isotopes (Soddy, 1913) and restricted to whole-rock geochemical analyses. This and complementary efforts examining U decay and utilizing U–Pb chemical geochronology (e.g., Barrell, 1917; Bateman, 1910; Boltwood, 1907; Holmes and Lawson, 1927) laid the foundation for what was to become one of the most important isotopic dating methods, capable of measuring the timescales of events from the early solar system ~4.57 Ga into the Pleistocene.

We now know that the element lead has four naturally occurring stable isotopes, ^{204}Pb, ^{206}Pb, ^{207}Pb, and ^{208}Pb, of which the latter three have a radiogenic component produced through the independent decay of ^{238}U, ^{235}U, and ^{232}Th, respectively. The abundance of high-U minerals in most rock types, as well as the resistance of many of these minerals to chemical and physical weathering, contributes to the popularity and prolificacy of the U–Pb system. Though zircon is by far the most commonly utilized mineral for U–Pb dating (Hanchar and Hoskin, 2003), monazite, apatite, xenotime, titanite, rutile, baddeleyite, allanite, and perovskite are also commonly dated and provide a spectrum of geochronologic and thermochronologic applications in igneous, metamorphic, hydrothermal, and epithermal systems (Corfu, 1988; Corfu et al., 1994; Crowley et al., 2009; Gregory et al., 2007; Hawkins and Bowring, 1999; Heaman, 1989; Heaman and LeCheminant, 1993; Mezger et al., 1991; Nemchin and Pidgeon, 1999; Oberli et al., 2004; Parrish, 1990; Rasmussen et al., 2005, 2006; Rubatto, 2002; Schaltegger, 2007; Schoene and Bowring, 2006; Storey et al., 2007; Verts et al., 1996; von Blanckenburg, 1992). Combined with whole-rock partial dissolution techniques of increasing sophistication (Amelin et al., 2009; Connelly and Bizzarro, 2009; Connelly et al., 2008; Wadhwa et al., 2009), the U–Pb system has provided

crucial time constraints for the formation of the solar system, the calibration of the geologic timescale, the rates of tectonothermal processes in the lithosphere, and the reconstruction of paleogeography and supercontinent cycles.

The amount of material in a given analysis has continually decreased and the precision of analyses has increased since mass spectrometers were first applied to U–Pb geochronology in the 1960s. The last decade has seen an explosion of U–Pb data in the literature (**Figure 1**), in part because of the ease of dating high-U minerals in situ through the application of laser ablation methods to geochronology. However, more time-intensive high-precision U–Pb geochronology has remained the standard to which all other geochronologic methods are compared. An increasing number of other radioisotope decay constants are calibrated directly against the U decay constants through geochronologic methods (Nebel et al., 2011; Renne et al., 2010; Scherer et al., 2001; Selby et al., 2007), and the timescales of early solar system differentiation based on the decay of extinct radionuclides are connected to the absolute U–Pb timescale (Kita et al., 2005; Wadhwa et al., 2009). This is in part because the U decay constants are the most precisely determined among all geochronologic decay schemes (Begemann et al., 2001; Jaffey et al., 1971), but also because their accuracy is cross-calibrated with one another through high-precision geochronology of closed-system minerals (Mattinson, 2000, 2010; Schoene et al., 2006). The benefit of the dual U decay thus goes further to provide an internal check for closed-system behavior over long timescales, cross-checking the accuracy of many age determinations and also yielding information on multiple geologic events from single datasets (Tera and Wasserburg, 1972a; Wetherill, 1956).

This chapter focuses on modern U–Th–Pb geochronology of relatively high-U–Th minerals in high-temperature systems. It does not adequately cover exciting related fields of geochronology, such as U-series dating, for which the reader is referred elsewhere (e.g., Bourdon et al., 2003; **Chapters 4.5** and **4.15**, and references therein). This chapter also does not describe in much detail the geochronology of low-U materials (e.g., carbonates; Rasbury and Cole, 2009) or the field of Pb isotopes (see summary in Faure and Mensing, 2005), though the principles discussed here are easily extended to those fields. This chapter outlines the decay schemes and geochemistry of parent and daughter products (**Section 4.10.2**), summarizes the most popular data visualization techniques and ways to interpret such data (**Sections 4.10.2** and **4.10.3**), describes the three analytical methods used to measure parent and daughter isotope ratios (**Section 4.10.4**), discusses the controls on the precision and accuracy of the method (**Section 4.10.5**), and finally illustrates a few of the most exciting modern applications of U-Th-Pb geochronology to problems in the earth sciences (**Section 4.10.6**). Though not nearly comprehensive, this chapter is intended to give the reader a basic understanding of the U–Th–Pb system and provide the tools to delve deeper into the literature with an appreciation for the complexity and richness of the method.

4.10.2 Decay of U and Th to Pb

4.10.2.1 Decay Mechanisms

The power of U–Th–Pb geochronology is largely drawn from the decay of multiple parent isotopes to different stable isotopes of Pb, each with different half-lives (**Figures 2** and **3(a)**). None of the parent isotopes decays directly to Pb, but instead follows a sequence of alpha and beta decays (which entails the ejection of an alpha or beta particle, respectively, from the nucleus) that create a series of intermediate daughter isotopes, and always lead to the same stable isotope of Pb (Bateman, 1910). The decay chains are summarized in **Figure 2**, with estimated decay constants and half-lives of the parent isotopes illustrated (see also Dickin, 2005; Faure and Mensing, 2005). The half-lives of each intermediate daughter are far shorter than that of the parent isotope; half-lives for intermediate daughter isotopes are given in **Figure 2** if greater than 10 years. To understand the effects of these complicated decay chains on U–Th–Pb geochronology, we must introduce the concept of secular equilibrium. A decay chain is in secular equilibrium when the product of the abundance of an isotope and its decay constant are equal among all intermediate daughter products and the parent isotope:

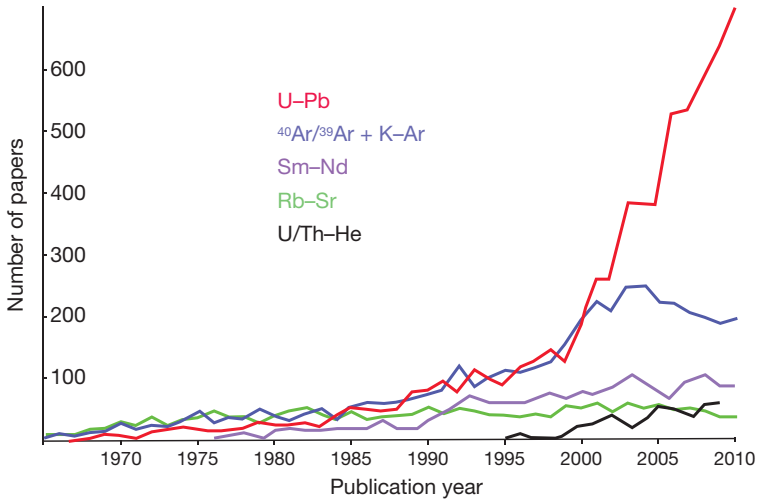

Figure 1 Plot of number of publications per year for various radioisotopic dating methods. Curves were constructed by counting all publications per year with the dating method listed in the title, as recorded on the web of knowledge (www.webofknowledge.com). A similar analysis on Google Scholar (scholar.google.com) reveals similar trends with slightly different magnitudes. A compilation that searched for the method listed anywhere in the paper revealed roughly the same relative trends, but with much higher values.

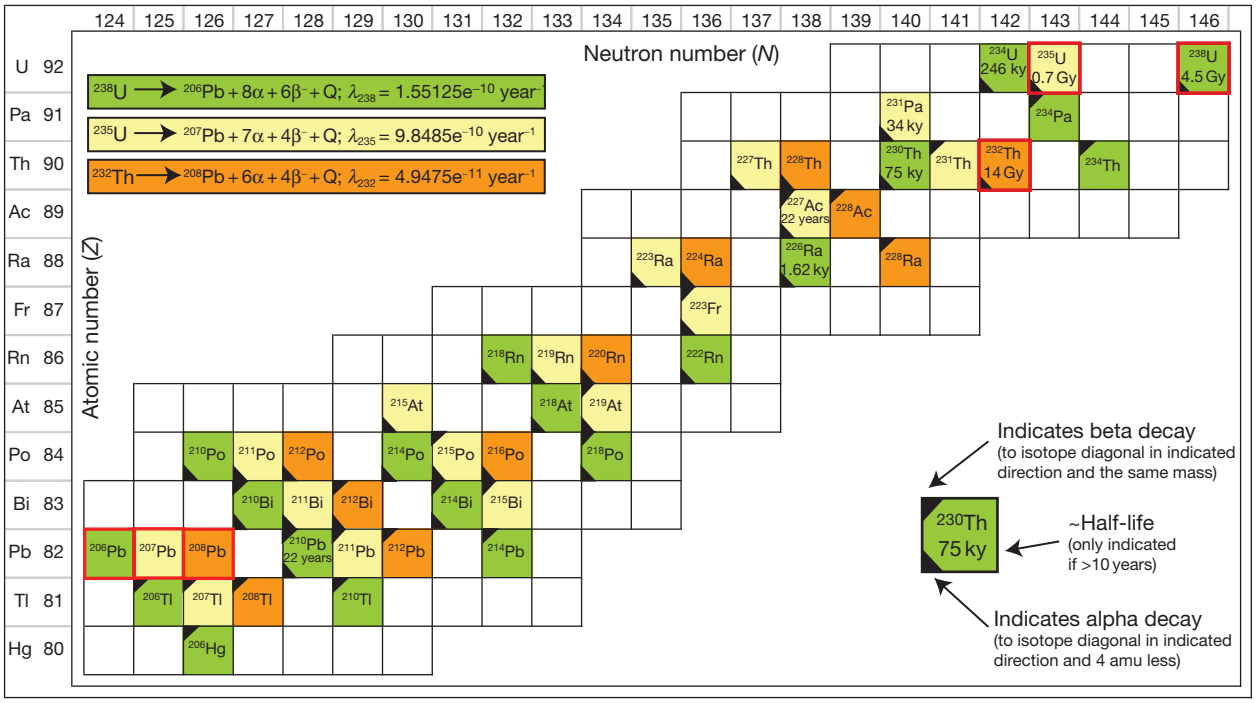

Figure 2 An illustration of the U–Th–Pb decay chains. Each isotope occurring in a given decay chain is color-coded to its parent isotope, which are outlined in red, as are the stable daughter isotopes of Pb. See inset for description of symbols used in each box. α is an alpha particle, β is a beta particle, and Q is energy released during the decay.

$$N_1\lambda_1 = N_2\lambda_2 = N_3\lambda_3 = \ldots \quad [1]$$

$$[N_1] = [N_2] = [N_3] \ldots \quad [2]$$

where N_1 is the moles of parent isotope 1 and λ_1 is its decay constant. Equation [2] rewrites this in the common nomenclature for *activity* of a given isotope (denoted by the square brackets), which describes its decay rate. In a closed system, any decay chain will reach secular equilibrium in a time proportional to the longest half-life of the intermediate daughter product. The system will remain in secular equilibrium until one or more of the isotopes in the chain is fractionated from the others, for instance by chemical partitioning in a magmatic system or low-temperature fractionation during chemical weathering. Two important implications arise from this formulation: (1) if a system is in secular equilibrium, one atom of ^{206}Pb is created for every atom of ^{238}U that decays, which is an implicit assumption when using the simplified dating equations employed in geochronology (see Section 4.10.2.2); and (2) if secular equilibrium is disturbed during crystallization or partial melting, the apparent age calculated by a geochronologist will be jeopardized – but only if the half-life of the isotope that is fractionated is significantly long. For example, even if a magma is in secular equilibrium, it is unlikely that the noble gas radon (Rn) is partitioned into zircon during crystallization. In secular equilibrium, there is one atom of ^{222}Rn for every 430 billion atoms of ^{238}U. Exclusion of all ^{222}Rn therefore will result in one fewer ^{206}Pb atom for every 430 billion parent atoms, or a calculated age that is too young by about 1 ppt, which is insignificant compared to precision on a calculated date, which is at best ~0.5‰ (see Section 4.10.4). However, several intermediate daughter products have sufficiently long half-lives that they must be considered in U–Pb geochronology, namely ^{230}Th and ^{231}Pa, and these will be discussed in Section 4.10.3. Other intermediate daughter products are also very important because they are exploited themselves as geochronometers of young materials. So-called U-series dating methods have been crucial for informing our understanding of the rates of magmatic and climatic processes in young systems (<250 ka), and are discussed in detail elsewhere (e.g., Bourdon et al., 2003; Chapters 4.5 and 4.15).

4.10.2.2 Age Equations

Treating each of the three decay systems independently permits the construction of three separate age equations, assuming secular equilibrium at the time of system closure. Derivation of the decay equation and isochron equations are given in Chapter 4.8, which in the U–Th–Pb system leads to the following classic isochron equations:

$$\left(\frac{^{206}\text{Pb}}{^{204}\text{Pb}}\right) = \left(\frac{^{206}\text{Pb}}{^{204}\text{Pb}}\right)_0 + \left(\frac{^{238}\text{U}}{^{204}\text{Pb}}\right)\left(e^{\lambda_{238}t} - 1\right) \quad [3]$$

$$\left(\frac{^{207}\text{Pb}}{^{204}\text{Pb}}\right) = \left(\frac{^{207}\text{Pb}}{^{204}\text{Pb}}\right)_0 + \left(\frac{^{235}\text{U}}{^{204}\text{Pb}}\right)\left(e^{\lambda_{235}t} - 1\right) \quad [4]$$

$$\left(\frac{^{208}\text{Pb}}{^{204}\text{Pb}}\right) = \left(\frac{^{208}\text{Pb}}{^{204}\text{Pb}}\right)_0 + \left(\frac{^{232}\text{Th}}{^{204}\text{Pb}}\right)\left(e^{\lambda_{232}t} - 1\right) \quad [5]$$

where the subscript 0 follows the ratio of the isotopic composition of Pb when the system closed (e.g., crystallization of a mineral), t is the time since the system closed, and λ_{238}, λ_{235}, and λ_{232} are the decay constants of ^{238}U, ^{235}U, and ^{232}Th. Note that initial Pb is colloquially called *common lead*, and denoted Pb_c. Here, Pb_c is used as initial Pb plus blank and

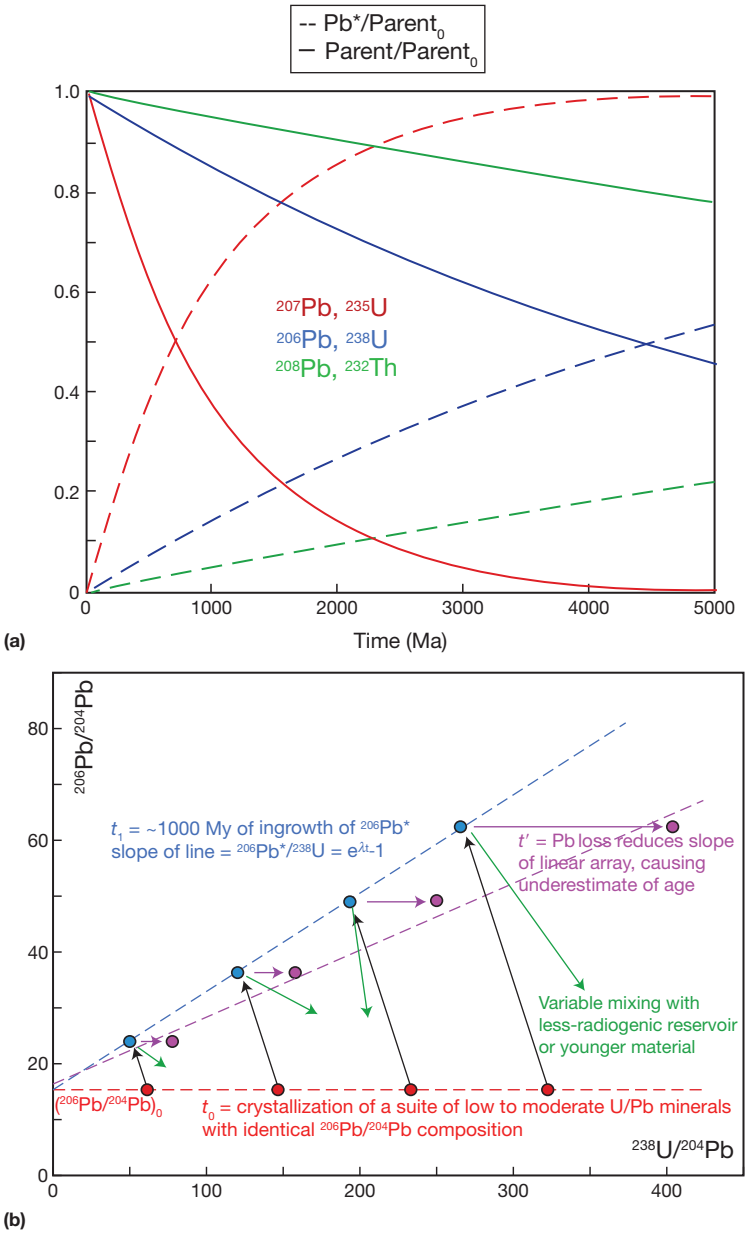

Figure 3 (a) Illustration of the different half-lives of ^{232}Th, ^{238}U, and ^{235}U through decay of the parent isotope and ingrowth of the daughter. Curves are color-coded by decay system. (b) An example of one of three possible parent–daughter isochron diagrams in the U–Th–Pb system. t_0, t_1, etc., refer to different times in the system's evolution and are color-coded to the positions of the points, which migrate as shown by the arrows. See **Section 4.10.2.2** and eqns [3]–[5].

contamination Pb (i.e., nonradiogenic Pb introduced during laboratory work or naturally prior to sampling). (It should be noted that other nomenclature also exists. For example, some prefer the term *nonradiogenic Pb* rather than *common Pb*, as used here.) As with isochron equations in other commonly used dating systems, a stable isotope of the daughter element is chosen for normalization, which in this case is ^{204}Pb, the only nonradiogenic isotope of Pb (**Figure 3(b)**). Normalization has several benefits. One is that it removes the systematic uncertainty of calculated moles of both parent isotope and daughter product, which is typically large compared to the precision of the isotopic ratio. In other words, one can measure ^{206}Pb/^{204}Pb much more precisely than one can measure the moles of ^{206}Pb, which is a function of the relatively poorly known concentration of the tracer solution or standard mineral used for the analysis (see **Section 4.10.3**). A second benefit is that it allows one to ignore the absolute concentration of both U and Pb and focus simply on their ratio, which again can be measured very precisely compared to the concentrations. Each of eqns [3]–[5] can be used to calculate a model age if the isotopic composition of initial Pb at $t = 0$ is known or if its contribution can be neglected, and if other sources of Pb_c have been accounted for. Alternatively, a collection of mineral or bulk rock analyses may form a linear

array on an isochron diagram (e.g., $^{206}Pb/^{204}Pb$ vs. $^{238}U/^{204}Pb$), where the slope of the line is equal to $e^{\lambda t} - 1$ and the y-intercept is equivalent to the initial isotopic composition of Pb; this is the classic isochron approach used in nearly all geochronologic methods and is shown graphically in **Figure 3(b)**.

In some mineral systems, as is commonly the case with zircon and monazite, the contribution of initial lead is negligible compared to the radiogenic component, in which case eqns [3]–[5] simplify to

$$\left(\frac{^{206}Pb^*}{^{238}U}\right) = \left(e^{\lambda_{238}t} - 1\right) \quad [6]$$

$$\left(\frac{^{207}Pb^*}{^{235}U}\right) = \left(e^{\lambda_{235}t} - 1\right) \quad [7]$$

$$\left(\frac{^{208}Pb^*}{^{232}Th}\right) = \left(e^{\lambda_{232}t} - 1\right) \quad [8]$$

where * stands for *radiogenic*.

An added benefit of the U–Pb dual decay system is that it permits a fourth isochron equation to be constructed, which comes about by dividing eqn [4] by eqn [3]:

$$\frac{\left(\frac{^{207}Pb}{^{204}Pb}\right) - \left(\frac{^{207}Pb}{^{204}Pb}\right)_0}{\left(\frac{^{206}Pb}{^{204}Pb}\right) - \left(\frac{^{206}Pb}{^{204}Pb}\right)_0} = \left(\frac{^{235}U}{^{238}U}\right)\frac{\left(e^{\lambda_{235}t} - 1\right)}{\left(e^{\lambda_{238}t} - 1\right)} = \left(\frac{^{207}Pb}{^{206}Pb}\right)^* \quad [9]$$

where * refers to the ratio of radiogenic $^{207}Pb/^{206}Pb$. This equation is especially useful as the present-day $^{235}U/^{238}U$ is assumed to be a known constant in terrestrial and meteoritic systems (though see **Section 4.10.5**), eliminating the need to measure U. The concentration of Pb can also be ignored. Equation [9] can be used to calculate an age by linear fitting in $^{206}Pb/^{204}Pb$–$^{207}Pb/^{204}Pb$ space, or if initial Pb is negligible, then the measured $(^{207}Pb/^{206}Pb)^*$ can be used to directly calculate a date. In both cases, the equation must be solved iteratively; this is commonly called the Pb–Pb date. Thus, by measuring U and Pb isotopes alone, one can calculate three isotopic dates, and in a closed system, all three would agree. Because, as with any dating method, the requirement of closed-system behavior is often violated, geochronologists have developed numerous graphical and numerical methods aimed to test the assumption of closed-system behavior and to extract additional information on the geologic history of samples by quantifying open-system behavior recorded by this system.

4.10.2.3 Visualization of U–Th–Pb Data

Because of the numerous equations that permit calculation of dates and Pb_0 compositions in U–Th–Pb geochronology, several popular graphical representations of data are used to display the numerous variables. While the same information can be pulled from any of these graphical depictions, different diagrams have been used as convenient ways of displaying different types of data.

4.10.2.3.1 2D isochrons

Equations [3]–[5] can be used to create traditional isochron plots that are used widely in many geochronometric systems, all of which are interpreted as outlined earlier (Holmes, 1946; Houtermans, 1946). The U–Pb system is also amenable to 3D isochrons (Ludwig, 1998; Wendt, 1984; Zheng, 1992), which simultaneously determine the initial $^{206}Pb/^{204}Pb$ and $^{207}Pb/^{204}Pb$ compositions and age for cogenetic samples. A suite of rocks and/or minerals can be used to calculate a date on 2D or 3D isochrons if each rock or mineral on the isochron (1) became a closed system at the same time, (2) has remained closed since that time, and (3) had the same initial isotopic composition of Pb. These prerequisites are the same as those for all other isochron calculations and need to be evaluated both statistically (Ludwig, 1998; Wendt and Carl, 1991; York, 1968; York et al., 2004) and using the geology of the samples measured.

Rearranging eqn [9] allows the construction of a Pb–Pb isochron diagram in $^{206}Pb/^{204}Pb$–$^{207}Pb/^{204}Pb$ space (Holmes, 1946; Houtermans, 1946). The main difference graphically is that all minerals or rocks that satisfy the isochron criteria start at the exact same point in $^{206}Pb/^{204}Pb$–$^{207}Pb/^{204}Pb$ space and follow an arc whose radius depends on the U/Pb in the sample (Armstrong, 1968; Stacey and Kramers, 1975). Samples with different U/Pb, despite following different paths, will still fall on a line whose slope can be used to calculate the time since system closure. Perhaps the most famous Pb–Pb isochron was calculated by Patterson (1956), who used terrestrial and meteorite samples to define an isochron whose date of 4.55 ± 0.07 Ga was interpreted as the time at which meteorites and Earth began evolving separately – in other words, the age of Earth. As with U–Pb isochrons, Pb–Pb isochrons can yield age information while avoiding the assumption of an initial Pb isotopic composition. It is more useful than U–Pb isochrons in systems where recent open-system behavior is suspected for U, or if the U measurement is difficult (e.g., Barfod et al., 2002; Chen et al., 2004; Toulkeridis et al., 2010). Modern meteorite geochronology employs a modification of the Pb–Pb isochron by plotting $^{204}Pb/^{206}Pb$ versus $^{207}Pb/^{206}Pb$. This approach allows very precise calculation of $^{207}Pb/^{206}Pb^*$, which is weighted toward samples that are the least sensitive to Pb_c (Amelin et al., 2009; Baker et al., 2005; Connelly et al., 2008; Wadhwa et al., 2009).

4.10.2.3.2 The Wetherill concordia plot

Early workers noted the important constraints that the dual decay of U to Pb could provide for geochronological applications. Wetherill (1956) introduced the concordia diagram, which plots $^{206}Pb^*/^{238}U$ versus $^{207}Pb^*/^{235}U$ from the same analyses. The parametric *concordia curve* can then be drawn as the set of solutions to eqns [6] and [7] for equal values of t (**Figure 3**), which is nonlinear because ^{238}U and ^{235}U have different half-lives. In other words, points on the concordia curve are where $^{207}Pb^*/^{235}U$ and $^{206}Pb^*/^{238}U$ both correspond to the same date. On the concordia plot, all samples that remained a closed system since the time of formation fall on the concordia curve; those that do not are called *discordant* and have experienced some form of open-system behavior.

This plot was quickly adopted by U–Pb geochronologists as a means of identifying and quantifying open-system behavior

in datable materials (Davis et al., 2003; Pidgeon et al., 1966; Russell and Ahrens, 1957; Tilton, 1960; Wasserburg, 1963). It has been used countless times since, and so understanding its use is essential for every earth scientist with an interest in geologic time, and it is briefly outlined here. The concordia plot is also discussed at length in the literature and also in several good textbooks (Dickin, 2005; Faure and Mensing, 2005). The discussion that follows assumes that all analyses have been corrected for Pb_c and thus contain only radiogenic lead.

Sections 4.10.3 and 4.10.5 summarize most of the geologic and analytical sources of discordance, respectively. Here the causes of large amounts of discordance are examined in order to introduce how to interpret data in concordia space, without going into detail about the mechanisms by which open-system behavior occurs. Pb loss, Pb gain, U loss, U gain, and mixing of different-aged material can all cause discordant arrays. Pb-loss and mixing, or some combination of these, are the only ones entertained regularly in the literature and have similar interpretations in concordia space. Some empirical and experimental evidence has been used to argue that U mobility may be important under certain conditions (e.g., Sinha et al., 1992; Williams et al., 1984).

When a mineral crystallizes and begins accumulating Pb* in a closed system, $^{207}Pb^*/^{235}U$ and $^{206}Pb^*/^{238}U$ evolve such that both ratios follow the concordia curve (Figure 4). If the system experiences a single episode of Pb loss, the lead leaving the system has a $^{207}Pb/^{206}Pb$ composition of the mineral at that time, which corresponds to its Pb–Pb date (eqn [9]). Multiple minerals that experience a similar evolution but with different amounts of Pb loss will initially fall on a discordia line that goes through the origin and intersects the concordia curve at the date that corresponds to the real age. (Please note the difference between a *date* and an *age*, which is described in Section 4.10.5.1.) In such a case, the Pb–Pb date will be identical to the upper intercept date. If the minerals then become closed systems again, they continue to accumulate Pb* and evolve on a trajectory such that the discordia array is preserved as a line. If one were to date these minerals 100 My later, the upper intercept date would correspond to the true formation age of the mineral and the lower intercept of the discordia line would

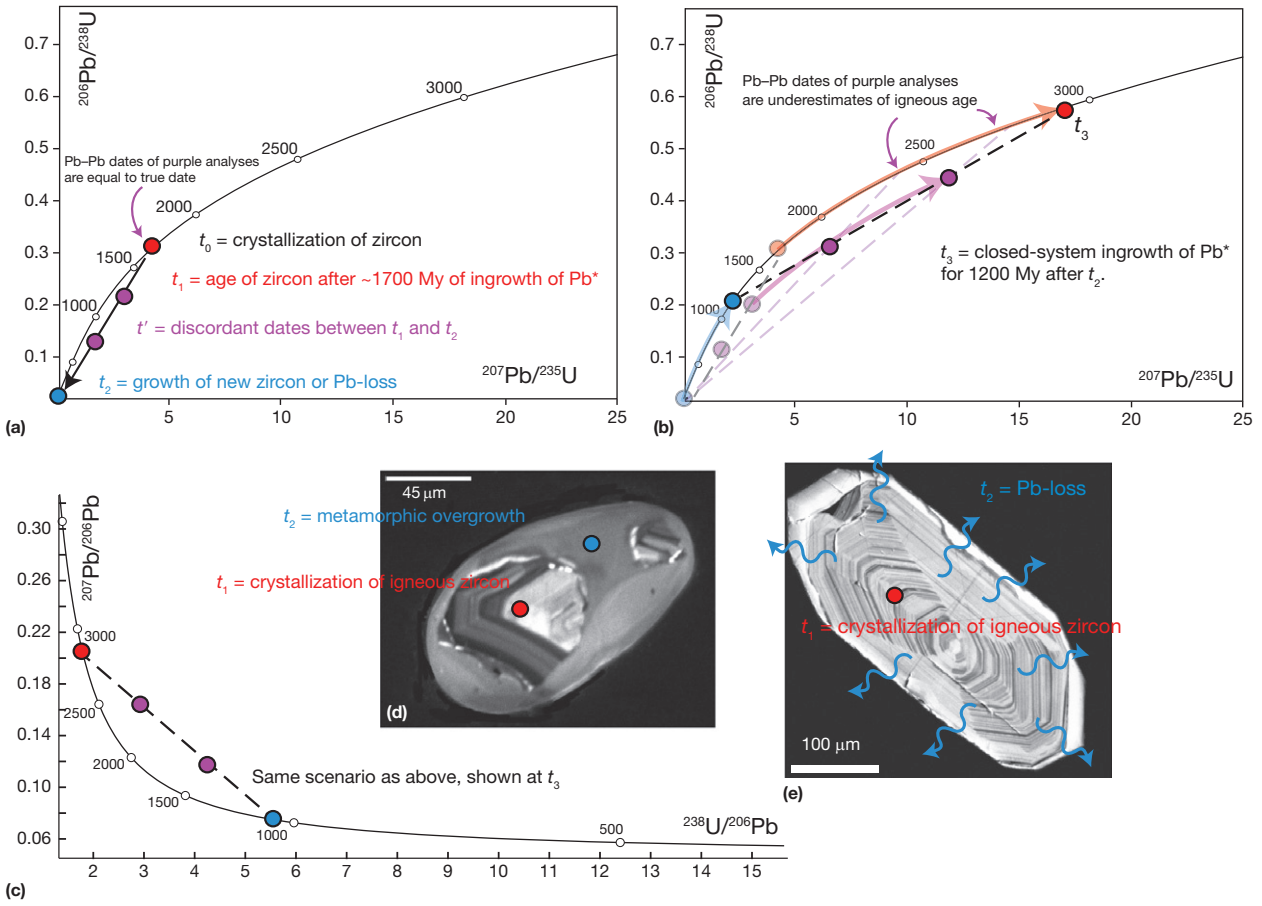

Figure 4 Graphical representation of zircon growth history in the Wetherill concordia diagram (a, b) and the Tera–Wasserburg (T–W) diagram (c). (a) Example of a 1700 Ma zircon losing Pb or mixing with metamorphic overgrowth. t_0 is the crystallization age of the zircons; after 1700 My of closed-system ingrowth of Pb, the zircons appears on concordia at t_1; at t_2 the zircon suffers Pb loss or growth of new zircon around old core; t' represents zircons that are discordant following partial Pb loss or mineral overgrowth at t_2. (b) The same data after the system has closed again and continues to evolve up the concordia curve. The discordia line defined by purple analyses now has an upper intercept with concordia representing the original igneous crystallization event at t_1, and a lower intercept age representing t_2, the time before the present at which Pb loss or overgrowth occurred. (c) The same scenario as in (b) but in a T–W diagram. (d) Illustration of how the scenario in (a) and (b) would possibly be recorded in the event of metamorphism as t_2. (e) The case where Pb loss happens at t_2. Zircon image in (d) is from Schmitz and Bowring (2004). Note color coordination from (a)–(c) with descriptions in (d) and (e).

intersect the concordia curve at a date corresponding to the time of the Pb-loss event. In such a case, none of the U–Pb or Pb–Pb dates of single minerals will have geologic meaning, but the discordia line would yield geologic insight.

If an analysis mixes two domains with different ages, for example an old zircon core and a younger zircon rim, the exact same effect is observed and the interpretation in concordia space is the same. This simple graphical analysis can be extended to multiple Pb-loss events or mixing of multiple aged end-members, though the data will become scattered off of a line, making robust geologic information difficult to extract.

4.10.2.3.3 Tera–Wasserburg diagram and 3D isochrons

Several other types of concordia diagrams can be constructed in the U–Th–Pb system by placing any two (or more) of the four utilizable clocks onto axes. Th–Pb versus U–Pb diagrams have been used (Searle et al., 2007; Steiger and Wasserburg, 1966; Villeneuve et al., 2000), especially for monazite, whose $^{206}Pb/^{238}U$ systematics are compromised by ^{230}Th disequilibrium due to very high Th/U (see **Section 4.10.3**; Searle et al., 2007; Villeneuve et al., 2000). The most popular alternative to the Wetherill diagram is the Tera–Wasserburg (T–W) concordia diagram, which places $^{238}U/^{206}Pb$ and $^{207}Pb/^{206}Pb$ on the *x*- and *y*-axes, respectively (Tera and Wasserburg, 1972a,b). If $^{238}U/^{206}Pb^*$ and $^{207}Pb^*/^{206}Pb^*$ (i.e., corrected for Pb_c, as is done on the Wetherill diagram) are plotted on the T–W diagram, concordant and discordant data can be interpreted identically to the Wetherill concordia diagram (**Figure 4**). However, if a cogenetic suite of samples fall off of concordia solely from variable contamination by a single initial Pb composition, then a line drawn through the dataset will intercept concordia at the true age and the $^{207}Pb/^{206}Pb$ axis at the composition of Pb_0 (i.e., where U = 0, so there is no Pb*). It therefore combines some of the power of isochron methods by displaying initial Pb compositions with the power of a concordia diagram by simultaneously testing for signs of open system behavior (**Figure 5**).

The power of linear regression in T–W space to identify Pb_c composition breaks down, however, if a sample is affected by Pb loss or mixing of multiple age domains. This could be identified if a discordia does not statistically fit a line, or if different age domains within the analyzed minerals can be dated. A statistically more rigorous way of testing these assumptions is by using a 3D isochron (Ludwig, 1998; Wendt, 1984), which simultaneously determines the initial $^{206}Pb/^{204}Pb$ and $^{207}Pb/^{204}Pb$ compositions and age for cogenetic samples (**Figure 5**). The method plots $^{238}U/^{206}Pb$ versus $^{207}Pb/^{206}Pb$ in one plane of the coordinate system and $^{204}Pb/^{206}Pb$ in the third dimension. A suite of cogenetic minerals whose spread is caused solely by Pb_c should fall on a line in this space, and so, in addition to providing high-precision dates, this method can test whether Pb loss or inheritance is important in a given high-Pb_c dataset (Ludwig, 1998). These methods have been applied successfully in numerous cases, and usually yield more precise estimates of Pb_c isotopic composition than 2D isochrons (Amelin and Zaitsev, 2002; Gelcich et al., 2005; Schoene and Bowring, 2006).

4.10.3 Causes of Discordance in the U–Th–Pb System

Because the U–Th–Pb system is amenable to scrutiny of open-system behavior, the causes of discordance have received much attention. As a result, some of these causes are well understood,

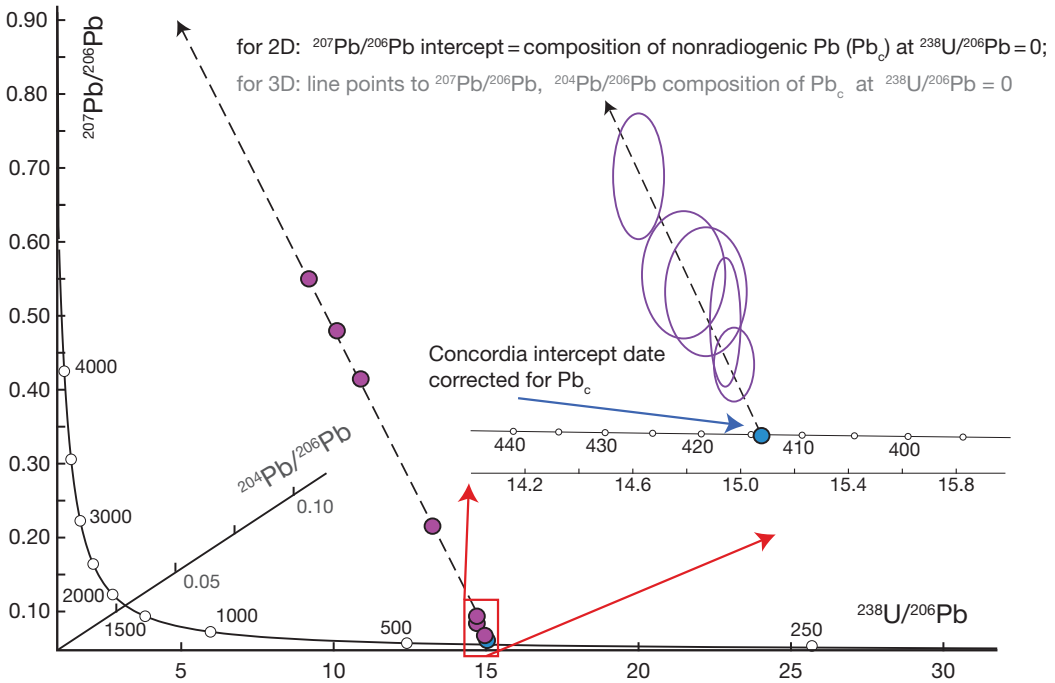

Figure 5 Tera–Wasserburg (T–W) concordia diagram shown in 2D and 3D. Note that if discordance is caused by mixture with initial Pb_c, the resulting linear fit to the data intersects the $^{207}Pb/^{206}Pb$ axis at higher values than would be expected for mixing with radiogenic Pb, for instance from an older component of the mineral. See text for discussion.

while others remain more enigmatic. Here, the term discordance is used synonymously with open-system behavior. However, as will be discussed in **Section 4.10.5**, many samples may have experienced open-system behavior but are still statistically concordant (i.e., overlap the concordia curve within uncertainty), especially in young rocks, or for data obtained using low-precision analytical techniques. Nonanalytical, or 'geologic,' reasons for discordance discussed here in some detail are (1) mixing, (2) Pb loss, (3) intermediate daughter product disequilibrium, and (4) initial Pb. Other factors causing discordance, such as the U isotopic composition of the sample and decay constant uncertainties, will be discussed in **Section 4.10.5**.

4.10.3.1 Mixing of Different Age Domains

It has long been known that zircon and other minerals can contain old cores and one or more generations of younger overgrowth that, if analyzed together, can lead to discordant arrays in concordia space. These were initially identified optically in mineral separates or grain-mount (Bickford et al., 1981; Corfu and Ayres, 1984; Krogh and Davis, 1975), later by backscatter electron imaging (Wayne and Sinha, 1988; Wayne et al., 1992), and finally cathodoluminescence imaging was widely popularized (Hanchar and Miller, 1993; Hanchar and Rudnick, 1995; Schenk, 1980). Backscattered and cathodoluminescence imaging have revealed internal zonation within minerals that may record whether different growth zones are igneous or metamorphic in origin, whether resorption occurred prior to overgrowth, etc. These simple yet powerful tools are now used ubiquitously by analysts doing in situ U–Pb geochronology as a means of identifying and isolating different growth domains in zircon, monazite, titanite, and apatite. The high spatial resolution of these techniques (see **Section 4.10.4**) has been crucial in revealing the metamorphic histories of rocks with complexly zoned minerals (e.g., Bowring et al., 1989; Cottle et al., 2009b; Harley and Kelly, 2007; Kelly and Harley, 2005; Rubatto, 2002; Schaltegger et al., 1999; Vavra et al., 1996). Grain imaging prior to isotope dilution thermal ionization mass spectrometry (ID-TIMS) is gaining increasing use as a means of avoiding grains with obvious inherited cores or by isolating different growth domains by mechanically breaking imaged grains prior to analysis (Corrie and Kohn, 2007; Crowley et al., 2007; Gordon et al., 2010; Hawkins and Bowring, 1999; Schoene and Bowring, 2007). Whichever technique is used, the goal is either to isolate mineral cores and rims in order to date those events with higher precision and accuracy than is achievable by calculating upper or lower intercept dates in concordia space, or to establish that the different spatial domains are not temporally resolvable (Dumond et al., 2008).

4.10.3.2 Pb Loss

A major focus of U–Pb geochronologists has been to understand discordia arrays in zircon analyses. Though mixing of growth domains with different ages is easily understood and is now often resolvable using high spatial resolution measurement techniques, the process of Pb loss has numerous possible causes that are difficult to quantify. The example given in **Figure 4** follows the common interpretation that the lower intercepts of discordant arrays represent geologically significant events that caused Pb loss in a suite of zircons. Tilton (1960) noted the odd coincidence that many zircon discordia arrays from different continents had broadly similar lower intercepts of ~600 Ma, but did not follow linear arrays, as would be expected from a single Pb-loss event. He instead derived formulas to explain Pb loss in concordia space as a result of volume diffusion of Pb through the zircon crystal lattice. He realized the conundrum of this model, namely that while many zircons remain closed systems through high-temperature metamorphism, others fall on discordant arrays with lower intercepts that are in fact younger than K–Ar dates in biotite (in which Ar diffuses at lower temperatures than 300 °C) from the same rocks. Following the detailed empirical study of Silver and Deutsch (1963), Wasserburg (1963) derived equations for a model in which Pb loss occurred by diffusion, but with a diffusion coefficient that was a function of U- and Th-induced radiation damage to the zircon lattice. Models for volume diffusion of Pb have now been described analytically and numerically, and applied to U–Pb thermochronometers such as titanite, apatite, and rutile. These applications will be highlighted separately in **Section 4.10.6**, while zircon is given special treatment here.

Radiation damage to zircon is a result of both alpha recoil and fission track accumulation (Deliens et al., 1977; Meldrum et al., 1998; Nasdala et al., 1996; Pidgeon et al., 1966; Silver and Deutsch, 1963), and has been shown to correlate roughly with the degree of discordance in some zircon suites (Nasdala et al., 1998). At temperatures above ~250 °C, radiation damage in zircon is annealed on short geologic timescales (Ketcham et al., 1999); experimental data for diffusion of Pb in zircon show it to be negligible at temperatures of even >900 °C in non-metamict crystals (Cherniak and Watson, 2001; Lee, 1997). Attempts at revising equations for radiation-induced Pb diffusion, for example by adopting short-circuit diffusion models (Lee, 1995), have not proven useful for zircon. Additional mechanisms that may contribute to Pb loss are crystal plastic deformation as a means of generating fast-diffusion pathways (Reddy et al., 2006) and low-temperature hydrothermal dissolution–reprecipitation (Geisler et al., 2002, 2003). Nonetheless, the conclusion remains that Pb loss should not occur in zircons except at low temperatures. Mezger and Krogstad (1997) inferred that Pb loss at high temperatures is a result of recrystallization of metamict zircon, and could result in meaningful or meaningless lower intercept dates. The concept of 'recrystallization,' however, is a nebulous and poorly defined process. Alternatively, it may be more reasonable that lower intercept dates that appear to have geologic meaning (i.e., they correspond to a known metamorphic event) may represent core–rim mixing arrays that are perhaps superimposed on low-temperature Pb loss in metamict zircons. Or, more simply, that the exact opposite of the traditional interpretation is correct: that lower intercept dates represent not the time at which Pb loss occurred, but the time at which Pb loss stopped due to high temperature annealing.

Whatever the exact mechanism of Pb loss in zircons, the most important advances in overcoming discordance have not been from understanding its cause but instead from eliminating it. In addition to methods of avoiding selection of metamict grains (e.g., Krogh, 1982a), these can be summarized in three advances: (1) the air abrasion technique (Krogh, 1982b), which

mechanically removes the outer, often higher-U and more metamict domains of grains prior to analysis of whole grains; (2) the use of in situ dating techniques, which have sufficient spatial resolution to attempt either avoiding domains that have undergone Pb loss or intentionally isolating different age domains that have been identified texturally; and (3) the invention of the chemical abrasion technique (Mattinson, 2005), which partially anneals zircons and then chemically dissolves discordant domains, leaving a closed-system residue amenable to analysis. The latter two techniques will be discussed in more detail in Sections 4.10.4 and 4.10.5.

4.10.3.3 Intermediate Daughter Product Disequilibrium

The assumption of secular equilibrium, outlined in Section 4.10.2.1, is crucial for simplifying the complicated U–Th–Pb decay chains into manageable equations from which a date can be calculated. This assumption is incorrect, however, if one or more of the intermediate daughter products is fractionated from its parent isotope such that the crystallized mineral is not in secular equilibrium immediately after formation (Mattinson, 1973; Schärer, 1984). This can occur due to fractionation of the intermediate product during partial melting or during crystallization of the resulting liquid. Though fractionation of intermediate products certainly occurs during partial melting processes, and has been documented in young volcanic rocks (e.g., Condomines et al., 2003, and references therein), the effect of this process on older minerals is difficult to quantify or even treat qualitatively. However, correcting for fractionation during crystallization is commonly attempted. Qualitatively, if an intermediate product is preferentially partitioned into the mineral over its parent, it will result in an excess amount of Pb*, and therefore an overestimate of the true age. Conversely, an age will be underestimated if an intermediate product is preferentially excluded during crystallization (Figure 6). Given the diversity of geochemical behavior of all elements in the three decay chains, it is unlikely that any mineral is, in fact, in secular equilibrium at the time of crystallization.

For reasons described in Section 4.10.2.1 and apparent in eqns [1] and [2], only intermediate products with long enough half-lives will be present or absent in enough quantity to affect a resulting date. The intermediate products that meet this criteria in the ^{238}U decay chain are ^{230}Th ($t_{1/2}=75.4$ ky) and ^{234}U ($t_{1/2}=245$ ky), but it is often assumed that ^{234}U is not significantly fractionated from ^{238}U at high temperatures. ^{231}Pa is the only relatively long-lived isotope in the ^{235}U decay chain. ^{230}Th disequilibrium has received the most attention in the literature, in part because very high Th/U minerals such as monazite induce strong Th and U fractionations from melt to mineral, resulting in excess ^{206}Pb that is easily recognizable when plotted against ^{207}Pb/^{235}U on a conventional concordia plot (Mattinson, 1973). Schärer (1984) and Parrish (1990) quantified these effects by relating the amount of intermediate product lost or gained relative to secular equilibrium during mineral crystallization using versions of eqn [10]:

$$t_{\text{excess}} = \left(\frac{1}{\lambda_{238}}\right) \ln\left[1 + (f-1)\left(\frac{\lambda_{238}}{\lambda_{230}}\right)\right] \qquad [10]$$

where

$$f = \left[\frac{(\text{Th/U})_{\text{mineral}}}{(\text{Th/U})_{\text{liquid}}}\right] \qquad [11]$$

Thus, f is equivalent to the ratio of the mineral/melt partition coefficients for Th and U for the phase of interest ($D^{\text{Th/U}}_{\text{mineral/melt}}$). In theory, if partition coefficients for minerals are invariant, then f should always be the same and one

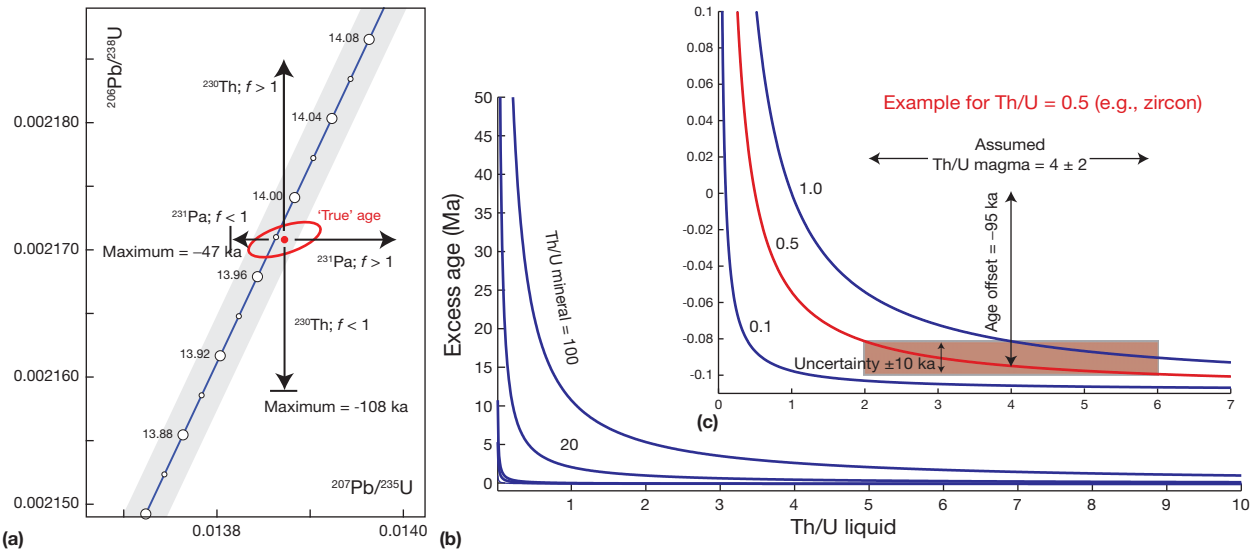

Figure 6 Illustration of intermediate daughter product disequilibrium (intermediate product D). (a) Depiction of what would happen to an ellipse in concordia space if it were moved from its true age by intermediate product disequilibrium of ^{230}Th and/or ^{231}Pa (concordia ticks are in Ma). (b) Plot showing the excess age expected, given the Th/U values of a liquid that the mineral crystallized from, for the Th/U values in the mineral indicated by each curve. For example, if a mineral crystallized with a Th/U of 20 from a liquid with Th/U of 1, the mineral would have a ^{206}Pb/^{238}U date that was ~3 Ma too old. (c) Magnification of panel (b) to illustrate where zircon commonly falls: $\text{Th/U}_{\text{mineral}} < \text{Th/U}_{\text{liquid}}$. Note that for a zircon of Th/U = 0.5 and an assumed Th/U magma of 4 ± 2, the total age offset of −95 ka is far greater than the uncertainty in the correction (±10 ka). Thus, it is better to estimate the $\text{Th/U}_{\text{liquid}}$ and propagate uncertainties than to ignore the correction.

could easily correct for intermediate product disequilibrium; in reality, the relative partition coefficients of Th and U for high-U minerals are not well understood. Published zircon/melt partition coefficients for Th and U are variable (Fukuoka and Kigoshi, 1974; Hanchar and van Westrenen, 2007; Hinton and Upton, 1991; Sano et al., 2002; Thomas et al., 2002) and may be dependent on temperature, pressure, and magma composition (Rubatto and Hermann, 2007). Partitioning of Th and U between melt and titanite and apatite have been determined experimentally (Prowatke and Klemme, 2005, 2006a,b), but the range observed in experiments (e.g., as a result of magma composition) precludes a bulk correction for intermediate product disequilibrium, even in magmatic minerals.

Because of the uncertainties in $D^{Th/U}{}_{mineral/melt}$ determined experimentally and the inconsistency of the f factor calculated empirically using ^{232}Th–^{208}Pb dates (Barth et al., 1994; Oberli et al., 2004), correcting for ^{230}Th disequilibrium is inherently imprecise. Fortunately, $Th/U_{mineral}$ can be measured directly during mass spectrometry or estimated by assuming concordance between the U–Pb and Th–Pb dates, measuring $^{208}Pb^*$, and then calculating ^{232}Th. This leaves one unknown, Th/U_{liquid}. One approach is to use the Th/U of the rock from which the mineral is extracted (Schärer et al., 1990). However, this estimate may be inaccurate because one must assume the rock represents a liquid composition and that U and Th have not been fractionated since crystallization. Another approach, for volcanic minerals, is to use the Th/U of the host glass (Bachmann et al., 2010; Schmitz and Bowring, 2001), assuming that the mineral grew directly from the liquid that quenched to form the glass.

For minerals where $f<1$, such as zircon and xenotime, the correction for ^{230}Th disequilibrium has a lower limit at $f=0$, yielding a date that is 110 ka too young (Schärer, 1984; using the ^{230}Th decay constant of Cheng et al., 2000; **Figure 6**). In such cases, it is common to assume a Th/U_{liquid}, given that this ratio usually falls between 2 and 6 in magmas. Equations [10] and [11] can be used to evaluate the influence of this assumption (**Figure 6**). Such an exercise shows that it is more accurate to make the correction assuming a Th/U_{liquid} than not make the correction at all. Propagating the uncertainty of the correction into final dates results in minimal added uncertainty, except for very young samples or samples hypothesized to have similar Th/U for the melt and mineral (Bachmann et al., 2010; Crowley et al., 2007). For minerals where $f \gg 1$, such as allanite and monazite (and sometimes titanite and apatite), the excess age resulting from initial ^{230}Th disequilibrium can be debilitating; many geochronologists simply avoid using the $^{206}Pb/^{238}U$ date in such cases (Cottle et al., 2009b; Crowley et al., 2009; Schoene and Bowring, 2006; Villeneuve et al., 2000).

The effect of ^{231}Pa disequilibrium is poorly understood, in part because there are no other isotopes of Pa that can be used as a proxy for Pa and U partitioning. Furthermore, Pa is not generally targeted in experimental partitioning studies. Schmitt (2007) measured $[^{231}Pa]/[^{235}U]$ in young volcanic zircons and found values slightly greater than 1, suggesting that only a 15 ka age excess would be present in older samples. Nonetheless, extreme ^{231}Pa disequilibrium has been documented in zircon (Anczkiewicz et al., 2001), which indicates the importance of future experimental studies to understand the effect of Pa partitioning on $^{207}Pb/^{235}U$ dates.

4.10.3.4 Correction for Initial Pb

Equations [3]–[5] illustrate the importance of correcting for the presence of initial lead (Pb_0; note the distinction used here that Pb_0 differs from Pb_c in that Pb_c is a more general term that includes laboratory blank Pb) in a system in order to obtain an accurate date. Both 2D and 3D isochrons can be used to solve for the isotopic composition of Pb_0 if a dataset meets the required assumptions that go into isochron calculations. On the T–W concordia diagram (part of most 3D isochrons; **Section 4.10.2.3.3**), the $^{207}Pb/^{206}Pb$ of Pb_0 is the y-intercept, given an otherwise closed system and adequate spread of data to define a line. The effect of Pb_c on a Wetherill concordia diagram is to create a discordia with slope equal to the $^{206}Pb/^{207}Pb^*(^{238}U/^{235}U)$ (i.e., the isotopic composition of U in the sample), though data are usually corrected for Pb_c before being plotted. A dataset in either concordia diagram can also form a linear array because of mixing or Pb loss. It is possible to determine whether Pb_c or mixing/Pb loss is responsible for the spread in data for young samples because the linear array created by Pb_c is at high angles to concordia and the upper intercept with concordia is >4.5 Ga. For Paleoproterozoic or Archean samples, however, the Pb_c array can be nearly parallel to discordias created by mixing/Pb loss, and it is thus dangerous to assume the source of the discordance.

Other methods for common Pb correction involve an assumption about its composition. For example, by measuring the moles of ^{204}Pb in a sample and assuming a $^{206}Pb/^{204}Pb$ of the Pb_c from a single source, one can calculate directly the amount of $^{206}Pb^*$ (Williams, 1998). If one assumes that total $^{206}Pb_c$ is composed of $^{206}Pb_0$ and ^{206}Pb from blank, or any number of sources, then it is also necessary to measure or assume the $^{206}Pb/^{204}Pb$ of the other sources, in which case the equations become slightly more complicated (Ludwig, 1980; McLean et al., 2011; Schmitz and Schoene, 2007). Assuming or measuring multiple sources of nonradiogenic Pb is standard in ID-TIMS, though the amount and composition of each is still difficult to determine accurately and, in cases where Pb^* is very low relative to Pb_c, this presents a significant source of uncertainty. In the case of zircon, it is easily argued that there is no Pb_0, and all Pb_c is introduced through one or more sources of laboratory contamination. The isotopic composition of Pb_0 adopted for other minerals is often assumed based on a bulk-Pb evolution model (e.g., Cumming and Richards, 1975; Stacey and Kramers, 1975) given an estimated crystallization age for the mineral. Alternatively, it can be estimated by dissolving or leaching Pb from coexisting low-U phases such as feldspar (Catanzaro and Hanson, 1971; Chamberlain and Bowring, 2000; Housh and Bowring, 1991); several papers make direct comparisons of these techniques (Chamberlain and Bowring, 2000; Schmitz and Bowring, 2001; Schoene and Bowring, 2006, 2007) with the general conclusion that analyzing cogenetic phases is more robust (**Figure 7**). However, Schoene and Bowring (2006) argue that apatite and titanite Pb_0 from a syenite were derived from an evolving source that is not defined by feldspar Pb and instead prefer the 3D isochron-derived Pb_0 composition.

As ^{204}Pb is always the least abundant Pb isotope present ($^{206}Pb/^{204}Pb \gg 1000$ is typical for zircon), ^{204}Pb is difficult to measure and is also affected by isobaric interferences.

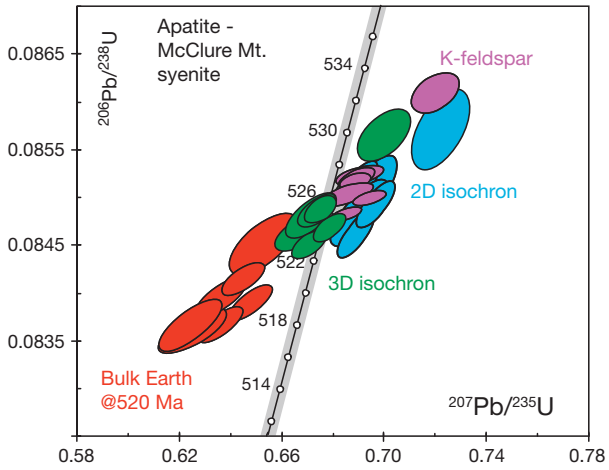

Figure 7 Effect of different methods of Pb_c correction, from Schoene and Bowring (2006). For isochron solutions, data are regressed to solve for the composition of Pb_c, then the data are re-reduced with the composition used for correction and plotted on the concordia diagram. For K-feldspar correction, K-feldspar was step-leached and the least radiogenic fraction was used to reduce the data. 'Bulk Earth' uses the Stacey and Kramers (1975) model at 520 Ma to perform the Pb_c correction. All uncertainties are 2σ.

In fact, in many analytical setups typical for LA-ICPMS U–Pb dating, ^{204}Pb is not measured due to the unresolvable isobaric interference from ^{204}Hg, requiring different methods of Pb_c correction (Andersen, 2002; Horstwood et al., 2003). Most of these are similar to the ^{204}Pb correction, but instead involve assuming an initial $^{207}Pb/^{206}Pb$ or $^{208}Pb/^{206}Pb$ and concordance between the U–Th systems (Williams, 1998). The former, '207 correction,' is essentially the same as fixing a $^{207}Pb/^{206}Pb$ intercept on a T–W concordia plot and regressing it through the data, and thus assumes concordance. If Pb loss and mixing are important in a dataset, then both the 208 and 207 corrections are inaccurate. Andersen (2002) presents a method of 204-absent Pb_c correction utilizing all three decay schemes that does not assume concordance, but instead must assume a time of Pb loss.

4.10.4 Measurement Techniques

There are three principal analytical methods used for U–Th–Pb geochronology: (1) ID-TIMS, (2) secondary ion mass spectrometry (SIMS), and (3) laser ablation inductively coupled plasma mass spectrometry (LA-ICPMS; Figure 8). Most modern applications of U–Th–Pb geochronology now involve either separating the minerals of interest by standard magnetic

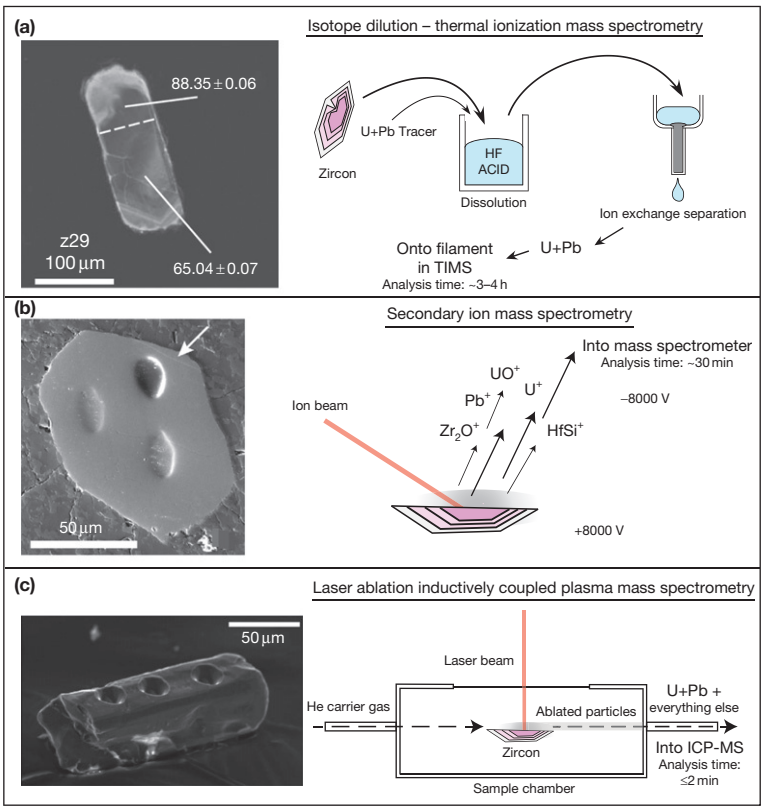

Figure 8 Cartoons depicting the three most common types of U–Th–Pb analysis. Each method shows an image of a zircon that was analyzed to illustrate sample size. Diagrams to the right illustrate how the method works. See **Section 4.10.4** of the text for more discussion. (a) Isotope dilution thermal ionization mass spectrometry (ID-TIMS). Image of microsampled zircon that was subsequently analyzed comes from Gordon et al. (2010). (b) Secondary ion mass spectrometry (SIMS). Image of zircon is from a lunar sample analyzed by Grange et al. (2011). (c) Laser ablation inductively coupled plasma mass spectrometry (LA-ICPMS). Image is from Cottle et al. (2009b).

and density techniques and dating single, carefully chosen mineral grains, or measuring grains in thin section or epoxy grain mounts using in situ techniques. Exceptions are studies involving dating low-U materials such as carbonates and meteorites, where different approaches must be taken (e.g., Connelly and Bizzarro, 2009; Rasbury and Cole, 2009). The nuts and bolts of these analytical methods and instrumentation are outlined in separate chapters of the *Treatise on Geochemistry* (see Volume 15), and so here the focus is only on those aspects that are the most important or unique to U–Pb geochronology, and the various sources of uncertainty that contribute to the precision of each technique. A more general discussion of precision and accuracy of the U–Pb method is given in **Section 4.10.5**.

Several methods for U–Th–Pb geochronology exist that do not measure both U and Pb isotopes or any isotopes at all. The zircon evaporation method, which places a zircon directly on a filament in a TIMS, measures $^{207}Pb/^{206}Pb$, and was applied widely to Archean rocks with the intention of eliminating discordance, which unfortunately cannot be tested without U measurements (Davis, 2008; Kober, 1986; Kröner and Todt, 1988; Kröner et al., 1996). Another method involves measuring U–Th–Pb elemental abundances but not isotopes. The U–Th–total Pb method, colloquially called electron microprobe U–Th–Pb dating, permits calculations of an age by measuring chemical composition on an electron microprobe (Cocherie et al., 1998; Montel et al., 1996). The limitations of this method are that one must assume concordance and no Pb_c, and the method is also restricted to minerals with enough U, Th, and Pb to be measured with adequate precision by electron microprobe (e.g., monazite). The advantage is the unrivaled spatial resolution of ~1 μm, which can be critical for resolving growth histories of polygenetic monazite (Mahan et al., 2006; Williams and Jercinovic, 2002; Williams et al., 2007).

4.10.4.1 ID-TIMS

ID-TIMS was pioneered in the 1950s by Alfred Nier and was the only tool for U–Pb geochronology for several decades. Initially, samples ranged from whole rocks to very large (many grams) aliquots of relatively pure mineral separates that were dissolved in steel vessels prior to analysis, with quoted precisions of a few percent on Pb/U ratios (**Figure 9**). Sample size has been reduced by many orders of magnitude and precision increased by a factor of 10–100, such that now some labs measure small fragments of single minerals to a precision better than 0.1% for a $^{206}Pb/^{238}U$ date (**Figures 8** and **9**). Other summaries of the ID-TIMS method applied to U–Pb geochronology can be found in Bowring et al. (2006) and Parrish and Noble (2003)

The well-documented complexity of zircon populations from single samples makes it necessary to measure single mineral grains by ID-TIMS. These are generally hand-picked under an optical microscope, though it is becoming more common to prescreen zircons via backscattered or cathodoluminescence imaging prior to analysis, as is routinely done in in situ methods. Remediation of Pb loss in zircons was accomplished for over 20 years by the air-abrasion method (Krogh, 1982b), removing the higher-U outer rims of zircons, which are often more radiation-damaged and prone to Pb loss. More recently, Pb-loss amelioration or elimination is approached through chemical abrasion (CA-TIMS; Mattinson, 2005), which selectively dissolves radiation-damaged or altered domains of zircon, regardless of their position within a grain. This method has improved considerably both the precision and accuracy of the ID-TIMS method and is discussed in **Section 4.10.5.5**.

Minerals selected for dating (±chemical abrasion) are spiked with a tracer solution (see below), dissolved in Teflon vessels in either HF or HCl, and U and Pb are ideally separated from other elements using ion exchange chemistry. This methodology has not changed since the introduction of Teflon to geochronology (Krogh, 1973), though all materials and vessels have been vastly downsized to account for smaller sample size and to reduce Pb blank (e.g., Parrish, 1987). Separating U and Pb through ion exchange chemistry serves two purposes: (1) because thermal ionization mass spectrometers are high-sensitivity, low-mass resolution instruments, potential isobaric interferences are best removed prior to analysis, and (2) other elements have a tendency to impede ionization of Pb and U on the filament, thereby reducing signal size and therefore precision.

TIMS involves placing a sample onto a metal filament (typically Re) and heating it to ionize the elements of interest, which are in turn accelerated into a magnetic sector mass spectrometer by applying an ~8000–10000 V electric potential near the filament under high vacuum (see **Chapter 15.18**). In U–Pb measurements, Pb ionizes predominantly as Pb^+ and U is measured either as the metal U^+ or as the oxide UO_2^+ species. For uranium oxide measurements, both U and Pb can be placed on the same filament in a silica gel emitter (e.g., Cameron et al., 1969; Gerstenberger and Haase, 1997) and analyzed at different temperatures. Uranium ratios must, in this case, be corrected for an assumed or measured isotope composition of oxygen (e.g., Schmitz and Bowring, 2001; Wasserburg et al., 1981). Uranium metal is analyzed by loading U onto a separate filament from Pb in a reducing substance or by using a triple-filament technique (Chen and Wasserburg, 1981; Condon et al., 2010; Hiess et al., 2012). Typical measurement times are on the order of a few hours for Pb, if measured on a single ion counter, and much faster if measured on faraday cups, though the latter is only possible with large samples (>100 pg Pb). Uranium can also be measured on an ion counter or faraday cups, but ideally the latter, given the higher precision that is possible (≥0.002% instead of ≥0.01%) for single minerals with a few nanograms of U. The high precision that is achieved by TIMS relative to other techniques is primarily a result of generating stable ion beams with relatively small and predictable mass-dependent fractionation over hours of analysis.

Isotope dilution refers to the process of spiking a sample with a known quantity of one or more tracer isotopes in order to convert ratios measured by mass spectrometry to moles of sample isotopes. A mixed U–Pb tracer is required for U–Pb measurements done by TIMS because both elements cannot be measured simultaneously during an analysis, and even if one tried to, the ionization efficiency is so different between the elements that a substantial and imprecise correction would have to be applied to account for elemental fractionation. Modern tracers for U–Pb ID-TIMS work involve some mixture of ^{205}Pb, ^{202}Pb, ^{233}U, ^{235}U, and ^{236}U. Of those isotopes, only ^{235}U is naturally occurring, making the equations used to

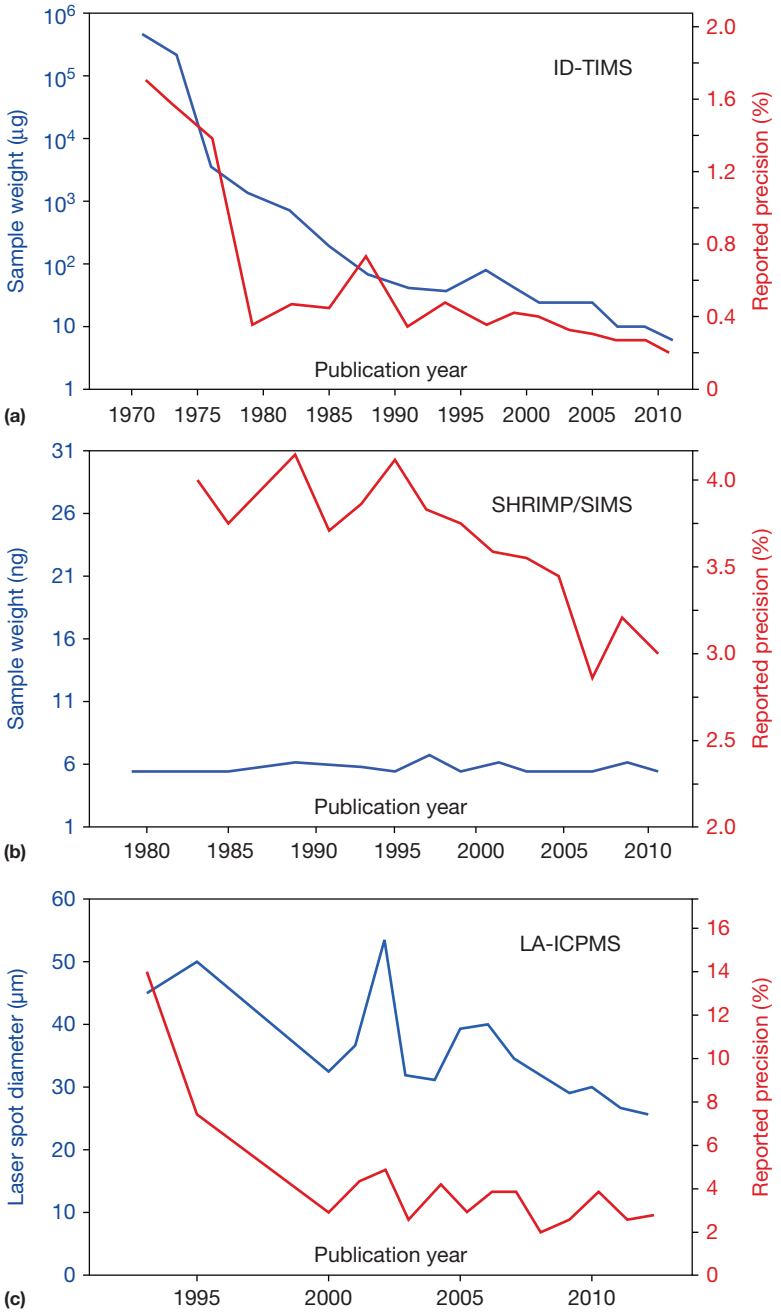

Figure 9 Plots of sample size and precision versus publication time for each method. Data were obtained by searching for the ten most cited papers for a given 1- or 2-year period and extracting the average 2σ uncertainty in $^{206}Pb/^{238}U$ dates or ratios for single analyses (not weighted means), then taking the average of the ten papers. Conspicuous outliers were excluded from the analysis if the data were anomalously imprecise or if the sample size was anomalously large, but not for the opposite cases. Thus, data are biased toward higher precision and smaller sample size (to emphasize state of the art). Sample weight is given for ID-TIMS and SHRIMP/SIMS, but not LA-ICPMS because spot depths are not consistently reported. All uncertainties are 2σ.

calculate moles of, for example, ^{206}Pb in the sample fairly simple:

$$\left(\frac{^{206}Pb}{^{205}Pb}\right)_{measured} = \left(\frac{^{206}Pb_{sample} + {}^{206}Pb_{blank} + {}^{206}Pb_{tracer}}{^{205}Pb_{tracer}}\right) \quad [12]$$

where $(^{206}Pb/^{205}Pb)_{measured}$ is already corrected for mass-dependent isotope fractionation during analysis, $^{206}Pb_{tracer}$ and $^{205}Pb_{tracer}$ are known, and $^{206}Pb_{blank}$ can be estimated from the amount of ^{204}Pb measured relative to ^{205}Pb and the $^{206}Pb/^{204}Pb$ of the blank. In minerals that contain initial Pb_c, this equation becomes slightly more complicated given the necessity to partition the ^{204}Pb into its blank Pb_c and Pb_0 components. Thorough examinations of these algorithms have been published recently (McLean et al., 2011; Schmitz and Schoene, 2007), building on previous work (Ludwig,

1980; Roddick, 1987). The correction for mass fractionation applied to $(^{206}Pb/^{205}Pb)_{measured}$ and all other Pb ratios is typically done either by (1) regularly measuring a standard of known composition and calculating the mean and variability of its mass fractionation, then applying the same correction to samples; or (2) using double spikes, where the ratio of two spike isotopes are known and can be used to calculate mass fractionation during each analysis. In the second case, ^{202}Pb and ^{205}Pb can be used (Amelin and Davis, 2006; Parrish and Krogh, 1987; Roddick et al., 1987; Schoene et al., 2010a; Todt et al., 1996) and ^{233}U and ^{236}U, or ^{235}U can be used (Roddick et al., 1987). Using ^{235}U as the second U spike isotope requires that a U isotopic composition be assumed for the sample (though see **Section 4.10.5.2**; full equations for this correction are given in Schmitz and Schoene, 2007).

As shown in **Figure 9**, ID-TIMS U–Pb geochronology is by far the most precise analytical technique. Initial advances in precision through the 1960s and 1970s were the result of better mass spectrometry and lower Pb contamination levels (blanks). The precipitous decline in sample size and increased precision in the late 1970s may have been entirely the result of the introduction of Teflon to isotope geochemistry (Krogh, 1973). The next 20 years saw little improvement in precision but several orders of magnitude decrease in sample size as workers pushed toward single mineral analyses (Lancelot et al., 1976; Michard-Vitrac et al., 1977; Oberli et al., 1990; Parrish, 1987, 1990; Von Blanckenburg, 1992). Further emphasis on better mass spectrometry, ionization efficiency of Pb and U, and continually lower Pb blanks – to the subpicogram level – has further reduced the uncertainty in reported dates, such that average precisions reported in the past few years on single zircons are about 0.2% of the reported date, but 0.05% is routinely achieved in some labs.

Due to reproducibility of mass fractionation and the use of isotope dilution, the sources of uncertainty in ID-TIMS U–Pb dating are both identifiable and quantifiable. Recent efforts to redraw data reduction and uncertainty estimation have resulted in transparent and well-documented software that is freely available and amenable to numerous mass spectrometer platforms (Bowring et al., 2011; McLean et al., 2011; Schmitz and Schoene, 2007). An interesting outcome of these efforts is the ability to quantify different sources and magnitudes of uncertainty from each U–Pb analysis, thereby providing targets for further improvement. **Figure 10** illustrates the most significant sources of uncertainty to three different single zircon analyses using pie charts. The charts are constructed by comparing the magnitudes of all sources of variance that sum up to the variance of the resulting date (Schmitz and Schoene, 2007), where the variance is the standard deviation squared. For other visualization diagrams that (importantly) contain more information about sources of covariance, see McLean et al. (2011) and Bowring et al. (2011). Note that the relative variance contributions from each variable can be quite different and depend on the age, Pb* content, Pb blank, etc. A user can thus identify the largest uncertainty contributions and aim to improve them in future work, through lower Pb blanks, a better constrained Pb blank isotopic composition, or better mass spectrometry.

It is worth noting, however, that a number of these sources of uncertainty are still difficult to quantify. The isotopic

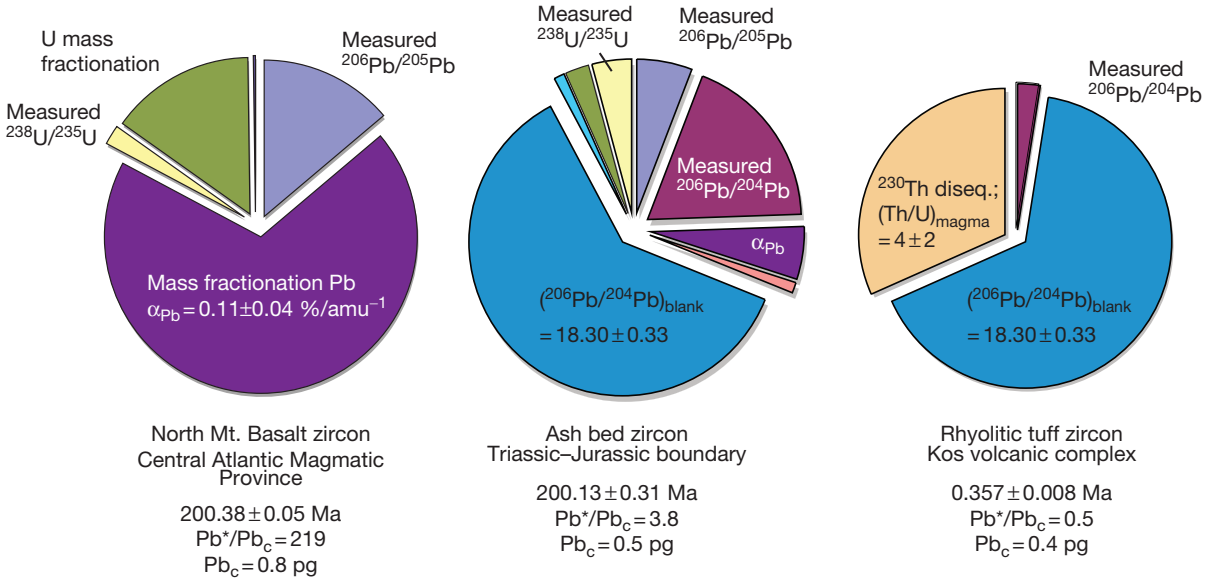

Figure 10 Pie charts illustrating the most important sources of uncertainty in ID-TIMS U–Pb analyses, and how they change as a function of age, Pb*/Pb$_c$, and Pb$_c$, and analytical precision. Dates are $^{206}Pb/^{238}U$ dates $\pm 2\sigma$ uncertainties and represent the square root of summed variances of the individual components. The two charts on the left are analyses from Schoene et al. (2010a,b), and the one on the right is from Bachmann et al. (2010). On the left chart, about 70% of the 0.05 Ma variance is derived from the variance in mass fractionation during mass spectrometry. This implies that using a double-Pb tracer will improve uncertainties drastically for this sample. In the center chart, where Pb* is very low, about 55% of the variance comes from the isotopic composition of the blank, and using a double-Pb spike will not increase precision markedly. The third chart illustrates the extreme example where correction for ^{230}Th disequilibrium contributes a significant percentage of the total uncertainty. Pie charts were generated using algorithms and modified spreadsheet from Schmitz and Schoene (2007).

composition of the Pb blank, which provides the basis for subtracting Pb_c isotopes from sample isotopes, is difficult to measure and potentially highly variable because the blank can come from many different potential sources (reagents, Re filaments, etc.). The correction for nonblank Pb_c, though not usually applicable to zircon, is also difficult to measure directly but is important for minerals with high initial Pb, such as titanite and apatite (see **Section 4.10.3.4**). Isobaric interferences such as ^{205}Tl and $BaPO_4$, though mostly removed during ion exchange chemistry prior to loading the sample onto the filament, still require careful consideration (e.g., Amelin and Davis, 2006). Pb mass fractionation during measurement is a significant source of uncertainty, especially when corrected using the mean of repeated standard measurements, as one must assign its reproducibility as an uncertainty in each measurement. The addition of a double-Pb spike, double-U spike tracer solution for isotope dilution dramatically lessens the uncertainty contribution from mass fractionation (Schoene et al., 2010a), which can reduce U–Pb and Pb–Pb date uncertainties by up to 50% for low-blank, high-Pb* analyses. Some studies using double-Pb spikes have also recognized the importance of mass-independent fractionation (e.g., Thirlwall, 2000), and though the magnitude of this effect is relatively small ($\sim$0.01% amu^{-1}), quantifying this will likely become more important in high-precision geochronology in the near future. Other targets for improved precision include lowering the Pb blank to femtogram levels, better calibration of nonspike isotopes in tracer solutions (e.g., ^{206}Pb), and improving the ionization efficiency for Pb and U.

4.10.4.2 SIMS

SIMS was developed in the 1970s as a means of measuring small domains of material for isotopic composition and elemental abundances (Andersen and Hinthorne, 1972a,b; Shimizu et al., 1978). SIMS was quickly recognized as a powerful tool for resolving dates within single zircons with complicated growth histories through U–Th–Pb geochronology (Compston et al., 1984; Hinthorne et al., 1979). The development of the sensitive high-resolution ion microprobe (SHRIMP) formed the foundation of modern SIMS U–Th–Pb geochronology (Compston et al., 1984), which remains a powerful tool to date small (<100 μm) minerals within their petrographic context and/or domains in single crystals that are revealed through various imaging techniques (see **Section 4.10.3.1**). Excellent descriptions of this technique applied to U–Th–Pb analysis are given elsewhere (Ireland and Williams, 2003; Williams, 1998), and here just the outline of the most important aspects is given.

The power of SIMS lies in its ability to ablate small-diameter spots (10–40 μm) with very shallow pit depth (<4 μm) by hitting the surface with a high-energy ion beam (typically O^- or O_2^-) under vacuum. A small portion of the liberated material forms atomic ions or molecular ionic compounds and is accelerated into a mass spectrometer (this process is called sputtering). Because ionized matter is composed of every element present in the targeted mineral, as well as their oxides and hydroxides, very high mass resolution is required to resolve potential isobaric interferences. The combination of a large-radius magnetic sector and electrostatic analyzer results in mass resolutions as high as 10 000. This allows one to distinguish between, for example, $^{206}Pb^+$ (M = 205.97) and $HfSi^+$ (M = 205.92), which is crucial for dating zircon by this method (Ireland and Williams, 2003).

Unlike TIMS geochronology, SIMS cannot use isotope dilution to calculate Pb/U. Instead, sample unknowns are analyzed in rotation with a mineral standard of known Pb/U and a correction is applied assuming that fractionation of Pb from U during sputtering is the same in both cases. Though this is generally not achievable, it was shown that Pb^+/U^+ covaries with UO^+/U^+ during an analytical session (Hinthorne et al., 1979). Because UO^+/U^+ can be measured directly, the offset of true Pb/U from sample to standard can be estimated with more confidence. Nonetheless, reproducibility requires that conditions for both standard and unknown are identical – from the flatness of the polished sample surface, to the pit size and beam intensity, to matching the matrix material (i.e., zircon standard for zircon unknown, but also matching compositions of zircons can be important; Black et al., 2004; Williams, 1998).

Reported precision on single SIMS U–Pb dates is on average $\sim$3%, which has only improved slightly in several decades of use. This lack of improvement is partly due to the inherent limitations in U/Pb fractionation during measurement and also a testament to the analytical rigor practiced by the pioneers of this method. Sputtering of analyzed material is done at very slow rates, leaving pits only a few microns deep over about 30 min of analysis time. Nonetheless, during the analysis time, elemental fractionation, coupled with compositional changes in the target mineral and standard, in addition to variable beam intensity limits the achievable precision (Ireland and Williams, 2003; Williams, 1998). Grain-to-grain reproducibility on standards over an analytical session or between sessions gives a good measure of the expected precision on unknowns (Stern and Amelin, 2003). Time-dependent averages based on standard measurement over a session can be calculated by linear or nonlinear regression and the associated uncertainties are propagated into each unknown (Ludwig, 2000b).

Analyzing secondary standards within grain mounts, whose dates should be identical relative to the primary standard over the course of an analytical session, reveals systematic offsets between different zircon standards. These are suspected to be due to 'matrix effects,' related to different Pb/U fractionation between minerals of potentially different composition (Black et al., 2003; Fletcher et al., 2010) or U-content (White and Ireland, 2012). The latter may be due to different Pb and U ionization efficiency in metamict zircon – a result of crystal lattice damage due to the decay of U (White and Ireland, 2012). This remains an important source of systematic uncertainty that has not been adequately characterized, and is difficult to propagate into the uncertainty of an unknown zircon, demonstrating the importance of having large quantities of well-characterized and homogeneous standard materials available to many labs (Black et al., 2003; Ireland and Williams, 2003; Wiedenbeck et al., 1995).

4.10.4.3 LA-ICPMS

LA-ICPMS, which involves lasing the surface of a mineral and carrying the resulting ablated aerosols into a mass spectrometer, was first applied to U–Pb geochronology in the 1990s

(Feng et al., 1993; Fryer et al., 1993; Hirata and Nesbitt, 1995). It has since become the most rapidly adopted method of U–Pb measurement because of its high spatial resolution, rapid analysis time, and affordability relative to SIMS. In fact, the explosion of U–Pb papers published since ~2003 (**Figure 1**) is probably due in large part to the advent and availability of LA-ICPMS data. Detailed coverage of the topic is beyond the scope of this chapter; reviews and recent examples of the more technical aspects of this rapidly evolving technique are given elsewhere (Arevalo et al., 2010; Cocherie and Robert, 2008; Gehrels et al., 2008; Horstwood et al., 2003; Kosler and Sylvester, 2003; Simonetti et al., 2005; Sylvester, 2008; Arevalo ToG Vo1. 15).

An LA-ICPMS system consists of two parts: (1) the laser ablation system, including the sample cell, and (2) the ICPMS. Laser ablation systems commonly used in U–Pb geochronology consist of a solid-state (e.g., Nd-YAG) or gas-source (e.g., Ar–F Excimer) laser of short wavelength (<266 nm). Detailed studies of different lasers and ablation techniques reveal that short-wavelength lasers coupled with carefully controlled pulse rates (typically on the nanosecond scale) and energy densities more efficiently ablate the tested materials with minimized heating and also reduced, more predictable elemental and isotopic fractionation (Guillong et al., 2003; Günther and Heinrich, 1999a; Günther et al., 1997). Recent advances in femtosecond-pulse-rate lasers continue to minimize elemental fractionation (Claverie et al., 2009; Garcia et al., 2008; Gonzalez et al., 2008; see **Section 4.10.5**).

The sample is ablated inside a sample cell with a laser-transparent window, and ablated particles are swept from the cell to the plasma torch by incorporation into a carrier gas. A range of carrier gases has been explored, noting that the choice of gas affects instrument sensitivity (Guillong and Heinrich, 2007; Günther and Heinrich, 1999b; Horn and Günther, 2003). As a result of these and complementary studies, most labs use He gas with or without a trace of N_2, Ar, and H. The size and geometry of the sample cell can also affect the efficiency and stability with which the particles are transported to the inductively coupled plasma (Cottle et al., 2009a; Kosler and Sylvester, 2003; Muller et al., 2009; Pisonero et al., 2006).

Several types of ICP-MS are used in laser ablation U–Th–Pb geochronology: quadrupole, single-, or multi-collector magnetic sector instruments. The latter two are increasing in popularity because of their versatility at measuring isotope ratios in many elemental systems, but reported precisions and duration of analysis (now typically less than a couple of minutes) for U–Th–Pb geochronology for each instrument are not very different. The magnetic sector instruments, however, have higher sensitivity and generally allow for smaller spot sizes in single grains (**Figure 8(c)**). ICP-MS analysis is discussed in depth in Arevelo (2012; Volume 15) of the treatise.

Multi-collector and single-collector magnetic sector or quadrupole instruments report similar uncertainties, implying that much of the uncertainty in LA-ICPMS U–Pb data comes from the complicated nature of the ablation process and/or transport to and ionization in the plasma. In particular, U and Pb fractionation at the ablation site can be quite variable and depend on (1) the depth within an ablation pit (Hergenroder, 2006; Horn et al., 2000; Kosler et al., 2005; Paton et al., 2010), (2) the process by which the laser forms aerosols, and the resulting particle size distribution (Guillong et al., 2003; Günther and Heinrich, 1999a; Günther et al., 1997), and (3) ionization in the plasma and the related complications introduced by choice of carrier gas (Guillong and Heinrich, 2007; Günther and Heinrich, 1999b; Horn and Günther, 2003).

In addition, as with SIMS, differences in ablation resulting from different matrix materials and/or compositions can result in systematic biases in U and Pb fractionation (Black et al., 2004; Kosler et al., 2005). While this effect may be expected between glasses and minerals of different matrices, a few studies document systematic biases even between zircon standards when compared to ID-TIMS dates, and this process is not yet well understood (Black et al., 2004; Gehrels et al., 2008). This assertion is substantiated by a large dataset from the Arizona Laserchron Center (**Figure 11**; G. Gehrels, personal communication). Analysis of numerous zircon standards against one primary standard (SL-1 Sri Lankan zircon) reveals that the mean of ten replicate analyses is within ~2% of the ID-TIMS age and the standard deviation of those means usually overlaps with the ID-TIMS age, as also reported by Gehrels et al. (2008). Systematic offset between different zircon standards is also observed, which Gehrels et al. (2008) attribute to matrix effects between zircon standards. The implication is that similar matrix effects may be important in zircon unknowns, and until the causes of systematic uncertainties from matrix effects are better understood, the precision on single analyses and weighted means derived from LA-ICPMS is ultimately limited by standard variability, which appears to be ~2% (Horstwood, 2008; Sylvester, 2008).

Because LA-ICPMS geochronology is being adopted so quickly by many laboratories, many different freely or commercially available software packages for data reduction and uncertainty analysis exist, in addition to other home-grown approaches (e.g., Chang et al., 2006; Gehrels et al., 2008; Horstwood, 2008; Paton et al., 2011; Petrus and Kamber, 2012; Sylvester, 2008; van Achterbergh et al., 2001). Reducing data using several common software-independent methods reveals differences in the resulting date and precision of up to several percent for the exact same analysis (Fisher et al., 2010). Recent community-driven efforts have adopted the goal of standardizing these procedures, and once transparency is achieved, further progress can be made at assessing the maximum achievable precision on U–Pb dates by LA-ICPMS. These efforts will parallel the current exploration of minimizing and/or correctly parameterizing U–Pb fractionation during LA-ICPMS analyses.

4.10.5 Precision and Accuracy of U–Th–Pb Geochronology

The previous section briefly outlined the three most widely used methods of obtaining U–Th–Pb dates and the achievable precision of each method at present. In addition to differences in spatial resolution of the different methods, the precision afforded by ID-TIMS and the in situ methods differs by 1–2 orders of magnitude (**Figures 8–11**). Furthermore, because TIMS instruments are far more stable (e.g., in terms of drift in elemental and isotopic fractionation) than LA-ICP-MS and SIMS setups and because isotope dilution ensures that ID-TIMS dates are measured relative to well-calibrated isotopic

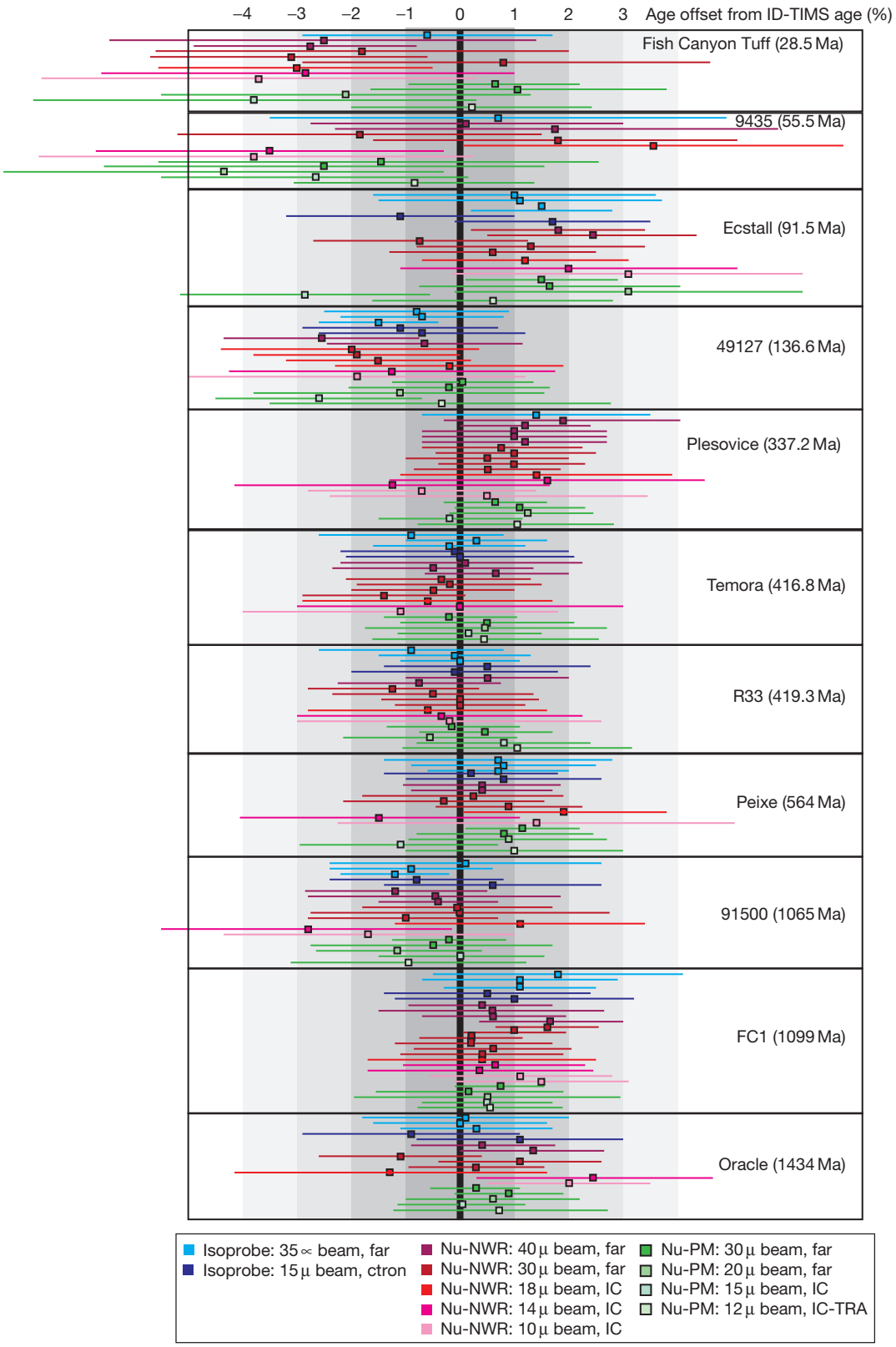

Figure 11 Comparison of $^{206}Pb/^{238}U$ LA-ICPMS ages with ID-TIMS ages for well-characterized zircons that range in age from 28 to 1434 Ma conducted in the Arizona Laserchron Center (figure courtesy of G. Gehrels, see Gehrels et al., 2008, for more details). All data are relative to the SL-1 zircon standard. Each square is the weighted mean of a set of ten LA-ICPMS measurements, and the error bars show the 2σ standard deviation of the weighted mean. No analyses were rejected. Data collected between 2006 and 2011. Isoprobe and Nu refer to the ICPMS used, and NWR and PM refer to the laser used. Far = faraday cups, ctron = channeltron, and IC = ion counters. Measurements in μ refer to spot size in μm.

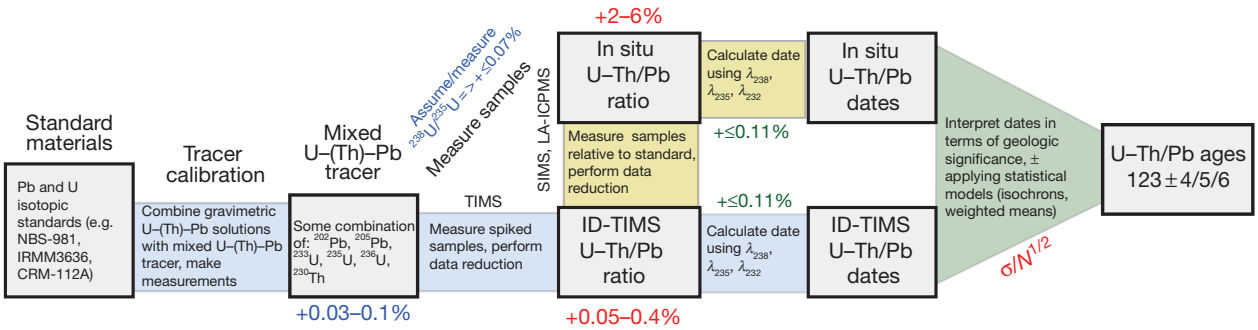

Figure 12 Simplified flow chart indicating the sources of internal (in red) and systematic (blue and green) uncertainties in U/Pb geochronology, tracking back to the standard materials used to calibrate tracers for ID-TIMS dating. Gray boxes contain either physical things or numbers and text between them describes the processes involved in getting from one box to another. $\sigma/N^{1/2}$ refers to the uncertainty reduction related to taking a weighted mean, where N is the number of analyses. The final number in the gray boxes illustrates a way of reporting uncertainties with various degrees of systematic uncertainties propagated for comparison with different types of data. See **Section 4.10.5.1** of the text for discussion. All uncertainties are 2σ.

standards, the precision and accuracy of TIMS dates are easier to quantify. For all these reasons, ages of reference standards used by the in situ techniques are calibrated by ID-TIMS (Figure 12). Further, because an increasing number of decay constants are calibrated against U–Pb dates (Nebel et al., 2011; Renne et al., 2010; Scherer et al., 2001; Selby et al., 2007), a discussion of the precision and accuracy of ID-TIMS geochronology in effect is a discussion of how well we know geologic time. Therefore, this section begins with a general discussion of the accuracy of U–Pb geochronology with an emphasis on ID-TIMS, followed by common statistical models used to interpret U–Pb dates, which is generally applicable to all methods.

4.10.5.1 Random and Systematic Uncertainties, Precision, and Accuracy

A discussion of precision and accuracy requires a few definitions that are relatively standard in isotope geochemistry. This terminology is generally consistent with that recommended by the Joint Committee for Guides in Metrology (JCGM; GUM, 2008; VIM, 2012), but here these terms are highlighted as they are used in the geochronology literature because this lexicon is derived from direct application to the problems faced by geochronologists. For a recent discussion on the application of the Guide to the expression of Uncertainty in Measurement (GUM, 2008) to isotope measurements, the reader is referred to Potts (2012) and Bürger et al. (2010). Here, random uncertainties are those that arise from random effects during measurement. One example is raw isotope ratios measured by mass spectrometry, before mass fractionation and other corrections have been made. Sometimes known as 'internal,' random uncertainties can be improved by making more measurements. Systematic uncertainty components vary predictably or remain constant no matter how many measurements are taken. Examples include uncertainties in the tracer isotope composition for TIMS, decay constants, or compositions of age standards. These are sometimes called 'external' uncertainties.

It is now common to report U/Pb ages with various levels of systematic uncertainties included, for example as a $^{206}Pb/^{238}U$ date of $123 \pm 4/5/6$, where 4 is the internal or random uncertainty, 5 is the uncertainty including the tracer calibration or standard age, and 6 is the uncertainty including decay constant uncertainties (Figure 12). When comparing $^{206}Pb/^{238}U$ dates generated from the same lab with the same tracer solution or primary age standard (assuming it's homogeneous), one should use 123 ± 4. When comparing to another $^{206}Pb/^{238}U$ date determined using a different tracer solution or age standard, 123 ± 5 is appropriate. When comparing to another dating method, such as $^{40}Ar/^{39}Ar$, 123 ± 6 would be the appropriate date to use.

Here the standard distinction between precision and accuracy is used: precision is a reflection of the reproducibility of an experiment, for example, the consistency of isotopic ratios measured from a single analysis on a mass spectrometer or calculated/derived precision through a weighted mean of numerous analyses; accuracy is a qualitative estimate of how well the mean and quoted uncertainty overlap the 'true value.' (Note that this definition of accuracy, though widely used in the geochronology literature, is slightly different than that recommended by the International Vocabulary of Metrology (VIM, 2012). In that terminology, accuracy is also affected by the precision of the measurement – i.e., a more precise estimate that overlaps with the true value is also more accurate than a less precise one. The standard use of accuracy in geochronology makes no reference to whether or not the measurement or date is precise, but simply whether it agrees with the true value – this definition more closely resembles what VIM (2012) refers to as 'trueness.') Precision is easier to measure than accuracy, because the latter involves both how well the quoted ratio or date reflects that of the sample (which is usually unknown for geologic studies) and how one interprets the data in terms of its geologic significance. The quoted uncertainties on dates of each method discussed earlier and shown in **Figure 9** are largely a gauge of the precision of the method. Whether those dates are actually accurate within that quoted precision is a separate issue, and is best addressed by measurement of similarly behaving standards. The example of a secondary standard was given for the in situ techniques as a means of deriving the correct precision for each analysis, but also helps address the accuracy. This leads to a final but important point, and that is the distinction between *dates* and *ages*. It is common to use the term *date* to reflect a number derived from solving eqns [6]–[8] for t, time. A date has no geologic significance until it is interpreted in terms of a process, at which point it becomes an age.

An *age* is therefore an interpretation of a date, or set of dates, and these interpretations are discussed further later in the chapter. Examples of ages that will arise are crystallization ages, eruption ages, cooling ages, etc. Both dates and ages can be precise or imprecise, accurate or inaccurate.

4.10.5.2 Isotopic Composition of Natural U

The $^{238}U/^{235}U$ of natural uranium in most terrestrial materials has been assumed to be constant and equal to 137.88 for 30 years. This value was adopted by Steiger and Jäger (1977), citing measurements from Cowan and Adler (1976) from a variety of uranium ore deposits. Recently, deviation of $^{238}U/^{235}U = 137.88$ of up to ~1‰ has been observed in low-temperature environments and crustal rocks, which may be the result of temperature-dependent mass fractionation, kinetic effects, or redox-sensitive partitioning (Bopp et al., 2009; Brennecka et al., 2011; Stirling et al., 2007; Weyer et al., 2008). Excess ^{235}U, measured in refractory inclusions in chondritic meteorites, has been attributed to decay of the short-lived nuclide ^{247}Cm in the early solar system (Brennecka et al., 2010).

Recent efforts in the ID-TIMS U–Pb dating community have been directed at determining the natural composition of U with reference to quantifiable SI units (e.g., kilogram, Becquerel, seconds). Directly applicable to U–Pb geochronology of crustal processes, Hiess et al. (2012) measured $^{238}U/^{235}U$ in zircon, titanite, monazite, apatite, xenotime, baddeleyite, and uraninite, relative to a ^{233}U–^{236}U tracer solution that was well calibrated gravimetrically (Condon et al., 2010; Richter et al., 2008). They found variability within these minerals of ≤1‰, and suggested that a value of 137.818 ± 0.045 be adopted for use in zircon geochronology.

The value of $^{238}U/^{235}U$ appears in several places during the calculation of an age. Most notable is its importance in the Pb–Pb age equation (eqn [9]), but this assumed value is also often used during mass spectrometry to correct for mass-dependent fractionation, for example during TIMS analyses with a ^{233}U–^{235}U tracer (see **Section 4.10.4.1**). Some analysts using low-precision dating techniques (see **Section 4.10.4**) or doing isotope dilution with a ^{233}U–^{236}U tracer do not even measure ^{235}U during mass spectrometry because of its low abundance, and thus assume a $^{238}U/^{235}U$ value of 137.88 to calculate $^{207}Pb/^{235}U$ dates. Adoption of a new $^{238}U/^{235}U$ value of ~137.82 could shift $^{206}Pb/^{238}U$ dates by as much as 0.03% for young samples, but is unimportant for old samples; $^{207}Pb/^{235}U$ dates can shift by as much as 0.07% for young samples and as little as 0.01% for samples >4 Ga (Hiess et al., 2012). Importantly, the ^{207}Pb–^{206}Pb dates from meteorites, used to calculate the age of the solar system and Earth, have been measured independently as well, resulting in Pb–Pb date increases by up to 1.4 Ma (Amelin et al., 2010).

4.10.5.3 U and Th Decay Constants

The uncertainties in decay constants are an important source of systematic uncertainty that affects the accuracy of U–Pb dates in absolute time, and also limits the precision to which U–Pb dates can be compared to dates from other radioisotopic systems. The uranium decay constants recommended for use by Steiger and Jäger (1977) were determined by Jaffey et al. (1971) by alpha counting methods on separate aliquots of enriched ^{235}U and ^{238}U, and were given 2σ uncertainties of ±0.137 and ±0.107%, respectively. These are by far the most precisely determined decay constants used in geochronology. Additionally, the accuracy of these numbers has been verified indirectly by U–Pb geochronology of closed-system minerals (Mattinson, 2000, 2010; Schoene et al., 2006). This can be done if a set of analyses are statistically equivalent in concordia space and the mineral remained a closed system. By using minerals with negligible Pb_c, eqns [6] and [7] can be solved for t and set equal to one another, and rearranged to

$$\frac{\lambda_{235}}{\lambda_{238}} = \frac{\ln\left(\frac{^{207}Pb^*}{^{235}U} + 1\right)}{\ln\left(\frac{^{206}Pb}{^{238}U} + 1\right)} \quad [13]$$

Equation [13] shows that minerals with very different ages should all give the same solution for the *ratio* of the uranium decay constants if the analyses are truly concordant (Mattinson, 2000), and that this ratio can be calculated with very high precision using multiple analyses. Such exercises have shown that this ratio is correct to within the $\pm 2\sigma$ uncertainty quoted by Jaffey et al. (1971), but that systematic discordance in the U–Pb system of about 0.3% exists within analyses spanning >3 Ga, suggesting that one or both of the mean values of the uranium decay constants are inaccurate (**Figure 13**). Though the alpha counting data for ^{238}U from Jaffey et al. (1971) appear more robust at face value, it is impossible to determine whether the inaccuracy exists in one or both of the decay constants. Nonetheless, these studies use λ_{238} to calculate a new λ_{235}, such that $^{207}Pb/^{235}U$ dates can be compared directly to $^{206}Pb/^{238}U$ dates without propagating decay constant uncertainties, though each of these studies cautions against its use given other outstanding sources of uncertainty (Mattinson, 2000, 2010; Schoene et al., 2006). For example, as discussed by Mattinson (2010), the calculated λ_{235} is also dependent on the assumed value of $^{238}U/^{235}U = 137.88$. Using the value of 137.818 ± 0.045 suggested by Hiess et al. (2012) would change the calculated λ_{235} by ~0.03%, though, as discussed in that paper (**Figure 13**), a single study with full traceability to SI units needs to be carried out before new values of λ_{235} are adopted for use in geochronology. Furthermore, increasing the absolute resolution of U–Pb geochronology beyond the 0.1% level and/or verification of the accuracy of the λ_{238} value from Jaffey et al. (1971) requires further counting experiments.

The ^{232}Th decay constant suggested by Steiger and Jäger (1977) has a value of 4.948×10^{-11} ($year^{-1}$) with an uncertainty of ~1%, and comes from an abstract (Le Roux and Glendenin, 1963) with minimal documentation. Sparse U–Th–Pb data are at least near a $^{208}Pb/^{232}Th$–$^{207}Pb/^{235}U$ concordia curve (e.g., Villeneuve et al., 2000), giving some support to its accuracy. Amelin and Zaitsev (2002) recalculated λ_{232} by correcting ^{208}Pb–^{232}Th apatite dates to zircon and baddeleyite $^{206}Pb/^{238}U$ dates, and obtained a value of 4.934×10^{-11} ($year^{-1}$) ±0.3%. Though some workers are using this value currently, a Th–Pb/U–Pb study with similar rigor to those cited for the U decay constants is warranted.

Regardless of the magnitude of the uncertainties of the decay constants, and until these constants are perfectly

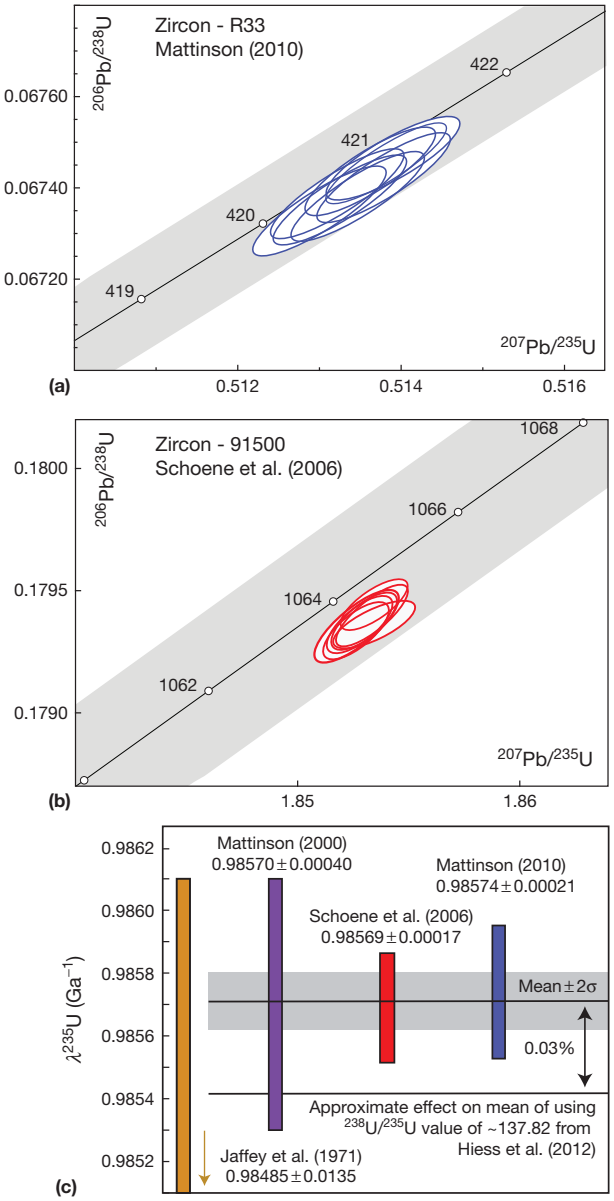

Figure 13 U decay constant uncertainties. (a) and (b) Two of the many examples presented in papers of systematic discordance in closed-system minerals using decay constants of Jaffey et al. (1971). This discordance is used to calculate a new ^{235}U decay constant, assuming an accurate ^{238}U decay constant using eqn [13] in the text. (c) Recalculated values for λ_{235}, assuming λ_{238} to be correct, from three studies with weighted mean plotted as well. Also pictured is the effect that using a natural U composition of 137.82 instead of 137.88 would have, as proposed by Hiess et al. (2012). All uncertainties are 2σ.

intercalibrated, it is important that decay constant uncertainties are considered when comparing $^{207}Pb/^{235}U$, $^{206}Pb/^{238}U$, and $^{207}Pb/^{206}Pb$ dates to each other. It is also important that, when using intercept dates and the concordia age (Ludwig, 1998, 2000a), one propagates the uncertainties in both U decay constants, because these calculations use both decay schemes (Begemann et al., 2001; Schoene et al., 2006) and thus both would change with adoption of a new ^{235}U decay constant. Also important is that studies utilizing only one decay constant need not propagate its uncertainty to calculate durations of, or intervals between, different events.

4.10.5.4 Tracer Calibration

As outlined in Section 4.10.4.1, the process of isotope dilution involves mixing a solution of known U/Pb with preferably nonnaturally occurring U and Pb isotopes with each unknown sample in order to calculate the U/Pb ratio of the sample. A U–Pb date determined by ID-TIMS is therefore no more accurate than the measured U/Pb of the tracer solution used. Because ^{202}Pb and ^{205}Pb are not available in large quantities and are difficult to obtain (Parrish and Krogh, 1987), it is impossible to mix the U/Pb tracer gravimetrically with high precision (i.e., by weighing aliquots of pure monoisotopic Pb). Instead, the tracer is calibrated against solutions of precisely determined U/Pb ratio and isotopic composition created by weighing high-purity metallic U (±Th) and Pb isotopic standards, then dissolving them together in the same acid. The tracer is preferably calibrated against multiple independently mixed gravimetric solutions (Schoene et al., 2006). Though most laboratories quote ~0.1% precision as a tracer uncertainty for home-made tracers, the methodology and data of the calibrations are not usually given. As part of the EARTHTIME initiative (www.Earth-time.org), a large aliquot of freely available mixed (^{202}Pb–)^{205}Pb–^{233}U–^{235}U tracer was mixed and calibrated with the goal of quantifying all known sources of uncertainty back to SI units. The results indicate that the limiting sources of uncertainty in tracer calibration are the isotopic composition and purity of uranium and lead isotope standards (Condon et al., 2010; Todt et al., 1996), in addition to uncertainties in mass spectrometry; these amount to ~0.03% uncertainty in a $^{206}Pb/^{238}U$ date. This is predominantly a systematic source of uncertainty, which need not be propagated into an age when compared to other U–Pb ages determined using the same tracer solution.

4.10.5.5 'Geologic' Uncertainty

As described in Section 4.10.3, mixing, Pb loss, intermediate daughter product disequilibrium, and incorrect Pb_c subtraction are all ways of jeopardizing the accuracy of a U–Pb date if not corrected for or interpreted correctly. These 'geologic' phenomena can act as either random or systematic uncertainties on a given sample or dataset. For example, a set of minerals with ubiquitous inherited cores that go unrecognized will bias each analysis, so that calculated dates are too old. Unremediated Pb loss will bias ages in the opposite direction; although each grain will be too young by a different amount, the net effect is a systematic bias toward younger dates. As described in Section 4.10.3.1, grain polishing and imaging prior to analysis by in situ methods is a common way to avoid systematic bias by inheritance. However, recent work documenting the timescales of mineral growth in magmatic systems shows that it may be common for minerals with high closure temperatures (e.g., zircon, monazite, and allanite) to grow over tens of thousands to millions of years without obvious textural evidence (Bachmann et al., 2007; Miller

et al., 2007; Schaltegger et al., 2009; Schmitt et al., 2010, 2011). Such extended growth periods can present subtle but important uncertainty in age interpretations if the goal is, for example, to date the timing of eruption of an ash bed or intrusion of a magma. This problem is an important source of systematic error when taking weighted means of many dates, which will be discussed in **Section 4.10.5.6**.

Accessing domains of closed-system zircon that has not undergone Pb loss was revolutionized by Mattinson (2005) with the advent of 'chemical abrasion' (CA)-ID-TIMS (**Figure 14**). This method involves annealing zircons prior to partial dissolution in HF acid to preferentially remove high-U, discordant domains of zircon (**Figure 14(a)** and **14(b)**). The resulting residue is then rinsed, spiked with a U/Pb tracer, and analyzed by TIMS. The original work of Mattinson (2005) involved a step-leaching technique on large aliquots of zircon in order to show that after a few leaching steps, the dates measured in the leachate reach a plateau and effectively represent closed-system zircon (**Figure 14(c)**). In order to adapt this method to single-grain zircon ID-TIMS work, Mundil et al. (2004) performed an aggressive 12-hour leaching step on single zircons following annealing (**Figure 14(a)**). This method has been adopted by most ID-TIMS U–Pb labs, and has all but replaced the air-abrasion method of Krogh (1973) after 30 years of uncontested service.

During those three decades, several studies examining leaching of metamict zircon were carried out, but without the annealing step they were unsuccessful and even induced open-system behavior, such as fractionation of ^{207}Pb from ^{206}Pb (Chen et al., 2002; Davis and Krogh, 2000; Krogh and Davis, 1975; Mattinson, 1994). CA-TIMS has made ultrahigh-precision Pb–Pb dating of concordant zircons possible in Archean terranes, where Pb loss is both ubiquitous and obvious (Das and Davis, 2010; Schoene and Bowring, 2007, 2010; Schoene et al., 2008), but has also instilled greater confidence in U–Pb dates in Phanerozoic samples where a Pb loss trajectory is masked because it parallels concordia. Studies spanning the CA-TIMS revolution provide stunning comparisons of air-abraded and chemically abraded zircon, with the latter

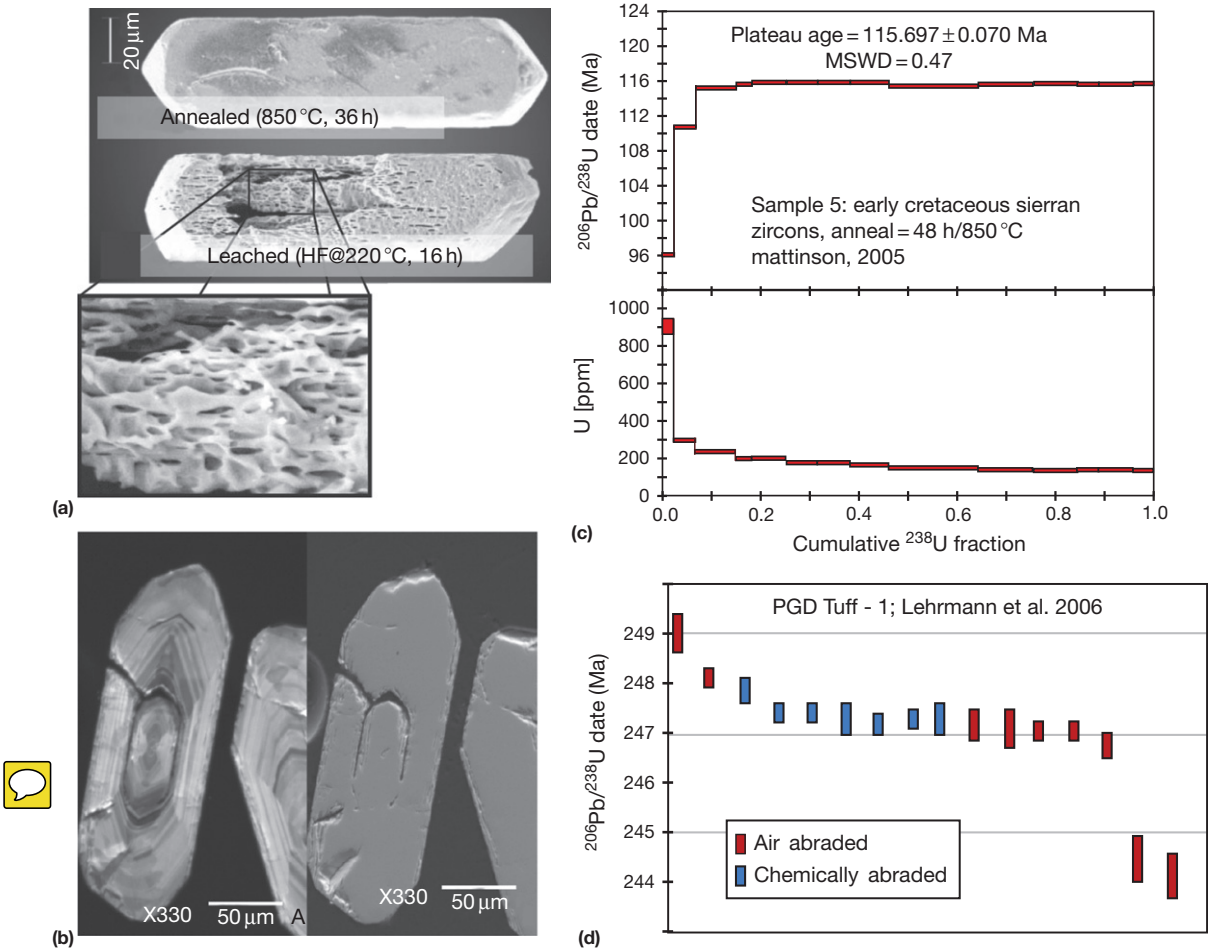

Figure 14 Chemical abrasion ID-TIMS (CA-TIMS) and its effect on zircon discordance. (a) Scanning electron microscope images of a zircon that was annealed and leached in HF overnight. Note preferential, nonsystematic dissolution of discordant domains within the crystal (from Mundil et al., 2004). (b) A cathodoluminescence image of a zircon following chemical abrasion, which shows that the HF was able to burrow into a grain and preferentially dissolve a high-U domain (Mundil et al., 2004). (c) An example of the step-leaching procedure used by Mattinson (2005) to develop the CA-TIMS method. Each cumulative ^{238}U fraction (*x*-axis) is leachate removed from the residue after a short leaching step. Note the initial discordance that is followed by many steps of equivalent-aged analyses, implying concordance. (d) A typical example of single-stage CA-TIMS from Lehrmann et al. (2006), showing air-abraded grains with substantial Pb loss versus chemically abraded grains that are more uniform in age. All uncertainties are 2σ.

consistently yielding older dates that are more likely to produce homogeneous clusters with a single $^{206}Pb/^{238}U$ date (Bowring et al., 2007; Mundil et al., 2004; Ovtcharova et al., 2006; Ramezani et al., 2007; Schoene and Bowring, 2006; **Figure 14(d)**). However, the technique is not perfect, especially when small sample size requires selection of imperfect (cloudy, cracked, magnetic, etc.) zircons for analysis, or in very metamict zircon (Das and Davis, 2010; Schoene et al., 2008, 2010a). Attempts to extend CA-TIMS to other minerals such as baddeleyite and monazite have not yet been as successful at remediating open-system behavior but have revealed interesting characteristics of these minerals during annealing and partial dissolution (Peterman et al., 2012; Rioux et al., 2010). Given the looming possibility that subtle residual Pb loss may remain in some zircon populations following CA-TIMS, open-system behavior in the form of Pb loss and prolonged zircon growth remain important sources of inaccuracy in U–Pb geochronology. Because of the different strengths of the three analytical techniques outlined earlier, understanding age information from minerals with complicated growth histories or subsequent Pb loss can be aided by using both high spatial resolution and high-precision techniques on the same grains.

4.10.5.6 Statistical Models

The previous discussion has focused entirely on the precision and accuracy of single dates arising from ID-TIMS, SIMS, and LA-ICPMS U–Pb geochronology. It is common, however, to pool many analyses from a single sample and apply statistical models to (1) increase the precision of an age interpretation, and (2) account for analytical scatter in the dataset. The two most commonly used statistical models in geochronology are the least-squares linear fit, such as an isochron, and a weighted mean. Both 2D and 3D isochrons are used in U–Pb geochronology and the assumptions they require are listed in **Section 4.10.2.3.1**. Assuming that it is geologically reasonable for these assumptions to be met, the accuracy of the age obtained from linear regression is typically evaluated by the goodness of fit. Of particular importance in isotopic data is that linear regressions can account both for the uncertainties in x and y variables, but also for the covariance of those uncertainties, as these variables are usually ratios with common numerators or denominators. A successful and widely used approach to this problem was presented by York (1967, 1968), and is commonly called the York fit. Variations and improvements on this method have been published (e.g., Brooks et al., 1972; Ludwig, 1991, 1998; York et al., 2004), and freeware exists for performing such calculations on a number of different types of geochronologic data (the most important and versatile being ISOPLOT; Ludwig, 1991).

In addition to estimates of the slopes and intercepts provided by these methods, it is critical in geochronology to evaluate the goodness of fit of the data to the statistical model, in this case a straight line. Geochronologists typically use the mean square of weighted deviates (MSWD), first introduced by York (1967, 1968), which is a variation on the common χ^2 statistic but which accounts for the degrees of freedom of the regression. A dataset that matches the statistical model gives an MSWD of 1, indicating that the scatter around the best-fit line is consistent with the uncertainties assigned to the data. An MSWD $\gg 1$ means the data scatter too much given the reported uncertainties, which can often be seen visually when the best-fit line lies far from the uncertainty envelopes, or 'error bars,' around the data. For an isochron, this means that one or more of the assumptions in **Section 4.10.2.3.1** has not been met.

An MSWD $\ll 1$ indicates that the uncertainties on the individual data are larger than expected given their observed scatter, which is seen on a plot where the best-fit line falls suspiciously close to the mean of each data point that has relatively large uncertainties. A very low MSWD may result from inappropriate propagation of systematic uncertainties into individual data points. Though it may appear to be a conservative approach to overestimate uncertainties, doing so can mask real systematic geologic uncertainty, and this, in turn, can bias a linear regression toward steeper or shallower slopes (and therefore different ages). An argument describing the acceptable distribution of MSWDs for a given number of data points used to fit a line is made by Wendt and Carl (1991), and is given by the following simple equation:

$$\sigma_{\mathrm{MSWD}} = \sqrt{\frac{2}{(N-2)}} \qquad [14]$$

Though this model is not rigorously adhered to in the literature, it provides an important guide for those wishing to better understand the distribution of their data in the hope of more accurately determining uncertainties and geologic interpretations.

In modern U–Pb geochronology, the weighted mean is the statistical model most often applied to a set of individual analyses, and the result is often interpreted as the best estimate of the age of a sample. The underlying assumption in weighted mean calculations is that the data represent a single value and that the variance of the means is due entirely to analytical scatter. As with the York fit, the uncertainties of individual data are weighted by the inverse of their variance, so those data with larger uncertainties have less weight (though see McLean et al. (2011) for an approach that accounts for systematic uncertainty, and can result in negative weights!). The result is the best estimate of that true value given the dispersion in the means and their associated uncertainties. Again, an MSWD can be calculated to assess whether the data do in fact meet the model prediction (though eqn [14] should be modified so the denominator reads $N - 1$.). This can be visually estimated by simply seeing whether a set of data points overlap within their 2σ uncertainties. A common tool to do so, colloquially called the 'weighted mean plot,' plots on one axis a date or ratio and successive analyses are lined up on the other axis (**Figure 15**).

A weighted mean functions much like the standard error in that it asks the question: how well do we know the mean? As such, the uncertainties in the estimate of the mean are reduced by $1/N^{1/2}$ (if the data have comparable uncertainties), meaning the more data you have, the better you know the mean of those data. It is thus a way to increase the precision of an age interpretation when the individual dates have larger uncertainties. Use of the weighted mean can, however, result in inaccurate ages if the mean of the samples does not reflect the (instantaneous) process that is being dated. Assuming that the petrogenetic origin of the dated minerals is accurately

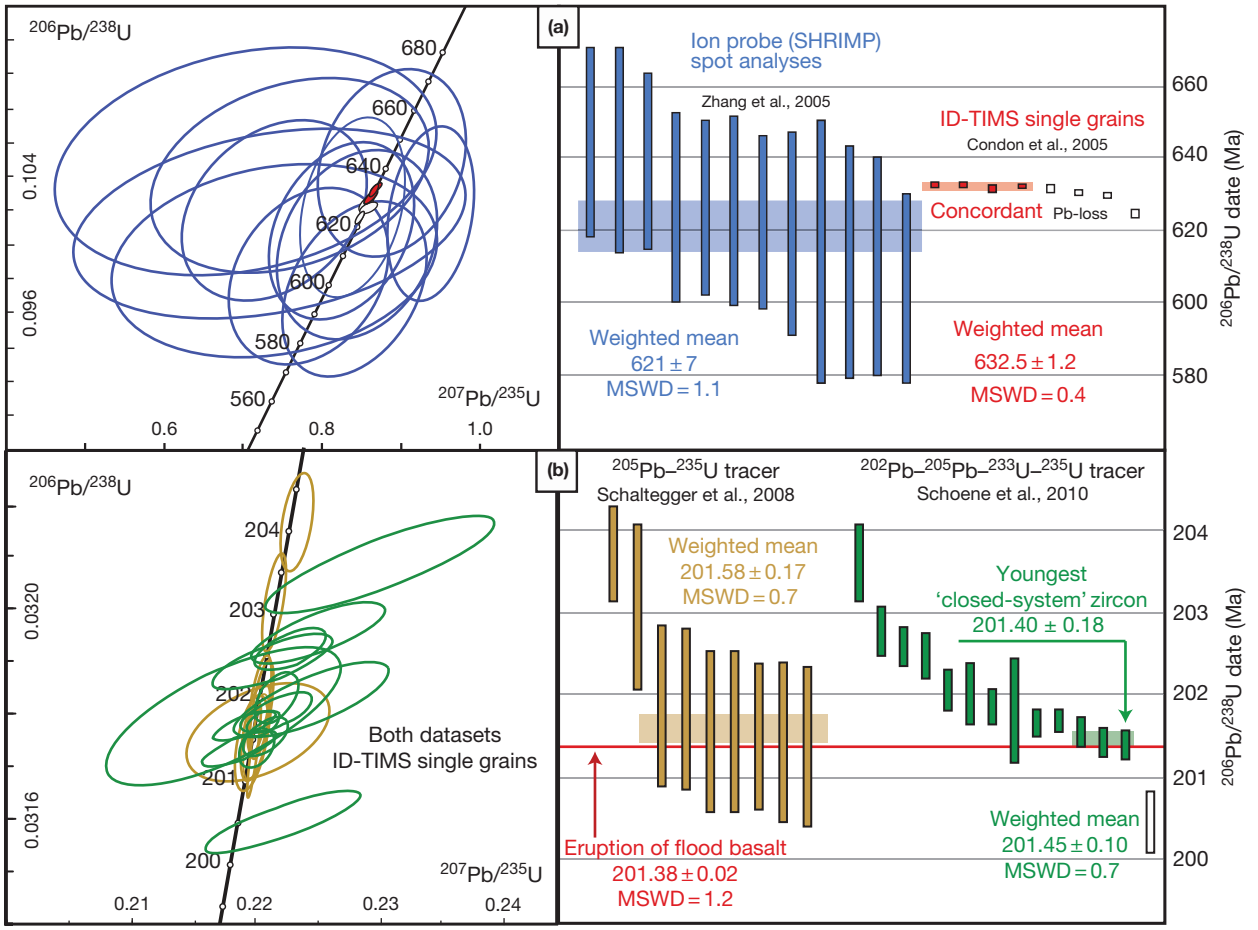

Figure 15 Examples of lower- versus higher-precision datasets on the exact same tuff samples. (a) SHRIMP analyses compared to ID-TIMS analyses, showing that large uncertainties from the SHRIMP likely mask small amounts of Pb loss, leading to a weighted-mean date that is statistically robust, but too young. (b) Lower-precision ID-TIMS data versus higher-precision ID-TIMS data from the same rhyolitic tuff, located just below the Triassic–Jurassic boundary. The lower-precision dataset likely hides pre-eruptive zircon growth, leading to a weighted-mean date that is biased slightly older, and does not overlap with the eruption of the flood basalt (also dated by ID-TIMS). The higher-precision dataset excludes older analyses and does overlap with the age of volcanism. All uncertainties are 2σ.

interpreted, an inaccurate age can result from a weighted mean with a statistically significant MSWD if a set of minerals is subject to 'geologic uncertainty' (e.g., Pb loss or mixing) whose effect is small relative to the uncertainties of individual data points. This is extremely important, and so two examples are given in **Figure 15**.

Pitfalls in interpreting weighted means are most easily illustrated by comparing low-precision datasets with high-precision datasets from the same sample. **Figure 15(a)** compares data from in situ U–Pb zircon geochronology by SHRIMP (Zhang et al., 2005) and whole-grain zircon ID-TIMS dating (Condon et al., 2005). The sample is a volcanic ash bed from the Neoproterozoic Duoshantuo Formation, which postdates the global Marinoan glaciation event. High-precision ID-TIMS data were obtained prior to the advent of chemical abrasion (**Section 4.10.5.5**) and exhibit a modest spread in dates, which the authors interpret as Pb loss. As such, they calculate a weighted mean date from the oldest homogeneous population of zircons, whose uncertainty in **Figure 15(a)** includes a tracer uncertainty of ~0.15%. The SHRIMP data show a single population of statistically indistinguishable analyses, though a weighted mean results in a $^{206}Pb/^{238}U$ age that is resolvably younger than the ID-TIMS estimate. An argument could be made that, although each individual SHRIMP analysis is accurate, the weighted mean is biased by subtle Pb loss toward a mean that is too young.

Another illustration of the complications of applying weighted means to datasets comes from an ash bed near the Triassic–Jurassic boundary (**Figure 15(b)**). In this example, the authors attempt to correlate the biostratigraphically calibrated end-Triassic mass extinction event with the onset of flood basalt volcanism in the Central Atlantic Magmatic Province (CAMP; Marzoli et al., 1999) from a section in Peru with abundant volcanic ash horizons. An initial dataset by CA-TIMS (Schaltegger et al., 2008), for a sample closest to the extinction horizon, used a $^{205}Pb–^{235}U$ tracer solution and reported a homogeneous population of zircon dates that were used to calculate a weighted mean age for the eruption of the ash bed. The calculated age is older than the very precisely dated North Mtn. Basalt – the lowermost basalt in the CAMP in North America – precluding a causal link. As discussed by Schaltegger et al. (2008), because the two ages were

determined using a different tracer solution in different labs, the potential for systematic biases existed.

A subsequent reanalysis of the ash bed using a ^{202}Pb–^{205}Pb–^{233}U–^{235}U tracer solution (Schoene et al., 2010a) results in a more precise dataset due to the reduced uncertainty related to mass fractionation during TIMS analysis. The newer dataset exhibits a substantial spread in dates that are no longer amenable to a statistically significant weighted mean age. Because these zircons were analyzed using chemical abrasion, the authors conclude that the spread is due to pre-eruptive zircon growth rather than Pb loss. Both a weighted mean of the youngest three analyses (barring one much younger grain, interpreted as Pb loss) and the youngest single-grain overlap in age with the eruption age calculated by Schaltegger et al. (2008), but the new study results in synchronicity with a redetermined age for the North Mtn. Basalt Schoene et al. (2010a) conclude that the dataset from Schaltegger et al. (2008) was subtly biased to appear too old by entrainment of pre-eruptive zircons in the volcanic ash, which are resolvable by the more precise dataset.

These two examples illustrate how the application of weighted means to both low- and high-precision datasets must be done with scrutiny. It is commonly known that the growth of high-U minerals and subsequent Pb loss or alteration can happen on timescales that are unresolvable at present by any geochronologic technique. Increasing precision in U–Pb datasets is usually met by increasing complexity in the resulting dates, and it has been shown repeatedly that arriving at high-precision ages through weighted means of many low-precision dates can be inaccurate due to unrecognized systematic bias. As such, the ultimate temporal resolution of U–Pb geochronology is limited by the precision of a single data point (Horstwood, 2008; Ludwig, 1991; Sylvester, 2008). For ID-TIMS, this precision is now similar in magnitude to the systematic uncertainties of decay constants and tracer calibration (**Figure 12**), but there is much room for improved precision with in situ methods before similar systematic uncertainties become limiting factors.

4.10.6 Applications: The Present and Future of U–Th–Pb Geochronology

4.10.6.1 Measuring Geologic Time and Earth History

Changes in the biosphere, atmosphere, hydrosphere, and the surface environment through Earth history are recorded within sedimentary rocks. Correlating disparate stratigraphic records with each other and with events in the solid Earth system requires high-precision geochronology. This is typically carried out by dating igneous minerals from volcanic tuffs that are intercalated in sedimentary strata (Tucker et al., 1990), thus providing an anchor in absolute time. These tie points also form the temporal framework of the geologic timescale (Gradstein et al., 2004). The periods, epochs and stages that comprise geologic time rely heavily on U–Pb geochronology for time constraints; the demand for absolute time and the abundance of U–Pb data dedicated toward this end are steadily increasing (Bowring and Schmitz, 2003; Bowring et al., 2006; Condon et al., 2005; Davydov et al., 2010; Furin et al., 2006; Hoffmann et al., 2004; Macdonald et al., 2010; Mazzini et al., 2010; Meyers et al., 2012; Mundil et al., 2003, 2004; Ovtcharova et al., 2006; Ramezani et al., 2007; Schaltegger et al., 2008; Schoene et al., 2010a; Smith et al., 2010).

Timescale geochronology requires the highest precision and accuracy, and therefore single-zircon ID-TIMS U–Pb dating is frequently the method of choice (Bowring and Schmitz, 2003; Bowring et al., 2006; Ireland and Williams, 2003). However, eruption ages determined by U–Pb ID-TIMS should also be subjected to considerable scrutiny. One example is the very subtle but important differences arising from increased precision and application of statistical models to ash bed zircon populations near the Triassic–Jurassic boundary discussed in **Section 4.10.5.6** and shown in **Figure 15(b)**. A further example arises from the Permian–Triassic boundary, as dated by ID-TIMS, which has yielded four different nonoverlapping ^{206}Pb/^{238}U ages in the last 14 years from the same stratigraphic section in Meishan, China: 251.4 ± 0.3 Ma (Bowring et al., 1998), >253 Ma (Mundil et al., 2001), 252.6 ± 0.2 Ma (Mundil et al., 2004), and most recently 252.17 ± 0.08 Ma (Shen et al., 2011; uncertainties do not include tracer calibration or decay constant contributions). While this evolving dataset is undoubtedly related to analytical improvements such as a switch from multigrain to single-grain analyses, application of CA-TIMS, decreased Pb blanks, and improved mass spectrometry, discrepancies may also be related to zircon selection, ash bed sample size and heterogeneity, Pb loss and inheritance in zircon populations, unresolved systematic errors biasing weighted mean calculations, and other interlaboratory biases. Interlaboratory bias is being actively addressed by the ID-TIMS community through interlaboratory calibration studies and distribution of freely available U–Pb tracer solutions to remove tracer bias (Condon et al., 2008). Recent studies carrying out high-precision comparison on homogeneous zircon populations show that agreement to better than 0.05% of the age is achievable on weighted means between multiple laboratories (Schoene et al., 2010a; Slama et al., 2008). However, for complicated datasets exhibiting considerable scatter in dates – as is becoming the norm – different geochronologists use different techniques to interpret an eruption age from a set of dates. Those who think a combination of Pb loss, inheritance, and analytical scatter are the most important sources of error extract the most statistically equivalent populations of zircons and apply weighted means (Davydov et al., 2010; Ramezani et al., 2007; Shen et al., 2011). Those who consider pre-eruptive growth of zircon as the source of the spread in dates focus on the youngest grain or subset of youngest grains from an ash bed as the best estimate of the eruption age (Meyers et al., 2012; Schmitz and Davydov, 2012; Schoene et al., 2010a). The latter approach has also been applied when significant reworking of ash material is suspected after initial eruption and deposition (Irmis et al., 2011).

How best to interpret complicated zircon populations in ash beds in the Mesozoic and Paleozoic can be aided by investigations of younger volcanic material where analytical uncertainty can be smaller relative to the observed spread in dates and significant Pb loss is not expected. Such studies using both U–Pb and U-series dating have revealed that, in some cases, all zircon in a magmatic system crystallizes in less than a few thousand years prior to eruption (Bachmann et al., 2010; Charlier and Wilson, 2010; Crowley et al., 2007; Schmitt et al., 2011),

while other tuffs contain zircon predating eruption by several hundred thousand to millions of years (Bachmann et al., 2007; Bacon and Lowenstern, 2005; Charlier et al., 2005; Claiborne et al., 2010; Schmitt et al., 2010). In all cases, it is important that a subset of zircon dates overlap with the eruption age, which may be estimated by $^{40}Ar/^{39}Ar$ or U–Th/He geochronology or may be known from historical records. It follows that in the absence of Pb loss, from a set of >10 ID-TIMS single-zircon dates from pre-Cenozoic ash beds, it is likely that the youngest one will overlap with the eruption age. Nonetheless, recent studies confirm that CA-TIMS is not 100% effective at eliminating Pb loss (Meyers et al., 2012; Schmitz and Davydov, 2012; Schoene et al., 2010a), which must be addressed by using large datasets (Shen et al., 2011) and taking advantage of the requirement that strata must get younger upward (Davydov et al., 2010; Guex et al., 2012; Meyers et al., 2012; Mundil et al., 2004; Schmitz and Davydov, 2012). Further understanding of zircon populations and increasing confidence in weighted mean calculations will come from integrating zircon textures and geochemistry with high-precision geochronology of ash bed zircons (Claiborne et al., 2010; Crowley et al., 2007; Schoene et al., 2010b, 2012).

U–Pb geochronology will undoubtedly play a large role in the further refinement of the geologic timescale (Gradstein et al., 2012). Data from the U–Pb system will be further integrated with other radioisotopic systems and results from orbital tuning (Kuiper et al., 2008; Meyers et al., 2012; Renne et al., 1998, 2010), along with bio-, chemo-, litho-, and magnetostratigraphic information, and increasingly higher-precision data will be required to address more specific hypotheses. Highlights include testing correlations between biostratigraphically calibrated mass extinction events and large igneous province eruptions, intercalibrating U–Pb data with potential Milankovitch cyclicity in orbitally tuned sections, measuring the tempo of the radiation of complex life in the early Paleozoic, and understanding the relationship between carbon cycling and glacial events. Continuing to increase precision in deposition ages for ash beds without sacrificing accuracy will require further work understanding the growth of zircon in magmatic systems and how it is transported during eruptive cycles and subsequent deposition.

4.10.6.2 Integration of Geochronology, Geochemistry, and Petrology

The accuracy of U–Th–Pb ages depends, in part, on correctly interpreting the meaning of a date, which can be aided by geochemical and/or petrographic information about the dated material. Such information provides a crucial context for generating pressure–temperature–time paths in metamorphic rocks by tying the growth of high-U accessory minerals to phase equilibria (see also **Chapter 4.7**). Geochemical and textural context can also be important for interpreting the timescales of igneous petrogenesis (see also **Chapter 4.5**). The ability of nondestructive in situ methods of U–Th–Pb geochronology has paved the way for this type of work through combining multiple analytical methods on single minerals with high spatial resolution. Integration of petrographic and geochemical data with ID-TIMS U–Th–Pb geochronology is logistically more challenging, often less direct, and more limited by sample size, but nonetheless essential if high-precision time constraints are necessary.

Though zircon zonation has served as a useful tool for deciphering metamorphic versus igneous growth histories (Corfu et al., 2003), determining its utility for tracking changing geochemical equilibria in metamorphic and igneous systems has not been straightforward. It was recognized long ago that Th/U is often higher in igneous than metamorphic zircon, and, more recently, rare earth element (REE) patterns in metamorphic zircon have been argued to be sensitive to the presence of garnet, and thus when coupled with geochronology, could fingerprint garnet growth or dissolution (Harley and Kelly, 2007; Kelly and Harley, 2005; Rubatto, 2002; Whitehouse and Platt, 2003). However, measured zircon–garnet–liquid partition coefficients are highly variable, and relatively few data documenting the effect of temperature, pressure, and bulk composition exist (Hanchar and van Westrenen, 2007; Rubatto and Hermann, 2007). Though several studies suggest that zircon REE patterns are not sensitive to magma composition (Hoskin and Ireland, 2000; Hoskin et al., 2000), other studies have argued that both REE and other trace elements vary significantly between rock types (Belousova et al., 2002, 2006; Heaman et al., 1990; Schoene et al., 2010b) and can track evolving magma composition in relative (Reid et al., 2011) or absolute (Schoene et al., 2012) time.

High-U phosphates (monazite, xenotime, and apatite) and allanite are involved in a host of metamorphic reactions (Bea and Montero, 1999; Finger et al., 1998; Spear and Pyle, 2002; Wing et al., 2003), which, when coupled with geochronology, can provide time constraints on metamorphism. SIMS U–Th–Pb dating of monazite preceded by geochemical and textural characterization has shown that monazite growth and geochemical composition are sensitive to the growth and dissolution of other high-REE minerals, such as garnet and allanite, and also to anatexis (**Figure 16(a)**; Gibson et al., 2004; Kohn and Malloy, 2004; Kohn et al., 2005; Zhu et al., 1997). ID-TIMS U–Pb dating of chemically and texturally characterized monazite, xenotime, and allanite is also feasible by removing grains from thin-section or grain mount and carrying out targeted microsampling of discreet domains (Corrie and Kohn, 2007; Hawkins and Bowring, 1997; Lanzirotti and Hanson, 1996; Romer and Siegesmund, 2003; Viskupic and Hodges, 2001). LA-ICPMS U–Th–Pb analysis of monazite is also widespread (Cottle et al., 2009a,b; Kosler et al., 2001; Paquette and Tiepolo, 2007; Willigers et al., 2002), though systematic and unexplained errors of up to 5% in monazite $^{206}Pb/^{238}U$ dates relative to ID-TIMS dates are not yet well understood (Kohn and Vervoort, 2008). U–Th–total Pb geochronology (**Section 4.10.4**) of monazite has been used to map and date geochemical zones at very high spatial resolution by measuring just elemental abundances of U, Th, and Pb (**Figure 16(d)**; Cocherie et al., 1998; Montel et al., 1996; Williams and Jercinovic, 2002). Recently, LA-ICPMS has also been applied to dating allanite (Darling et al., 2012; Gregory et al., 2007) and apatite (Chew et al., 2011), which are important in a wide range of igneous rocks and participants in numerous metamorphic reactions (Spear, 2010; Spear and Pyle, 2002).

SIMS and LA-ICPMS have been used to characterize metamorphic reactions involving titanite, which had previously been known to form multiple populations in single hand

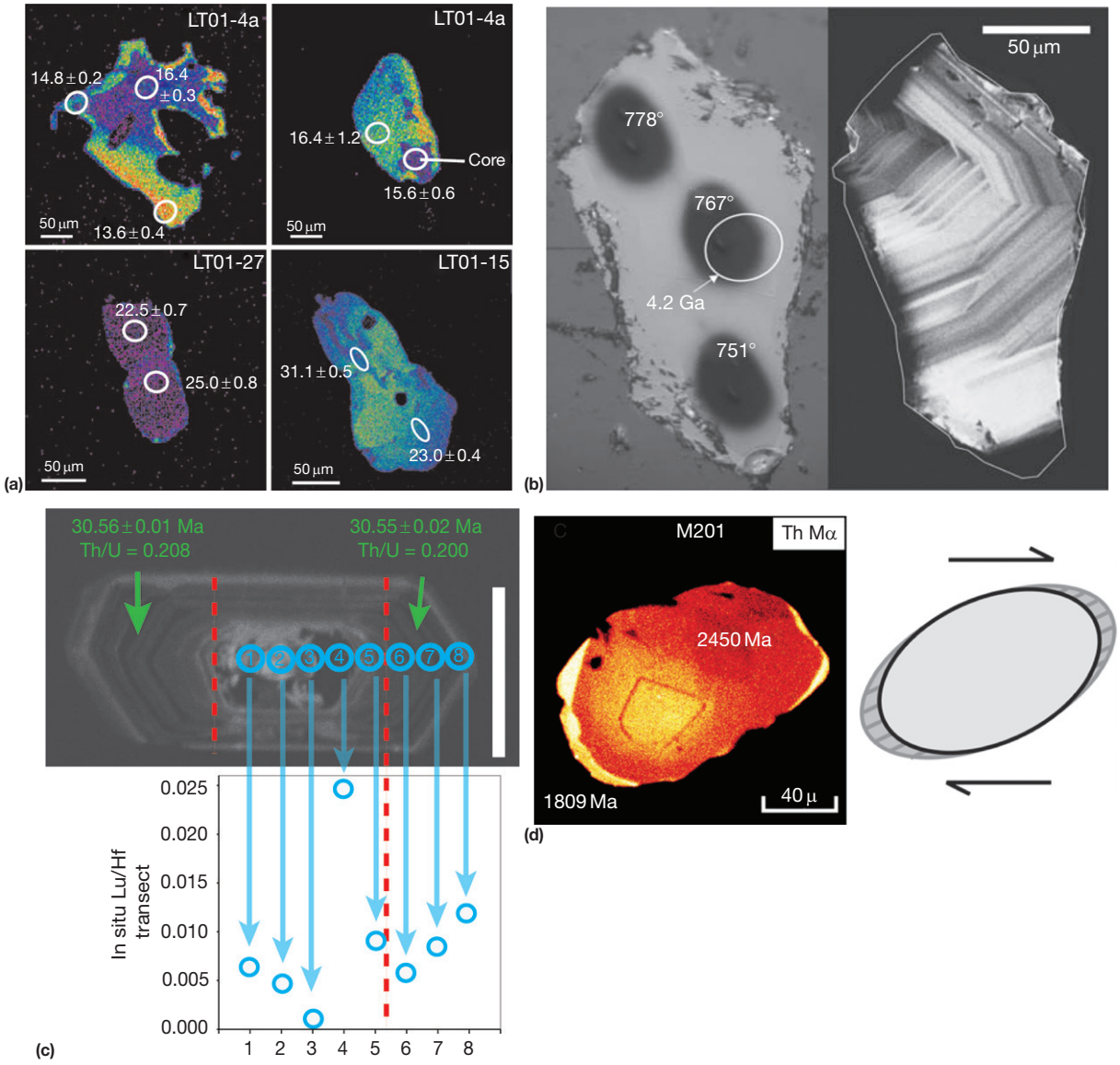

Figure 16 Combining geochronology and geochemistry. (a) Using element maps of monazite to guide SIMS ^{232}Th–^{208}Pb geochronology, from Kohn et al. (2005). Color indicates Y content, with more yellow colors indicating higher concentrations. Uncertainties are 2σ. (b) Combining Ti-in-zircon thermometry (results indicated by temperatures in °C) with in situ SIMS U–Pb geochronology, from Watson and Harrison (2005). Image on left is backscatter electron; image on right is cathodoluminescence showing igneous oscillatory zonation. (c) Electron microprobe U–Th–total Pb dating of monazite in situ, from Williams and Jercinovic (2002). Image on left is color scaled for Th content of monazite. Bright, high-Th, rim is interpreted to have formed in pressure shadows resulting from dextral shear, indicated by a cartoon on the right, constraining shearing to ~1800 Ma. (d) Example of combining in situ geochemical analysis with ID-TIMS geochronology. Blue circles on CL image show spot analyses for geochemistry determined by LA-ICPMS (J. Cottle, unpublished data), projected onto Lu/Hf graph below. Zircon was subsequently fragmented along red dashed lines and the tips were analyzed by ID-TIMS (K. Samperton, J. Crowley, M. Schmitz, and B. Schoene, unpublished data). Dates are ^{206}Pb/^{238}U, uncertainties are 2σ.

samples (Corfu and Stone, 1998; Frost et al., 2000; Verts et al., 1996). Aleinikoff et al. (2002) identified multiple generations of metamorphic titanite based on geochemistry and SIMS U–Pb analysis. Storey et al. (2007) conducted a similar study using LA-ICPMS on titanite, rutile, and apatite and argued that multiple chemically distinct zones in titanite recorded a protracted growth history.

A relatively new development is the application of mineral thermometry directly to high-U minerals. These thermometers are calibrated both empirically and experimentally and posit that the concentration of certain elements partitioned into a mineral structure is a strong function of temperature, assuming equilibrium partitioning and negligible subsequent loss or gain. An example is the Ti-in-zircon thermometer (**Figure 16(b)**; Ferry and Watson, 2007; Watson et al., 2006), which has been applied to Earth's oldest zircons as a means of understanding crustal genesis (Watson and Harrison, 2005), and also to a wide range of magmatic and metamorphic systems. This tool is most commonly applied by in situ methods because both temperature and date can be measured on the same growth zone within

single zircons. A limitation to its accuracy is that the activity of Ti in the melt must be assumed, measured, or argued to be unity, for example if cogenetic rutile is present (Ferry and Watson, 2007). Furthermore, there is evidence that Ti partitioning into zircon may be controlled by factors other than temperature, for example nonequilibrium partitioning, pressure, or magma composition (Fu et al., 2008; Hofmann et al., 2009). Other thermometers such as Zr-in-rutile (Ferry and Watson, 2007; Zack et al., 2004) and Zr-in-titanite (Hayden et al., 2008) will also be powerful tools for relating temperature to time, though these systems are more sensitive to pressure and subsequent Zr diffusion (Cherniak, 2006; Cherniak et al., 2007). Nonetheless, there is potential for combining these thermometers with U–Pb thermochronology and geochronology to elucidate high-temperature thermal histories that are inaccessible by thermochronology alone (Blackburn et al., 2012b; Meinhold, 2010).

Certainly with the number of labs now interested in conducting LA-ICPMS U–Pb geochronology on non-zircon minerals, new insight will be gained into the growth and cooling histories they record (e.g., Gao et al., 2011; Li et al., 2010; Poujol et al., 2010). Advances in this field will arise from more seamless integration of geochemical data with geochronological data from the exact same volume of analyzed material. One method recently developed is to split the aerosol stream arising from laser ablation and feed it into two ICPMSs – one for geochemical analysis and a multicollector instrument dedicated to U–Pb and Hf isotopic measurements (Yuan et al., 2008). Methods integrating ID-TIMS U–Pb measurements with trace element analysis by solution ICPMS (ID-TIMS-TEA) from the same volume of material can provide geochemical data coupled with high-precision dates (Schoene et al., 2010b, 2012), which build on previous efforts that retain aliquots containing isotopes and elements during ion separation chemistry for subsequent analysis (Amelin, 2009; Amelin et al., 1999; Crowley et al., 2006; Heaman et al., 1990; Lanzirotti and Hanson, 1996). These latter techniques emphasize the importance of integrating multiple methods – high spatial resolution with high temporal resolution (**Figure 16(d)**) – to gain a richer understanding of the geochemical, structural, and thermal history of rocks with time.

4.10.6.3 Detrital Zircon Analysis

LA-ICPMS provides a fast and affordable way to generate a huge amount of U–Pb isotopic data, which is ideal for characterizing complex detrital zircon populations (Fedo et al., 2003). Because of the availability of and excitement for detrital zircon studies, one may speculate that the sharp increase in U–Pb publications relative to other geochronologic methods shown in **Figure 1** is strongly influenced by this application. Gehrels (2011) outlines three main motivations for detrital zircon studies: (1) to characterize the provenance of sediment compared to known sources, (2) to correlate sedimentary units, assuming identical provenance, and (3) to quantify the maximum depositional age of strata in the absence of datable volcanic material.

Provenance studies have proven useful in paleogeographic reconstructions, identifying tectonically induced drainage pattern switches, placing time constraints on uplift, and fingerprinting pulses of magmatism (e.g., Bruguier et al., 1997; DeGraaff-Surpless et al., 2002; Dickinson and Gehrels, 2003;

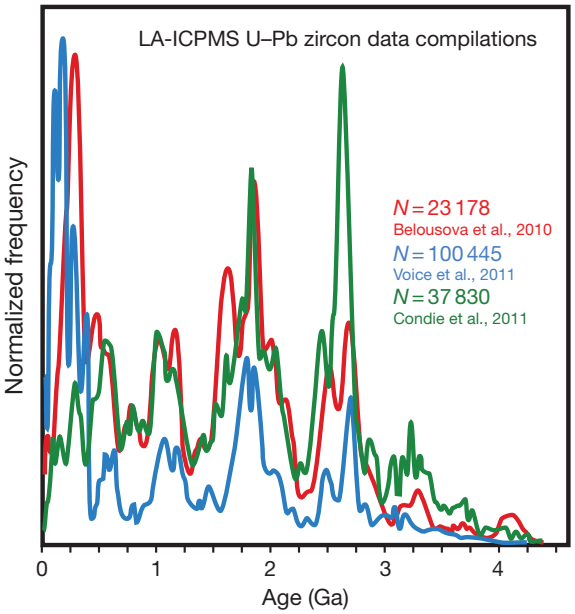

Figure 17 Summary of recent zircon LA-ICPMS U–Pb date compilations, illustrating the massive influx of such data. *N* is the number of analyses included in each compilation. Most of the data are detrital zircon data from young sediments, though several thousand from Condie et al. (2011) are orogenic granitoids of various ages. Data such as these are used to debate periodic continental growth versus preservation bias, crustal volume as a function of time, in addition to more focused studies on individual orogenic belts and sedimentary strata.

Ireland et al., 1998; LaMaskin, 2012; Rainbird et al., 1992; Stewart et al., 2001). Using detrital zircons to correlate sedimentary strata has been a powerful tool for paleogeographic reconstructions (Murphy et al., 2004) and has led to improved tectonic models for orogenic belts such as the Himalaya, where the difficulty of correlating sedimentary sequences along strike has hindered an understanding of precollision basin geometries (DiPietro and Isachsen, 2001; Gehrels et al., 2003; Long et al., 2011; Myrow et al., 2009).

In the absence of datable ash beds, detrital zircon geochronology can provide maximum ages for deposition of sedimentary strata (Robb et al., 1990), which is aided by analyzing a large number of zircons (e.g., >100) and thus is not ideally done by ID-TIMS (Dickinson and Gehrels, 2009; Hervé et al., 2003). In studies where higher-precision time constraints are required, it is possible to target the youngest zircon population, identified by LA-ICPMS or SIMS, for ID-TIMS analysis.

Despite the successes of detrital zircon analysis, several challenges still remain. There is currently no consensus on the best way to interpret detrital zircon spectra in terms of the significance of peak heights (when plotted on probability density function diagrams; **Figure 17**), differences in the relative abundances of peaks between samples in stratigraphic succession, or what statistics can be applied to spectra (Gehrels, 2011). Furthermore, several recent studies on modern sediments highlight the impact that biased provenance sampling, especially with low sampling resolution (Hietpas et al., 2011b; Moecher and Samson, 2006), and grain-size sorting during sediment transport can have on depositional age interpretations

(Hietpas et al., 2011b). As workers continue to decide how to interpret detrital zircon spectra quantitatively and apply statistical models to these data, equal effort could be applied to understanding these sources of 'geologic' bias. The addition of other detrital minerals such as monazite will also likely play a role in deciphering ages and provenance of sedimentary units (Hietpas et al., 2010, 2011a; Suzuki and Adachi, 1994; White et al., 2001).

The abundance of detrital and bedrock zircon U–Pb data produced by in situ methods, especially when coupled with isotopic tracers such as Hf and O, has also supplied new constraints on the rates and mechanisms of continental growth through Earth history (see also **Chapter 4.11**). Tens of thousands of zircon U–Pb (**Figure 17**) and Hf analyses have been used to spark debates about pulsed continental growth versus preservation bias, and growth models such as subduction versus plume-related crust production (Belousova et al., 2010; Condie et al., 2009, 2011; Dhuime et al., 2012; Hawkesworth and Kemp, 2006; Lancaster et al., 2011; Voice et al., 2011).

4.10.6.4 Lithospheric Thermal Evolution Through U–Pb Thermochronology

The U–Th–Pb system has the unique quality that several high-U minerals undergo significant diffusive loss of Pb at mid- to lower-crustal temperatures, but become retentive near Earth's surface (**Figure 18(a)**). These minerals may therefore be exploited for U–Pb thermochronology, which is based on temperature-sensitive volume diffusion of Pb through the crystal lattice. Diffusion kinetics of Pb have been determined experimentally (Cherniak, 1993; Cherniak and Watson, 2000, 2001; Cherniak et al., 1991), yielding nominal closure temperatures (T_c; Dodson, 1973, 1986) for apatite ($T_c = 450$–$550\,^{\circ}C$), rutile ($T_c = 400$–$500\,^{\circ}C$; though see Blackburn et al., 2012b, whose values are used in **Figure 18**; Schmitz and Bowring, 2003a), and titanite ($T_c = 550$–$650\,^{\circ}C$; **Figure 18(a)**). These are broadly consistent with empirical measurements and intercalibration with $^{40}Ar/^{39}Ar$ dates in hornblende ($T_c = 450$–$550\,^{\circ}C$; Harrison, 1981). The relatively high closure temperatures of these minerals make them suitable to track mid- to lower-crustal cooling and exhumation over billions of years (**Figure 18(b)**).

Early workers recognized that titanite and apatite could be robust U–Pb geochronometers (Catanzaro and Hanson, 1971; Hanson et al., 1971; Oosthuyzen and Burger, 1973; Tilton and Grunenfelder, 1968), but more widespread application of these minerals for calibrating postorogenic cooling and exhumation was not employed until much later (Corfu, 1988; Corfu et al., 1985; Mezger et al., 1989, 1991; Tucker et al., 1986). Mezger et al. (1989) recognized that rutile dates were grain size-dependent, as predicted by Dodson (1973), suggesting that volume diffusion was the primary mechanism of Pb loss in this mineral, allowing more quantitative analysis of temperature time paths in this system. Kooijman et al. (2010) measured age gradients within single rutiles by LA-ICPMS in support of volume diffusion as the Pb loss mechanism, and calculated time-dependent cooling histories of $<1\,^{\circ}C\,My^{-1}$ during post-Grenvillian stabilization in eastern Canada. Chamberlain and Bowring (2000) measured U–Pb cooling ages in apatite and titanite across several terranes in the western United States and also calculate very slow cooling rates of $<0.3\,^{\circ}C\,My^{-1}$ following ~ 1.4 Ga continental assembly. Hawkins and Bowring (1999) exploited the variation of age with grain size in titanite to extract quantitative temperature–time histories during ~ 1.6 Ga post-metamorphic cooling paths in the Grand Canyon, USA. This property was also utilized by Schoene and Bowring (2007) in both apatite and titanite from the same ~ 3.2 Ga rock in Swaziland, and they used a finite-difference forward-diffusion model to derive a unique nonlinear T–t path during exhumation from the lower to the upper crust. These studies are consistent with models for long-term structural and thermal resilience of cratonic lithosphere (Artemieva, 2011; Jordan, 1988), though rocks collected at the surface often do not capture the more recent thermal history of the middle and lower crust, required to address the importance of lithospheric reheating events (Heizler et al., 1997; Schmitz and Bowring, 2003b; Shaw et al., 2004).

In a novel application of U–Pb thermochronology, Schmitz and Bowring (2003a) determined cooling histories of rutile from lower-crustal xenoliths in the Kaapvaal craton. These data were used to calibrate the relaxation of cratonic geotherms following mid-Proterozoic thermal perturbation and subsequent Mesozoic lithospheric heating coincident with kimberlite eruption. Blackburn et al. (2011) conducted a similar study on kimberlite-borne lower crustal xenoliths from the Rocky Mountain region, USA. Using rutile U–Pb dates from three xenoliths, each representing different crustal depths, they employed a finite difference diffusion model to show that systematic discordance spanning >1 Ga is inconsistent with Pb loss from reheating events. Instead, they fit T–t paths to the rutile data to illustrate that $\leq 0.1\,^{\circ}C\,My^{-1}$ cooling in the lower crust is required and that the results fit the analytical solution for diffusive Pb loss derived by Tilton (1960, **Figure 18(c)**). A subsequent contribution coupled these and other U–Pb thermochronometric data to model extremely long-term cratonic exhumation rates of <2 m My^{-1} (Blackburn et al., 2012a).

Though U–Pb thermochronology is a powerful and underutilized tool for understanding the long-term thermal history of continents, as outlined in **Section 4.10.6.2**, the minerals titanite, apatite, and rutile can be involved in numerous metamorphic reactions, complicating their interpretation in some rocks. Additionally, there is still debate regarding the closure temperatures of rutile (Blackburn et al., 2012b; Cherniak and Watson, 2000; Schmitz and Bowring, 2003a; Vry and Baker, 2006), and examples of retention of radiogenic Pb in titanite through granulite grade metamorphic events are confounding (Kylander-Clark et al., 2008; Tucker et al., 1986).

4.10.6.5 Calibrating the Archean

There is general consensus that Earth's heat budget was higher in the Archean and that there must have been some transitional period with regard to tectonic processes following Earth's accretion to the relatively well-understood modern system. Our understanding of tectonic and magmatic processes in the Archean is hampered in part because the precision of geochronology in such old rocks is limited. In order to make robust comparisons with potential modern-day analogues for Archean terranes, it is necessary to produce time constraints relevant to the pace of plate tectonics.

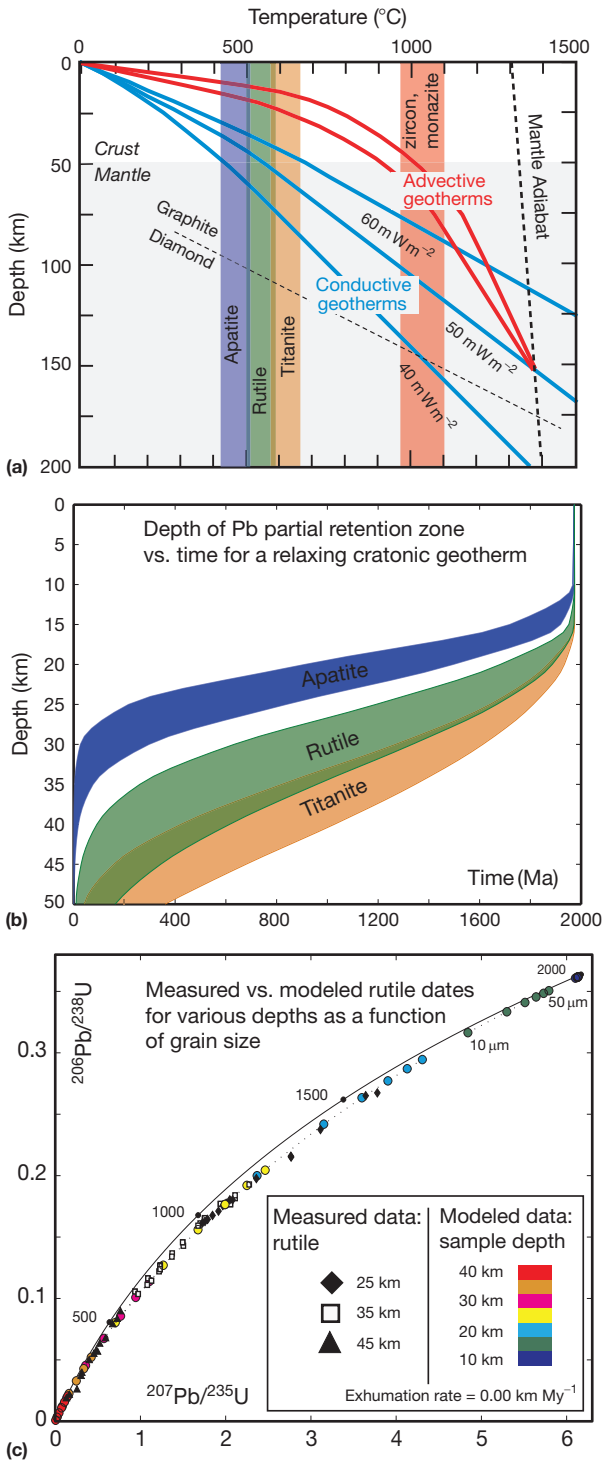

Figure 18 U–Pb thermochronology applied to craton thermal evolution. (a) Temperature versus depth through a generic cratonic lithosphere illustrating advective 'hot' geotherms compared to steady-state conductive 'cold' cratonic geotherms for different surface heat flow values (mW m^{-2}). Intersection of geotherms with mantle adiabat defines the base of the thermal lithosphere. Graphite/diamond transition shown as dotted line. Nominal closure temperatures for U–Pb thermochronometers shown as vertical colored lines (references in text). (b) An example showing how the $^{206}Pb/^{238}U$ partial retention zones (PRZ) of each thermochronometer move downward through the crust as a function of time during relaxation from a hot geotherm to a cold geotherm over 2 Ga. Limits of colored envelopes encompass the PRZ for 10–50 µm grains using diffusion kinetics cited in the text. (c) Actual rutile U–Pb data from middle to lower crustal xenoliths from Blackburn et al. (2011) compared to the results of a numerical diffusion model. Black and white symbols are measured data from samples originating from various crustal depths, and colored circles show the range of closure times for 10–50 µm grains from variable crustal depth for a conductively relaxing geotherm given no surface erosion (Blackburn et al., 2011, 2012a,b). Note the good agreement between measured rutile dates and modeled dates, which preclude significant reheating as a source of discordance of the real data. All uncertainties are 2σ.

The test of open-system behavior that is afforded by the dual decay of ^{235}U to ^{207}Pb and ^{238}U to ^{206}Pb is highly beneficial in Archean rocks because Pb loss results in a spread of data that falls far from the concordia curve. Pb loss in Archean zircons is ubiquitous, and because it is common for these minerals to also record complex polymetamorphic growth histories, single whole-grain analysis by TIMS has traditionally been difficult. Isolating the timing of multiple growth events is best done through textural imaging in grain mount or thin section, followed by U–Pb dating by SIMS or LA-ICPMS, but these analytical techniques are limited to a few percent precision. When coupled with Pb loss that may be masked by low precision, untangling the sequence of events during a single orogenic episode in the Archean is rarely possible.

The chemical-abrasion method (CA-TIMS; Mattinson, 2005; **Section 4.10.5.5**) has vastly improved our ability to resolve Pb loss by ID-TIMS in otherwise terminally discordant zircons. Leaching old radiation-damaged grains in HF frequently removes >90% of the original zircon, leaving <5 µm fragments of low-U zircon (Schoene and Bowring, 2007, 2010; Schoene et al., 2008). Analytical precision of U–Pb dates on such low-U (and therefore low-Pb) residues is, on average, 0.1–0.2%, compared to <0.1% precision of younger, higher-U zircon with greater intensity Pb ion beams. This level of precision is not ideal for age determination, but is adequate to resolve concordance in single grains. Establishing concordance for individual analyses permits use of the $^{207}Pb/^{206}Pb$ date with confidence in its accuracy, and this is by far the most precise date available for Archean rocks (Mattinson, 1987). Relatively high amounts of $^{206}Pb^*$ and $^{207}Pb^*$ in old zircons, along with modern sub-picogram Pb blanks, allows for precision in $^{207}Pb/^{206}Pb$ dates as low as 0.01% for weighted means of less than five analyses. Therefore, when analyzing zircons with relatively simple growth histories (i.e., single-stage growth), CA-TIMS analysis has the potential to resolve Archean events within 1 Ma of each other – essential when addressing typical, short-duration tectonic episodes or magmatic events.

Application of CA-TIMS with <1 Ma resolution, combined with field mapping and geochemistry, has resolved timescales of batholith construction through pulses of tonalitic to granodioritic magma during synmagmatic contraction ~3.2 Ga in the eastern Kaapvaal craton (Schoene and Bowring, 2010; Schoene et al., 2008; **Figure 19**). Furthermore, high-precision geochronology coupled with geochemistry provides a means of time-series analysis of Archean magmatic events that can be used to evaluate the geochemical *evolution* of the magmatic

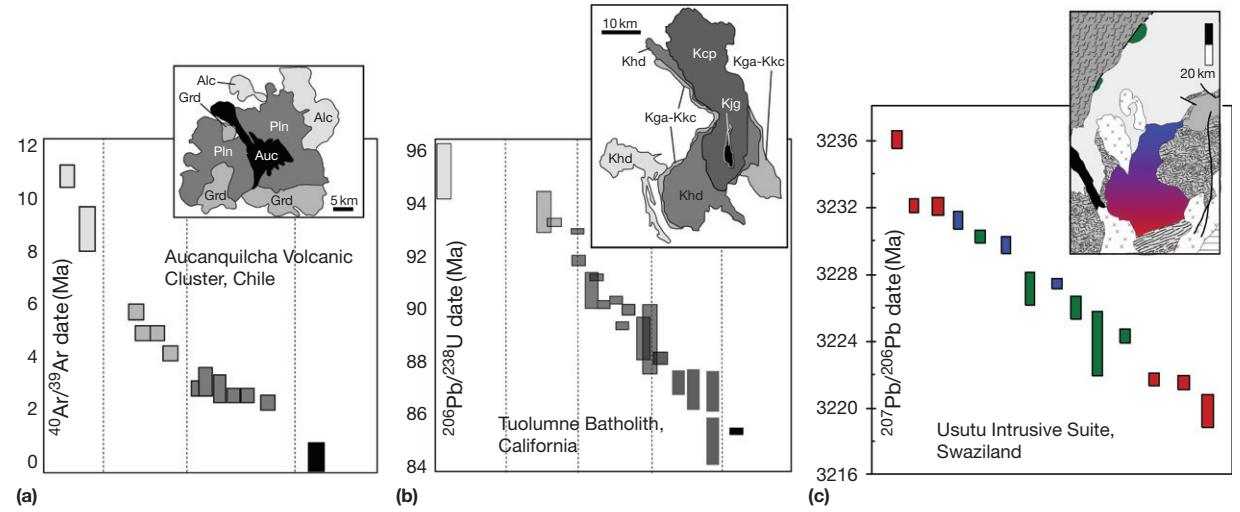

Figure 19 The longevity of magmatic systems from the Neogene to the Archean. (a) and (b) Modified from Grunder et al. (2006), with additional data inserted to panel (b). (a) $^{40}Ar/^{39}Ar$ eruption dates for extrusive units in the Aucanquilcha Volcanic Cluster, Chile, possibly in the waning stages of activity in the present, thus indicating about 11 My of magmatic history. (b) Compilation of weighted-mean $^{206}Pb/^{238}U$ zircon dates for magmatic rocks from the Tuolumne Batholith, California, from Coleman and Glazner (1997), Coleman et al. (2004), Burgess and Miller (2008), and Memeti et al. (2010), indicating assembly of the batholith over 10–12 My. Different shades of gray indicate different mapped lithologies, ranging from diorite to granodiorite. (c) $^{207}Pb/^{206}Pb$ weighted-mean dates for concordant zircons from tonalite to granodiorite samples of the Usutu Intrusive Suite, Swaziland, from Schoene and Bowring (2010). Colors correspond to geographic location on map. (a)–(c) Illustrations showing that ultra-high-precision geochronology of concordant zircons on Archean rocks approaches the resolution necessary to understand the construction of magmatic systems in the Archean, and relating these to tectonic models for Archean geodynamics. These data, when combined with geochemistry and field observations, also make for robust comparisons with younger magmatic systems, which have previously been unachievable. All uncertainties are 2σ.

system, which is critical for evaluating the tectonic process. Comparison of these data to the tempo of batholith construction observed in Mesozoic and Cenozoic arcs reveals a striking similarity (Figure 19). Further detailed analysis of the geochemical and structural evolution of Archean magmatic systems with high temporal resolution will provide a means to further test hypotheses regarding plate-tectonic versus plume-related lithospheric evolution through Earth history.

Acknowledgments

Though the (completely objective) views in this chapter are my own, I am tremendously lucky to have interacted with and learned from an amazing team of geochronologists at MIT and University of Geneva over the past dozen years. I am also extremely fortunate to have been supported and taught by a spectrum of people including the pioneers and up-and-comers in isotope geology through the EARTHTIME consortium, thoughtful paper reviews, and many fruitful international meetings. Although it is impossible to cover such a rich field of science in such a short document, I apologize for all the oversights and omissions in this chapter. R. Rudnick is thanked for both the invitation to write this chapter and her subsequent patience. Discussions with N. McLean and his comments on the manuscript are gratefully acknowledged. Very thoughtful reviews by L. Heaman and Y. Amelin are gratefully acknowledged. Data for Figure 9 was compiled with the help of M. Barboni, J. Husson, and C.B. Keller. Thanks to G. Gehrels, T. Blackburn, and M. Schmitz for providing Figures 11, 18(b), 18(c), and 18(a), respectively. This work is dedicated to my grandfather, M.A. Bayly, who passed away during its writing. He is an inspiration for those who aspire to greatness in support of their family, community, and profession.

References

Aleinikoff JN, Wintsch RP, Fanning CM, and Dorais MJ (2002) U–Pb geochronology of zircon and polygenetic titanite from the Glastonbury Complex, Connecticut, USA: An integrated SEM, EMPA, TIMS, and SHRIMP study. *Chemical Geology* 188: 125–147.

Amelin Y (2009) Sm–Nd and U–Pb systematics of single titanite grains. *Chemical Geology* 261: 53–61.

Amelin Y, Connelly J, Zartman RE, Chen JH, Gopel C, and Neymark LA (2009) Modern U–Pb chronometry of meteorites: Advancing to higher time resolution reveals new problems. *Geochimica et Cosmochimica Acta* 73: 5212–5223.

Amelin Y and Davis WJ (2006) Isotopic analysis of lead in sub-nanogram quantities by TIMS using a ^{202}Pb–^{205}Pb spike. *Journal of Analytical Atomic Spectrometry* 21: 1053–1061.

Amelin Y, Kaltenbach A, Iizuka T, et al. (2010) U–Pb chronology of the Solar System's oldest solids with variable $^{238}U/^{235}U$. *Earth and Planetary Science Letters* 300: 343–350.

Amelin Y, Lee D-C, Halliday AN, and Pidgeon RT (1999) Nature of the Earth's earliest crust from hafnium isotopes in single detrital zircons. *Nature* 399: 252–255.

Amelin Y and Zaitsev AN (2002) Precise geochronology of phoscorites and carbonatites: The critical role of U-series disequilibrium in age interpretations. *Geochimica et Cosmochimica Acta* 66: 2399–2419.

Anczkiewicz R, Oberli F, Burg JP, Villa IM, Günther D, and Meier M (2001) Timing of normal faulting along the Indus Suture in Pakistan Himalaya and a case of major $^{231}Pa/^{235}U$ initial disquilibrium in zircon. *Earth and Planetary Science Letters* 191: 101–114.

Andersen T (2002) Correction of common lead in U–Pb analyses that do not report ^{204}Pb. *Chemical Geology* 192: 59–79.

Andersen CA and Hinthorne JR (1972a) Ion microprobe mass analyzer. *Science* 175: 853–860.

Andersen CA and Hinthorne JR (1972b) U, Th, Pb and REE abundances and $^{207}Pb/^{206}Pb$ ages of individual minerals in returned lunar material by ion microprobe mass analysis. *Earth and Planetary Science Letters* 14: 195–200.

Arevalo R, Bellucci J, and McDonough WF (2010) GGR Biennial Review: Advances in laser ablation and solution ICP-MS from 2008 to 2009 with particular emphasis on sensitivity enhancements, mitigation of fractionation effects and exploration of new applications. *Geostandards and Geoanalytical Research* 34: 327–341.

Armstrong RL (1968) A model for the evolution of strontium and lead isotopes in a dynamic Earth. *Reviews of Geophysics* 6: 175–199.

Artemieva IM (2011) *The Lithosphere, An Interdisciplinary Approach*. Cambridge: Cambridge University Press.

Bachmann O, Charlier BLA, and Lowenstern JB (2007) Zircon crystallization and recycling in the magma chamber of the rhyolitic Kos Plateau Tuff (Aegean arc). *Geology* 35: 73–76.

Bachmann O, Schoene B, Schnyder C, and Spikings R (2010) The $^{40}Ar/^{39}Ar$ and U/Pb dating of young rhyolites in the Kos-Nisyros volcanic complex, Eastern Aegean Arc, Greece: Age discordance due to excess ^{40}Ar in biotite. *Geochemistry, Geophysics, Geosystems* 11: Q0AA08.

Bacon CR and Lowenstern JB (2005) Late Pleistocene granodiorite source for recycled zircon and phenocrysts in rhyodacite lava at Crater Lake, Oregon. *Earth and Planetary Science Letters* 233: 277–293.

Baker J, Bizzarro M, Wittig N, Connelly J, and Haack H (2005) Early planetesimal melting from an age of 4.5662 Gyr for differentiated meteorites. *Nature* 436: 1127–1131.

Barfod GH, Albarède F, Knoll AH, et al. (2002) New Lu–Hf and Pb–Pb age constraints on the earliest animal fossils. *Earth and Planetary Science Letters* 201: 203–212.

Barrell J (1917) Rhythms and the measurement of geologic time. *Bulletin of the Geological Society of America* 18: 745–904.

Barth S, Oberli F, and Meier M (1994) Th–Pb versus U–Pb isotope systematics in allanite from co-genetic rhyolite and granodiorite: Implications for geochronology. *Earth and Planetary Science Letters* 124: 149–159.

Bateman H (1910) Solution of a system of differential equations occurring in the theory of radioactive transformations. *Proceedings of the Cambridge Philosophical Society* 15: 423–427.

Bea F and Montero P (1999) Behavior of accessory phases and redistribution of Zr, REE, Y, Th, and U during metamorphism and partial melting of metapelites in the lower crust: An example from the Kinzigite Formation of Ivrea-Verbano, NW Italy. *Geochimica et Cosmochimica Acta* 63: 1133–1153.

Begemann F, Ludwig KR, Lugmair GW, et al. (2001) Call for an improved set of decay constants for geochronological use. *Geochimica et Cosmochimica Acta* 65: 111–121.

Belousova EA, Griffin WL, and O'Reilly SY (2006) Zircon crystal morphology, trace element signatures and Hf isotope composition as a tool for petrogenetic modelling: Examples from Eastern Australian granitoids. *Journal of Petrology* 47: 329–353.

Belousova EA, Griffin WL, O'Reilly SY, and Fisher NI (2002) Igneous zircon: Trace element composition as an indicator of source rock type. *Contributions to Mineralogy and Petrology* 143: 602–622.

Belousova EA, Kostitsyn YA, Griffin WL, Begg GC, O'Reilly SY, and Pearson NJ (2010) The growth of the continental crust: Constraints from zircon Hf-isotope data. *Lithos* 119: 457–466.

Bickford ME, Chase RB, Nelson BK, Shuster RD, and Arruda EC (1981) U–Pb studies of zircon cores and overgrowths, and monazite: Implications for age and petrogenesis of the northeastern Idaho Batholith. *Journal of Geology* 89: 433–457.

Black LP, Kamo S, Allen CM, et al. (2004) Improved $^{206}Pb/^{238}U$ microprobe geochronology by the monitoring of a trace-element-related matrix effect; SHRIMP, ID-TIMS, ELA-ICP-MS and oxygen isotope documentation for a series of zircon standards. *Chemical Geology* 205: 115–140.

Black LP, Kamo SL, Williams IS, et al. (2003) The application of SHRIMP to Phanerozoic geochronology: A critical appraisal of four zircon standards. *Chemical Geology* 200: 171–188.

Blackburn TJ, Bowring SA, Perron JT, Mahan KH, Dudas FO, and Barnhart KR (2012a) An exhumation history of continents over billion-year time scales. *Science* 335: 73–76.

Blackburn T, Bowring S, Schoene B, Mahan K, and Dudas F (2011) U–Pb thermochronology: Creating a temporal record of lithosphere thermal evolution. *Contributions to Mineralogy and Petrology* 162: 479–500.

Blackburn T, Shimizu N, Bowring SA, Schoene B, and Mahan KH (2012b) Zirconium in rutile speedometry: New constraints on lower crustal cooling rates and residence temperatures. *Earth and Planetary Science Letters* 317–318: 231–240.

Boltwood BB (1907) On the ultimate disintegration products of the radioactive elements. Part II. The disintegration products of uranium. *American Journal of Science* 23: 77–88.

Bopp CJ, Lundstrom CC, Johnson TM, and Glessner JJG (2009) Variations in $^{238}U/^{235}U$ in uranium ore deposits: Isotopic signatures of the U reduction process? *Geology* 37: 611–614.

Bourdon B, Turner S, Henderson GM, and Lundstrom CC (2003) Introduction to U-series geochemistry. *Reviews in Mineralogy and Geochemistry* 52: 1–21.

Bowring SA, Erwin DH, Jin YG, Martin MW, Davidek K, and Wang W (1998) U/Pb zircon geochronology and tempo of the end-Permian mass extinction. *Science* 280: 1039–1045.

Bowring SA, Grotzinger JP, Condon DJ, Ramezani J, Newall MJ, and Allen PA (2007) Geochronologic constraints on the chronostratigraphic framework of the Neoproterozoic Huqf Supergroup, Sultanate of Oman. *American Journal of Science* 307: 1097–1145.

Bowring JF, McLean NM, and Bowring SA (2011) Engineering cyber infrastructure for U–Pb geochronology: Tripoli and U–Pb redux. *Geochemistry, Geophysics, Geosystems* 12: Q0AA19.

Bowring SA and Schmitz MD (2003) High-precision U–Pb zircon geochronology and the stratigraphic record. In: Hanchar JM and Hoskin PWO (eds.) *Zircon. Reviews in Mineralogy and Geochemistry*, vol. 53, pp. 305–326. Washington, DC: Mineralogical Society of America.

Bowring SA, Schoene B, Crowley JL, Ramezani J, and Condon DC (2006) High-precision U–Pb zircon geochronology and the stratigraphic record: Progress and promise. In: Olszewski T (ed.) *Geochronology: Emerging Opportunities. Paleontological Society Papers*, vol. 12, pp. 25–45. Philidelphia, PA: The Paleontological Society.

Bowring SA, Williams IS, and Compston W (1989) 3.96 Ga gneisses from the Slave province, Northwest Territories, Canada. *Geology* 17: 971–975.

Brennecka GA, Wasylenki LE, Bargar JR, Weyer S, and Anbar AD (2011) Uranium isotope fractionation during adsorption to Mn-oxyhydroxides. *Environmental Science & Technology* 45: 1370–1375.

Brennecka GA, Weyer S, Wadhwa M, Janney PE, Zipfel J, and Anbar AD (2010) $^{238}U/^{235}U$ variations in meteorites: Extant ^{247}Cm and implications for Pb–Pb dating. *Science* 327: 449–451.

Brooks C, Hart SR, and Wendt I (1972) Realistic use of two-error regression treatments as applied to rubidium–strontium data. *Reviews of Geophysics* 10: 551–577.

Bruguier O, Lancelot JR, and Malavieille J (1997) U–Pb dating on single detrital zircon grains from the Triassic Songpan-Ganze flysch (Central China): Provenance and tectonic correlations. *Earth and Planetary Science Letters* 152: 217–231.

Bürger S, Essex RM, Mathew KJ, Richter S, and Thomas RB (2010) Implementation of guide to the expression of uncertainty in measurement (GUM) to multi-collector TIMS uranium isotope ratio metrology. *International Journal of Mass Spectrometry* 294: 65–76.

Burgess SD and Miller JS (2008) Construction, solidification and internal differentiation of a large felsic arc pluton: Cathedral Peak granodiorite, Sierra Nevada Batholith. In: Annen C and Zellmer GF (eds.) *Dynamics of Crustal Magma Transfer, Storage and Differentiation, Geological Society Special Publication 304*, pp. 203–233. London: Geological Society of London.

Cameron AE, Smith DH, and Walker RL (1969) Mass spectrometry of nanogram-size samples of lead. *Analytical Chemistry* 41: 525–526.

Catanzaro EJ and Hanson GN (1971) U–Pb ages for sphene from early Precambrian igneous rocks in northeastern minnesota–northwestern Ontario. *Canadian Journal of Earth Sciences* 8: 1319–1324.

Chamberlain KR and Bowring SA (2000) Apatite-feldspar U–Pb thermochronometer: A reliable mid-range ($\sim$450 °C), diffusion controlled system. *Chemical Geology* 172: 173–200.

Chang Z, Vervoort JD, McClelland WC, and Knaack C (2006) U–Pb dating of zircon by LA-ICP-MS. *Geochemistry, Geophysics, Geosystems* 7: Q05009.

Charlier BLA and Wilson CJN (2010) Chronology and evolution of caldera-forming and post-caldera magma systems at Okataina Volcano, New Zealand from zircon U–Th model-age spectra. *Journal of Petrology* 51: 1121–1141.

Charlier BLA, Wilson CJN, Lowenstern JB, Blake S, Van Calstren PW, and Davidson JP (2005) Magma generation at a large hyperactive silicic volcano (Taupo, New Zealand) revealed by U–Th and U–Pb systematics in zircons. *Journal of Petrology* 46: 3–32.

Chen DF, Dong WQ, Zhu BQ, and Chen XP (2004) Pb/Pb ages of Neoproterozoic Doushantuo phosphorites in South China: Constraints on early Metazoan evolution and glaciation events. *Precambrian Research* 132: 123–132.

Chen F, Siebel W, and Satir M (2002) Zircon U–Pb and Pb-isotope fractionation during stepwise HF acid leaching and geochronological implications. *Chemical Geology* 191: 155–164.

Chen JH and Wasserburg GJ (1981) Isotopic determination of uranium in picomole and subpicomol quantities. *Analytical Chemistry* 53: 2060–2067.
Cheng H, Edwards RL, Hoff J, Gallup CD, Richards DA, and Asmerom Y (2000) The half-lives of uranium-234 and thorium-230. *Chemical Geology* 169: 17–33.
Cherniak DJ (1993) Lead diffusion in titanite and preliminary results on the effects of radiation damage on Pb transport. *Chemical Geology* 110: 177–194.
Cherniak D (2006) Zr diffusion in titanite. *Contributions to Mineralogy and Petrology* 152: 639–647.
Cherniak DJ, Lanford WA, and Ryerson FJ (1991) Lead diffusion in apatite and zircon using ion implantation and Rutherford Backscattering techniques. *Geochimica et Cosmochimica Acta* 55: 1663–1673.
Cherniak DJ, Manchester J, and Watson EB (2007) Zr and Hf diffusion in rutile. *Earth and Planetary Science Letters* 261: 267–279.
Cherniak DJ and Watson EB (2000) Pb diffusion in rutile. *Contributions to Mineralogy and Petrology* 139: 198–207.
Cherniak DJ and Watson EB (2001) Pb diffusion in zircon. *Chemical Geology* 172: 5–24.
Chew DM, Sylvester PJ, and Tubrett MN (2011) U–Pb and Th–Pb dating of apatite by LA-ICPMS. *Chemical Geology* 280: 200–216.
Claiborne LL, Miller CF, Flanagan DM, Clynne MA, and Wooden JL (2010) Zircon reveals protracted magma storage and recycling beneath Mount St. Helens. *Geology* 38: 1011–1014.
Claverie F, Fernandez B, Pecheyran C, Alexis J, and Donard OFX (2009) Elemental fractionation effects in high repetition rate IR femtosecond laser ablation ICP-MS analysis of glasses. *Journal of Analytical Atomic Spectrometry* 24: 891–902.
Cocherie A, Legendre O, Peucat JJ, and Kouamelan AN (1998) Geochronology of polygenetic monazites constrained by in situ electron microprobe Th–U–total lead determination: Implications for lead behaviour in monazite. *Geochimica et Cosmochimica Acta* 62: 2475–2497.
Cocherie A and Robert M (2008) Laser ablation coupled with ICP-MS applied to U–Pb zircon geochronology: A review of recent advances. *Gondwana Research* 14: 597–608.
Coleman DS and Glazner AF (1997) The Sierra Crest Magmatic Event: Rapid formation of juvenile crust during the Late Cretaceous in California. *International Geology Review* 39: 768–787.
Coleman DS, Gray W, and Glazner AF (2004) Rethinking the emplacement and evolution of zoned plutons: Geochronologic evidence for incremental assembly of the Tuolumne Intrusive Suite, California. *Geology* 32: 433–436.
Compston W, Williams IS, and Meyer C (1984) U–Pb geochronology of zircons from lunar Breccia 73217 using a sensitive high mass-resolution ion microprobe. *Journal of Geophysical Research* 89: B525–B534.
Condie KC, Belousova E, Griffin WL, and Sircombe KN (2009) Granitoid events in space and time: Constraints from igneous and detrital zircon age spectra. *Gondwana Research* 15: 228–242.
Condie KC, Bickford ME, Aster RC, Belousova E, and Scholl DW (2011) Episodic zircon ages, Hf isotopic composition, and the preservation rate of continental crust. *Geological Society of America Bulletin* 123: 951–957.
Condomines M, Gauthier P-J, and Sigmarsson O (2003) Timescales of magma chamber processes and dating of young volcanic rocks. In: Bourdon B, Henderson GM, Lundstrom CC, and Turner SP (eds.) *Uranium-Series Geochemistry*. *Reviews in Mineralogy and Geochemistry* 52: 125–174. Washington, DC: Mineralogical Society of America.
Condon DJ, McLean N, Noble SR, and Bowring SA (2010) Isotopic composition ($^{238}U/^{235}U$) of some commonly used uranium reference materials. *Geochimica et Cosmochimica Acta* 74: 7127–7143.
Condon D, Mclean N, Schoene B, Bowring S, Parrish R, and Noble S (2008) Synthetic U–Pb 'standard' solutions for ID-TIMS geochronology. *Geochimica et Cosmochimica Acta* 72: A175.
Condon DJ, Zhu M, Bowring SA, Wang W, Yang A, and Jin Y (2005) U–Pb ages from the Neoproterozoic Duoshantuo Formation, China. *Science* 308: 95–98.
Connelly JN, Amelin Y, Krot AN, and Bizzarro M (2008) Chronology of the solar system's oldest solids. *The Astrophysical Journal Letters* 675: L121.
Connelly JN and Bizzarro M (2009) Pb–Pb dating of chondrules from CV chondrites by progressive dissolution. *Chemical Geology* 259: 143–151.
Corfu F (1988) Differential response of U–Pb systems in coexisting accessory minerals, Winnepeg River Subprovince, Canadian Shield: Implications for Archean crustal growth and stabilization. *Contributions to Mineralogy and Petrology* 98: 312–325.
Corfu F and Ayres LD (1984) U–Pb age and genetic significance of heterogeneous zircon populations in rocks from the Favourable Lake Area, Northwestern Ontario. *Contributions to Mineralogy and Petrology* 88: 86–101.
Corfu F, Hanchar JM, Hoskin PWO, and Kinny P (2003) Atlas of zircon textures. In: Hanchar JM and Hoskin PWO (eds.) *Zircon*. *Reviews in Mineralogy and Geochemistry*, vol. 53, pp. 468–500. Washington, DC: Mineralogical Society of America.
Corfu F, Heaman LM, and Rogers G (1994) Polymetamorphic evolution of the Lewisian complex, NW Scotland, as recorded by U–Pb isotopic compositions of zircon, titanite and rutile. *Contributions to Mineralogy and Petrology* 117: 215–228.
Corfu F, Krogh TE, and Ayres LD (1985) U–Pb zircon and sphene geochronology of a composite Archean granitoid batholith, Favourable Lake area, northwestern Ontario. *Canadian Journal of Earth Sciences* 22: 1436–1451.
Corfu F and Stone D (1998) The significance of titanite and apatite U–Pb ages: Constraints for the post-magmatic thermal-hydrothermal evolution of a batholithic complex, Berens River area, northwestern Superior Province, Canada. *Geochimica et Cosmochimica Acta* 62: 2979–2995.
Corrie SL and Kohn MJ (2007) Resolving the timing of orogenesis in the Western Blue Ridge, southern Appalachians, via *in situ* ID-TIMS monazite geochronology. *Geology* 35: 627–630.
Cottle JM, Horstwood MSA, and Parrish RR (2009a) A new approach to single shot laser ablation analysis and its application to in situ Pb/U geochronology. *Journal of Analytical Atomic Spectrometry* 24: 1355–1363.
Cottle JM, Searle MP, Horstwood MSA, and Waters DJ (2009b) Timing of midcrustal metamorphism, melting, and deformation in the Mount Everest Region of Southern Tibet revealed by U–Th–Pb geochronology. *Journal of Geology* 117: 643–664.
Cowan GA and Adler HH (1976) The variability of the natural abundance of ^{235}U. *Geochimica et Cosmochimica Acta* 40: 1487–1490.
Crowley JL, Schmitz MD, Bowring SA, Williams ML, and Karlstrom KE (2006) U–Pb and Hf isotopic analysis of zircon in lower crustal xenoliths from the Navajo volcanic field: 1.4 Ga mafic magmatism and metamorphism beneath the Colorado Plateau. *Contributions to Mineralogy and Petrology* 151: 313–330.
Crowley JL, Schoene B, and Bowring SA (2007) U–Pb dating of zircon in the Bishop Tuff at the millennial scale. *Geology* 35: 1123–1126.
Crowley JL, Waters DJ, Searle MP, and Bowring SA (2009) Pleistocene melting and rapid exhumation of the Nanga Parbat massif, Pakistan: Age and *P–T* conditions of accessory mineral growth in migmatite and leucogranite. *Earth and Planetary Science Letters* 288: 408–420.
Cumming GL and Richards JR (1975) Ore lead isotope ratios in a continuously changing Earth. *Earth and Planetary Science Letters* 28: 155–171.
Darling JR, Storey CD, and Engi M (2012) Allanite U–Th–Pb geochronology by laser ablation ICPMS. *Chemical Geology* 292–293: 103–115.
Das A and Davis DW (2010) Response of Precambrian zircon to the chemical abrasion (CA-TIMS) method and implications for improvement of age determinations. *Geochimica et Cosmochimica Acta* 74: 5333–5348.
Davis DW (2008) Sub-million-year age resolution of Precambrian igneous events by thermal extraction-thermal ionization mass spectrometer Pb dating of zircon: Application to crystallization of the Sudbury impact melt sheet. *Geology* 36: 383–386.
Davis DW and Krogh TE (2000) Preferential dissolution of ^{234}U and radiogenic Pb from alpha-recoil-damaged lattive sites in zircon: Implications for thermal histories and Pb isotopic fractionation in the near surface environment. *Chemical Geology* 172: 41–58.
Davis DW, Williams IS, and Krogh TE (2003) Historical development of zircon geochronology. In: Hanchar JM and Hoskin PWO (eds.) *Zircon*. *Reviews in Mineralogy and Geochemistry*, vol. 53, pp. 145–181. Washington, DC: Mineralogical Society of America.
Davydov VI, Crowley JL, Schmitz MD, and Poletaev VI (2010) High-precision U–Pb zircon age calibration of the global Carboniferous time scale and Milankovitch band cyclicity in the Donets Basin, eastern Ukraine. *Geochemistry, Geophysics, Geosystems* 11: Q0AA04.
DeGraaff-Surpless K, Graham SA, Wooden JL, and McWilliams MO (2002) Detrital zircon provenance analysis of the Great Valley Group, California: Evolution of an arc–forearc system. *Geological Society of America Bulletin* 114: 1564–1580.
Deliens M, Delhal J, and Tarte P (1977) Metamictization and U–Pb systematics – A study by infrared absorption spectrometry of Precambrian zircons. *Earth and Planetary Science Letters* 33: 331–344.
Dhuime B, Hawkesworth CJ, Cawood PA, and Storey CD (2012) A change in the geodynamics of continental growth 3 billion years ago. *Science* 335: 1334–1336.
Dickin AP (2005) *Radiogenic Isotope Geology*, 2nd edn. Cambridge, UK: Cambridge University Press.
Dickinson WR and Gehrels GE (2003) U–Pb ages of detrital zircons from Permian and Jurassic eolian sandstones of the Colorado Plateau, USA: Paleogeographic implications. *Sedimentary Geology* 163: 29–66.
Dickinson WR and Gehrels GE (2009) Use of U–Pb ages of detrital zircons to infer maximum depositional ages of strata: A test against a Colorado Plateau Mesozoic database. *Earth and Planetary Science Letters* 288: 115–125.
DiPietro JA and Isachsen CE (2001) U–Pb zircon ages from the Indian plate in northwest Pakistan and their significance to Himalayan and pre-Himalayan geologic history. *Tectonics* 20: 510–525.

Dodson MH (1973) Closure temperature in cooling geochronological and petrological systems. *Contributions to Mineralogy and Petrology* 40: 259–274.
Dodson MH (1986) Closure profiles in cooling systems. *Materials Science Forum* 7: 145–154.
Dumond G, McLean N, Williams ML, Jercinovic MJ, and Bowring SA (2008) High-resolution dating of granite petrogenesis and deformation in a lower crustal shear zone: Athabasca granulite terrane, western Canadian Shield. *Chemical Geology* 254: 175–196.
Faure G and Mensing TM (2005) *Isotopes – Principles and Applications*, 3rd edn. Hoboken, NJ: Wiley.
Fedo CM, Sircombe KN, and Rainbird RH (2003) Detrital zircon analysis of the sedimentary record. In: Hanchar JM and Hoskin PWO (eds.) *Zircon. Reviews in Mineralogy and Geochemistry*, 53: 277–303. Washington, DC: Mineralogical Society of America.
Feng R, Machado N, and Ludden J (1993) Lead geochronology of zircon by LaserProbe-inductively coupled plasma mass spectrometry (LP-ICPMS). *Geochimica et Cosmochimica Acta* 57: 3479–3486.
Ferry J and Watson E (2007) New thermodynamic models and revised calibrations for the Ti-in-zircon and Zr-in-rutile thermometers. *Contributions to Mineralogy and Petrology* 154: 429–437.
Finger F, Broska I, Roberts MP, and Schermaier A (1998) Replacement of primary monazite by apatite–allanite–epidote coronas in an amphibolite facies granite gneiss from the Eastern Alps. *American Mineralogist* 83: 248–258.
Fisher CM, Longerich HP, Jackson SE, and Hanchar JM (2010) Data acquisition and calculation of U–Pb isotopic analyses using laser ablation (single collector) inductively coupled plasma mass spectrometry. *Journal of Analytical Atomic Spectrometry* 25: 1905–1920.
Fletcher IR, McNaughton NJ, Davis WJ, and Rasmussen B (2010) Matrix effects and calibration limitations in ion probe U–Pb and Th–Pb dating of monazite. *Chemical Geology* 270: 31–44.
Frost BR, Chamberlain KR, and Schumacher JC (2000) Sphene (titanite): Phase relations and role as a geochronometer. *Chemical Geology* 172: 131–148.
Fryer BJ, Jackson SE, and Longerich HP (1993) The application of laser ablation microprobe-inductively coupled plasma-mass spectrometry (LAM-ICP-MS) to in situ U–Pb geochronology. *Chemical Geology* 109: 1–8.
Fu B, Page F, Cavosie A, et al. (2008) Ti-in-zircon thermometry: Applications and limitations. *Contributions to Mineralogy and Petrology* 156: 197–215.
Fukuoka T and Kigoshi K (1974) Discordant Io-ages and the uranium and thorium distribution between zircon and host rocks. *Geochemical Journal* 8: 117–122.
Furin S, Preto N, Rigo M, et al. (2006) High-precision U–Pb zircon age from the Triassic of Italy: Implications for the Triassic time scale and the Carnian origin of calcareous nannoplankton and dinosaurs. *Geology* 34: 1009–1012.
Gao XY, Zheng YF, and Chen YX (2011) U–Pb ages and trace elements in metamorphic zircon and titanite from UHP eclogite in the Dabie orogen: Constraints on *P–T–t* path. *Journal of Metamorphic Geology* 29: 721–740.
Garcia CC, Lindner H, von Bohlen A, Vadla C, and Niemax K (2008) Elemental fractionation and stoichiometric sampling in femtosecond laser ablation. *Journal of Analytical Atomic Spectrometry* 23: 470–478.
Gehrels G (2011) Detrital zircon U–Pb geochronology: Current methods and new opportunities. In: Busby C and Azor A (eds.) *Tectonics of Sedimentary Basins: Recent Advances*, pp. 45–62. Hoboken, NJ: Wiley.
Gehrels G, DeCelles PG, Martin A, Ojha TP, and Pinhassi G (2003) Initiation of the Himalayan orogen as an early Paleozoic thin-skinned thrust belt. *GSA Today* 13: 4–9.
Gehrels GE, Valencia VA, and Ruiz J (2008) Enhanced precision, accuracy, efficiency, and spatial resolution of U–Pb ages by laser ablation-multicollector-inductively coupled plasma-mass spectrometry. *Geochemistry, Geophysics, Geosystems* 9: Q03017.
Geisler T, Pidgeon RT, Kurtz R, van Bronswijk W, and Schleicher H (2003) Experimental hydrothermal alteration of partially metamict zircon. *American Mineralogist* 88: 1496–1513.
Geisler T, Pidgeon RT, van Bronswijk W, and Kurtz R (2002) Transport of uranium, thorium, and lead in metamict zircon under low-temperature hydrothermal conditions. *Chemical Geology* 191: 141–154.
Gelcich S, Davis DW, and Spooner ETC (2005) Testing the apatite-magnetite geochronometer: U–Pb and $^{40}Ar/^{39}Ar$ geochronology of plutonic rocks, massive magnetite–apatite tabular bodies, and IOCG mineralization in Northern Chile. *Geochimica et Cosmochimica Acta* 69: 3367–3384.
Gerstenberger H and Haase G (1997) A highly effective emitter substance for mass spectrometric Pb isotope ratio determinations. *Chemical Geology* 136: 309–312.
Gibson HD, Carr SD, Brown RL, and Hamilton MA (2004) Correlations between chemical and age domains in monazite, and metamorphic reactions involving major pelitic phases: An integration of ID-TIMS and SHRIMP geochronology with Y, Th, U X-ray mapping. *Chemical Geology* 211: 237–260.
Glazner AF, Bartley JM, Coleman DS, Gray W, and Taylor RZ (2004) Are plutons assembled over millions of year by amalgamation from small magma chambers?. *GSA Today* 14: 4–11.
Gonzalez JJ, Oropeza D, Mao X, and Russo RE (2008) Assessment of the precision and accuracy of thorium (^{232}Th) and uranium (^{238}U) measured by quadrupole based inductively coupled plasma-mass spectrometry using liquid nebulization, nanosecond and femtosecond laser ablation. *Journal of Analytical Atomic Spectrometry* 23: 229–234.
Gordon SM, Bowring SA, Whitney DL, Miller RB, and McLean N (2010) Time scales of metamorphism, deformation, and crustal melting in a Continental Arc, North Cascades USA. *Geological Society of America Bulletin* 122: 1308–1330.
Gradstein FM, Ogg JG, Schmitz MD, and Ogg GM (2012) *The Geologic Timescale 2012*. Oxford, UK: Elsevier.
Gradstein FM, Ogg JG, Smith AG, Bleeker W, and Lourens LJ (2004) A new geologic time scale with special reference to the Precambrian and Neogene. *Episodes* 27: 83–100.
Grange ML, Nemchin AA, Timms N, Pidgeon RT, and Meyer C (2011) Complex magmatic and impact history prior to 4.1 Ga recorded in zircon from Apollo 17 South Massif aphanitic breccia 73235. *Geochimica et Cosmochimica Acta* 75: 2213–2232.
Gregory CJ, Rubatto D, Allen CM, Williams IS, Hermann J, and Ireland T (2007) Allanite micro-geochronology: A LA-ICP-MS and SHRIMP U–Th–Pb study. *Chemical Geology* 245: 162–182.
Grunder AL, Klemetti EW, Feeley TC, and McKee CM (2006) Eleven million years of arc volcanism at the Aucanquilcha Volcanic Cluster, northern Chilean Andes: Implications for the life span and emplacement of plutons. *Earth and Environmental Science Transactions of the Royal Society of Edinburgh* 97: 415–436.
Guex J, Schoene B, Bartolini A, et al. (2012) Geochronological constraints on post-extinction recovery of the ammonoids and carbon cycle perturbations during the Early Jurassic. *Palaeogeography, Palaeoclimatology, Palaeoecology* 346–347: 1–11.
Guillong M and Heinrich CA (2007) Sensitivity enhancement in laser ablation ICP-MS using small amounts of hydrogen in the carrier gas. *Journal of Analytical Atomic Spectrometry* 22: 1488–1494.
Guillong M, Horn I, and Günther D (2003) A comparison of 266 nm, 213 nm and 193 nm produced from a single solid state Nd:YAG laser for laser ablation ICP-MS. *Journal of Analytical Atomic Spectrometry* 18: 1224–1230.
GUM: Joint Committee for Guides in Metrology (2008) Evaluation of measurement data–guide to the expression of uncertainty in measurement (GUM). JCGM, vol. 100. www.bipm.org/en/publications/guides/gum.html.
Günther D, Frischknecht R, Heinrich CA, and Kahlert H-J (1997) Capabilities of an argon fluoride 193 nm excimer laser for laser ablation inductively coupled plasma mass spectometry microanalysis of geological materials. *Journal of Analytical Atomic Spectrometry* 12: 939–944.
Günther D and Heinrich CA (1999a) Comparison of the ablation behaviour of 266 nm Nd:YAG and 193 nm ArF excimer lasers for LA-ICP-MS analysis. *Journal of Analytical Atomic Spectrometry* 14: 1369–1374.
Günther D and Heinrich CA (1999b) Enhanced sensitivity in laser ablation-ICP mass spectrometry using helium–argon mixtures as aerosol carrier. *Journal of Analytical Atomic Spectrometry* 14: 1363–1368.
Hanchar JM and Hoskin PWO (2003) *Zircon. Reviews in Mineralogy and Geochemistry*, vol. 153. Washington, DC: The Mineralogical Society of America.
Hanchar JM and Miller CF (1993) Zircon zonation patterns as revealed by cathodoluminescence and backscattered electron images. Implications for interpretation of complex crustal histories. *Chemical Geology* 110: 1–13.
Hanchar JM and Rudnick R (1995) Revealing hidden structures. The application of cathodoluninescence and back-scattered electron imaging to dating zircons from lower crustal xenoliths. *Lithos* 36: 289–303.
Hanchar JM and van Westrenen W (2007) Rare earth element behavior in zircon-melt systems. *Elements* 3: 37–42.
Hanson GN, Catanzaro EJ, and Anderson DH (1971) U–Pb for sphene in a contact metamorphic zone. *Earth and Planetary Science Letters* 12: 231–237.
Harley SL and Kelly NM (2007) The impact of zircon–garnet REE distribution data on the interpretation of zircon U–Pb ages in complex high-grade terrains: An example from the Rauer Islands, East Antarctica. *Chemical Geology* 241: 62–87.
Harrison TM (1981) Diffusion of ^{40}Ar in hornblende. *Contributions to Mineralogy and Petrology* 78: 324–331.
Hawkesworth CJ and Kemp AIS (2006) Evolution of the continental crust. *Nature* 443: 811–817.

Hawkins DP and Bowring SA (1997) U–Pb systematics of monazite and xenotime: Case studies from the Paleoproterozoic of the Grand Canyon, Arizona. *Contributions to Mineralogy and Petrology* 127: 87–103.

Hawkins DP and Bowring SA (1999) U–Pb monzaite, xenotime and titanite geochronological constraints on the prograde to post-peak metamorphic thermal history of Paleoproterozoic migmatites from the Grand Canyon, Arizona. *Contributions to Mineralogy and Petrology* 134: 150–169.

Hayden L, Watson E, and Wark D (2008) A thermobarometer for sphene (titanite). *Contributions to Mineralogy and Petrology* 155: 529–540.

Heaman LM (1989) The nature of the subcontinental mantle from Sr–Nd–Pb isotopic studies on kimberlitic perovskite. *Earth and Planetary Science Letters* 92: 323–334.

Heaman LM, Bowins R, and Crocket J (1990) The chemical composition of igneous zircon suites: Implications for geochemical tracer studies. *Geochimica et Cosmochimica Acta* 54: 1597–1607.

Heaman LM and LeCheminant AN (1993) Paragenesis and U–Pb systematics of baddeleyite (ZrO_2). *Chemical Geology* 110: 95–126.

Heizler MT, Ralser S, and Karlstrom KE (1997) Late Proterozoic (Grenville?) deformation in central New Mexico determined from single-crystal muscovite $^{40}Ar/^{39}Ar$ age spectra. *Precambrian Research* 84: 1–15.

Hergenroder R (2006) Hydrodynamic sputtering as a possible source for fractionation in LA-ICP-MS. *Journal of Analytical Atomic Spectrometry* 21: 517–524.

Hervé F, Fanning CM, and Pankhurst RJ (2003) Detrital zircon age patterns and provenance of the metamorphic complexes of southern Chile. *Journal of South American Earth Sciences* 16: 107–123.

Hiess J, Condon DJ, McLean N, and Noble SR (2012) $^{238}U/^{235}U$ systematics in terrestrial uranium-bearing minerals. *Science* 335: 1610–1614.

Hietpas J, Samson S, and Moecher D (2011a) A direct comparison of the ages of detrital monazite versus detrital zircon in Appalachian foreland basin sandstones: Searching for the record of Phanerozoic orogenic events. *Earth and Planetary Science Letters* 310: 488–497.

Hietpas J, Samson S, Moecher D, and Chakraborty S (2011b) Enhancing tectonic and provenance information from detrital zircon studies: Assessing terrane-scale sampling and grain-scale characterization. *Journal of the Geological Society* 168: 309–318.

Hietpas J, Samson S, Moecher D, and Schmitt AK (2010) Recovering tectonic events from the sedimentary record: Detrital monazite plays in high fidelity. *Geology* 38: 167–170.

Hinthorne JR, Andersen CA, Conrad RL, and Lovering JF (1979) Single-grain $^{207}Pb/^{206}Pb$ and U/Pb age determinations with a 10-μm spatial resolution using the ion microprobe mass analyzer (IMMA). *Chemical Geology* 25: 271–303.

Hinton RW and Upton BGJ (1991) The chemistry of zircon: Variations within and between large crystals from syenite and alakali basalt xenoliths. *Geochimica et Cosmochimica Acta* 55: 3287–3302.

Hirata T and Nesbitt RW (1995) U–Pb isotope geochronology of zircon: Evaluation of the laser probe-inductively coupled plasma mass spectrometry technique. *Geochimica et Cosmochimica Acta* 59: 2491–2500.

Hoffmann KH, Condon DJ, Bowring SA, and Crowley JL (2004) U–Pb zircon date from the Neoproterozoic Ghaub Formation, Namibia: Constraints on Marinoan glaciation. *Geology* 32: 817–820.

Hofmann A, Valley J, Watson E, Cavosie A, and Eiler J (2009) Sub-micron scale distributions of trace elements in zircon. *Contributions to Mineralogy and Petrology* 158: 317–335.

Holmes A (1911) The association of lead with uranium in rock-minerals and its application to the measurement of geological time. *Proceedings of the Royal Society of London* 85: 248–256.

Holmes A (1946) An estimate of the age of the Earth. *Nature* 157: 680–684.

Holmes A and Lawson RW (1927) Factors inolves in the calculation of the ages of radioactive minerals. *American Journal of Science* 13: 327–344.

Horn I and Günther D (2003) The influence of ablation carrier gasses Ar, He and Ne on the particle size distribution and transport efficiencies of laser ablation-induced aerosols: Implications for LA-ICP-MS. *Applied Surface Science* 207: 144–157.

Horn I, Rudnick RL, and McDonough WF (2000) Precise elemental and isotope ratio determination by simultaneous solution nebulization and laser ablation-ICP-MS: Application to U–Pb geochronology. *Chemical Geology* 164: 281–301.

Horstwood MSA (2008) Data reduction strategies, uncertainty assessment and resolution of LA-(MC-)ICP-MS isotope data. In: Sylvester PJ (ed.) *Laser Ablation ICP-MS in the Earth Sciences: Current Practices and Outstanding Issues*. *Mineralogical Association of Canada Short Course Series*, vol. 40, pp. 283–303. Quebec: Mineralogical Association of Canada.

Horstwood MSA, Foster GL, Parrish RR, Noble SR, and Nowell GM (2003) Common-Pb corrected in situ U–Pb accessory mineral geochronology by LA-MC-ICP-MS. *Journal of Analytical Atomic Spectrometry* 18: 837–846.

Hoskin PWO and Ireland TR (2000) Rare earth element chemistry of zircon and its use as a provenance indicator. *Geology* 28: 627–630.

Hoskin PWO, Kinny PD, Wyborn D, and Chappell BW (2000) Identifying accessory mineral saturation during differentiation in granitoid magmas: An integrated approach. *Journal of Petrology* 41: 1365–1396.

Housh T and Bowring SA (1991) Lead isotopic heterogeneities within alkali feldspars: Implications for the determination of initial lead isotopic compositions. *Geochimica et Cosmochimica Acta* 55: 2309–2316.

Houtermans FG (1946) Die isotopenhäufigkeiten im natürlichen blei und das alter des urans. *Naturwissenschaften* 33: 185–186.

Ireland TR, Flöttmann T, Fanning CM, Gibson GM, and Preiss WV (1998) Development of the early Paleozoic Pacific margin of Gondwana from detrital-zircon ages across the Delamerian orogen. *Geology* 26: 243–246.

Ireland TR and Williams IS (2003) Considerations in zircon geochronology by SIMS. In: Hanchar JM and Hoskin PWO (eds.) *Zircon*. *Reviews in Mineralogy and Geochemistry*, vol. 53, pp. 215–241. Washington, DC: Mineralogical Society of America.

Irmis RB, Mundil R, Martz JW, and Parker WG (2011) High-resolution U–Pb ages from the Upper Triassic Chinle Formation (New Mexico, USA) support a diachronous rise of dinosaurs. *Earth and Planetary Science Letters* 309: 258–267.

Jaffey AH, Flynn KF, Glendenin LE, Bentley WC, and Essling AM (1971) Precision measurement of half-lives and specific activities of ^{235}U and ^{238}U. *Physical Review C* 4: 1889–1906.

Jordan TH (1988) Structure and formation of the continental tectosphere. In: Menzies MA and Cox KG (eds.) *Oceanic and Continental Lithosphere: Similarities and Differences*, pp. 11–37. London: Oxford University Press.

Kelly NM and Harley SL (2005) An integrated microtextural and chemical approach to zircon geochronology: Refining the Archaean history of the Napier Complex, east Antarctica. *Contributions to Mineralogy and Petrology* 149: 57–84.

Ketcham RA, Donelick RA, and Carlson WD (1999) Variability of apatite fission-track annealing kinetics: III. Extrapolation to geological time scales. *American Mineralogist* 84: 1235–1255.

Kita NT, Huss GR, Tachibana S, Amelin Y, Nyquist LE, and Hutcheon ID (2005) Constraints on the origin of chondrules and CAIs from short-lived and long-lived radionlucides. In: Krot AN, Scott ERD, and Reipurth B (eds.) *Chondrites and the Protoplanetary Disc*, *ASP Conference Series*, vol. 341, pp. 558–587. San Francisco: Astronomical Society of the Pacific.

Kober B (1986) Whole-grain evaporation for $^{207}Pb/^{206}Pb$-age-investigations on single zircons using a double-filament thermal ion source. *Contributions to Mineralogy and Petrology* 93: 482–490.

Kohn MJ and Malloy MA (2004) Formation of monazite via prograde metamorphic reactions among common silicates: Implications for age determinations. *Geochimica et Cosmochimica Acta* 68: 101–113.

Kohn MJ and Vervoort JD (2008) U–Th–Pb dating of monazite by single-collector ICP-MS: Pitfalls and potential. *Geochemistry, Geophysics, Geosystems* 9: Q04031.

Kohn MJ, Wieland MS, Parkinson CD, and Upreti BN (2005) Five generations of monazite in Langtang gneisses: Implications for chronology of the Himalayan metamorphic core. *Journal of Metamorphic Geology* 23: 399–406.

Kooijman E, Mezger K, and Berndt J (2010) Constraints on the U–Pb systematics of metamorphic rutile from in situ LA-ICP-MS analysis. *Earth and Planetary Science Letters* 293: 321–330.

Kosler J and Sylvester PJ (2003) Present trends and the future of zircon in geochronology: Laser ablation ICPMS. In: Hanchar JM and Hoskin PWO (eds.) *Zircon*. *Reviews in Mineralogy and Geochemistry*, vol. 53, pp. 243–275. Washington, DC: Mineralogical Society of America.

Kosler J, Tubrett MN, and Sylvester PJ (2001) Application of laser ablation ICP-MS to U–Th–Pb dating of monazite. *Geostandards Newsletter* 25: 375–386.

Kosler J, Wiedenbeck M, Wirth R, Hovorka J, Sylvester P, and Mikova J (2005) Chemical and phase composition of particles produced by laser ablation of silicate glass and zircon—Implications for elemental fractionation during ICP-MS analysis. *Journal of Analytical Atomic Spectrometry* 20: 402–409.

Krogh TE (1973) A low contamination method for hydrothermal decomposition of zircon and extraction of U and Pb for isotopic age determination. *Geochimica et Cosmochimica Acta* 37: 485–494.

Krogh TE (1982a) Improved accuracy of U–Pb zircon dating by selection of more concordant fractions using a high gradient magnetic separation technique. *Geochimica et Cosmochimica Acta* 46: 631–635.

Krogh TE (1982b) Improved accuracy of U–Pb zircon ages by the creation of more concordant systems using an air abrasion technique. *Geochimica et Cosmochimica Acta* 46: 637–649.

Krogh TE and Davis GL (1975) Alteration in zircons and differential dissolution of altered an metamict zircon. *Carnegie Institution of Washington Yearbook* 74: 619–623.

Kröner A, Hegner E, Wendt JI, and Byerly GR (1996) The oldest part of the Barberton granitoid–greenstone terrain, South Africa: Evidence for crust formation between 3.5 and 3.7 Ga. *Precambrian Research* 78: 105–124.

Kröner A and Todt W (1988) Single zircon dating constraining the maximum age of the Barberton Greenstone Belt, southern Africa. *Journal of Geophysical Research* 93: 15329–15337.

Kuiper KF, Deino A, Hilgen FJ, Krijgsman W, Renne PR, and Wijbrans JR (2008) Synchronizing rocks clocks of Earth history. *Science* 320: 500–504.

Kylander-Clark ARC, Hacker BR, and Mattinson JM (2008) Slow exhumation of UHP terranes: Titanite and rutile ages of the Western Gneiss Region, Norway. *Earth and Planetary Science Letters* 272: 531–540.

LaMaskin TA (2012) Detrital zircon facies of Cordilleran terranes in western North America. *GSA Today* 22: 4–11.

Lancaster PJ, Storey CD, Hawkesworth CJ, and Dhuime B (2011) Understanding the roles of crustal growth and preservation in the detrital zircon record. *Earth and Planetary Science Letters* 305: 405–412.

Lancelot J, Vitrac A, and Allegre CJ (1976) Uranium and lead isotopic dating with grain-by-grain zircon analysis: A study of complex geological history with a single rock. *Earth and Planetary Science Letters* 29: 357–366.

Lanzirotti A and Hanson GN (1996) Geochronology and geochemistry of multiple generations of monazite from the Wepawaug Schist, Connecticut, USA: Implications for monazite stability in metamorphic rocks. *Contributions to Mineralogy and Petrology* 125: 332–340.

Le Roux LJ and Glendenin LE (1963) Half-life of ^{232}Th. In: *National Conference on Nuclear Energy, Application of Isotopes and Radiation*. Proceedings of the National Conference on Nuclear Energy held in Pretoria, April 5–8 1963, pp. 83–94. Pelindaba: South African Atomic Energy Board.

Lee JKW (1995) Multipath diffusion in geochronology. *Contributions to Mineralogy and Petrology* 120: 60–82.

Lee JKW (1997) Pb, U, and Th diffusion in natural zircon. *Nature* 390: 159–162.

Lehrmann DJ, Ramezani J, Bowring SA, et al. (2006) Timing of recovery from the end-Permian extinction: Geochronologic and biostratigraphic constraints from south China. *Geology* 34: 1053–1056.

Li J-W, Deng X-D, Zhou M-F, Liu Y-S, Zhao X-F, and Guo J-L (2010) Laser ablation ICP-MS titanite U–Th–Pb dating of hydrothermal ore deposits: A case study of the Tonglushan Cu–Fe–Au skarn deposit, SE Hubei Province, China. *Chemical Geology* 270: 56–67.

Long S, McQuarrie N, Tobgay T, Rose C, Gehrels G, and Grujic D (2011) Tectonostratigraphy of the Lesser Himalaya of Bhutan: Implications for the along-strike stratigraphic continuity of the northern Indian margin. *Geological Society of America Bulletin* 123: 1406–1426.

Ludwig KR (1980) Calculation of uncertainties of U–Pb isotope data. *Earth and Planetary Science Letters* 46: 212–220.

Ludwig KR (1991) ISOPLOT–A plotting and regression program for radiogenic-isotope data. *US Geological Survey Open-File Report, 91–445*. Denver, CO: US Geological Survey.

Ludwig KR (1998) On the treatment of concordant uranium–lead ages. *Geochimica et Cosmochimica Acta* 62: 665–676.

Ludwig KR (2000a) Decay constant errors in U–Pb concordia–intercept ages. *Chemical Geology* 166: 315–318.

Ludwig KR (2000b) *SQUID 1.00, A User's Manual, Berkeley Geochronology Center Special Publication* No. 2. Berkeley, CA: Berkeley Geochronology Center.

Macdonald FA, Schmitz MD, Crowley JL, et al. (2010) Calibrating the Cryogenian. *Science* 327: 1241–1243.

Mahan KH, Goncalves P, Williams ML, and Jercinovic MJ (2006) Dating metamorphic reactions and fluid flow: Application to exhumation of high-P granulites in a crustal-scale shear zone, western Canadian Shield. *Journal of Metamorphic Geology* 24: 193–217.

Marzoli A, Renne PR, Piccirillo EM, Ernesto M, Bellieni G, and De Min A (1999) Extensive 200-million-year-old continental flood basalts of the Central Atlantic Magmatic Province. *Science* 284: 616–618.

Mattinson JM (1973) Anomalous isotopic composition of lead in young zircons. *Carnegie Institution of Washington Yearbook* 72: 613–616.

Mattinson JM (1987) U–Pb ages of zircons: A basic examination of error propagation. *Chemical Geology* 66: 151–162.

Mattinson JM (1994) A study of complex discordance in zircons using step-wise dissolution techniques. *Contributions to Mineralogy and Petrology* 116: 117–129.

Mattinson JM (2000) Revising the "gold standard" – the uranium decay constants of Jaffey et al., 1971. *Eos, Transactions American Geophysical Union, Spring Meeting Supplement*, Abstract V61A-02.

Mattinson JM (2005) Zircon U–Pb chemical-abrasion ("CA-TIMS") method: Combined annealing and multi-step dissolution analysis for improved precision and accuracy of zircon ages. *Chemical Geology* 220: 47–56.

Mattinson JM (2010) Analysis of the relative decay constants of ^{235}U and ^{238}U by multi-step CA-TIMS measurements of closed-system natural zircon samples. *Chemical Geology* 275: 186–198.

Mazzini A, Svensen H, Leanza HA, Corfu F, and Planke S (2010) Early Jurassic shale chemostratigraphy and U–Pb ages from the Neuquén Basin (Argentina): Implications for the Toarcian Oceanic Anoxic Event. *Earth and Planetary Science Letters* 297: 633–645.

McLean NM, Bowring JF, and Bowring SA (2011) An algorithm for U–Pb isotope dilution data reduction and uncertainty propagation. *Geochemistry, Geophysics, Geosystems* 12: Q0AA18.

Meinhold G (2010) Rutile and its applications in earth sciences. *Earth-Science Reviews* 102: 1–28.

Meldrum A, Boatner LA, Weber WJ, and Ewing RC (1998) Radiation damage in zircon and monazite. *Geochimica et Cosmochimica Acta* 62: 2509–2520.

Memeti V, Paterson S, Matzel J, Mundil R, and Okaya D (2010) Magmatic lobes as "snapshots" of magma chamber growth and evolution in large, composite batholiths: An example from the Tuolumne intrusion, Sierra Nevada, California. *Geological Society of America Bulletin* 122: 1912–1931.

Meyers SR, Siewert SE, Singer BS, et al. (2012) Intercalibration of radioisotopic and astrochronologic time scales for the Cenomanian–Turonian boundary interval, Western Interior Basin, USA. *Geology* 40: 7–10.

Mezger K, Hanson GN, and Bohlen SR (1989) High-precision U–Pb ages of metamorphic rutile: Application to the cooling history of high-grade terranes. *Earth and Planetary Science Letters* 96: 106–118.

Mezger K and Krogstad EJ (1997) Interpretation of discordant U–Pb zircon ages: An evaluation. *Journal of Metamorphic Geology* 15: 127–140.

Mezger K, Rawnsley CM, Bohlen SR, and Hanson GN (1991) U–Pb garnet, sphene, monazite, and rutile ages: Implications for the duration of high-grade metamorphism and cooling histories, Adirondack Mts, New York. *Journal of Geology* 99: 415–428.

Michard-Vitrac A, Lancelot J, Allegre CJ, and Moorbath S (1977) U–Pb ages on single zircons from the Early Precambrian rocks of West Greenland and the Minnesota River Valley. *Earth and Planetary Science Letters* 35: 449–453.

Miller JS, Matzel JP, Miller CF, Burgess SD, and Miller RB (2007) Zircon growth and recycling during the assembly of large, composite arc plutons. *Journal of Volcanology and Geothermal Research* 167: 282–299.

Moecher DP and Samson SD (2006) Differential zircon fertility of source terranes and natural bias in the detrital zircon record: Implications for sedimentary provenance analysis. *Earth and Planetary Science Letters* 247: 252–266.

Montel J-M, Foret S, Veschambre ML, Nicollet C, and Provost A (1996) Electron microprobe dating of monazite. *Chemical Geology* 131: 37–53.

Muller W, Shelley M, Miller P, and Broude S (2009) Initial performance metrics of a new custom-designed ArF excimer LA-ICPMS system coupled to a two-volume laser-ablation cell. *Journal of Analytical Atomic Spectrometry* 24: 209–214.

Mundil R, Ludwig KR, Metcalfe I, and Renne PR (2004) Age and timing of the Permian mass extinctions: U/Pb dating of closed-system zircons. *Science* 305: 1760–1763.

Mundil R, Metcalfe I, Ludwig KR, Renne PR, Oberli F, and Nicoll RS (2001) Timing of the Permian–Triassic biotic crisis: Implications from new zircon U/Pb age data (and their limitations). *Earth and Planetary Science Letters* 187: 131–145.

Mundil R, Zühlke R, Bechstädt T, et al. (2003) Cyclicities in Triassic platform carbonates: Synchronizing radio-isotopic and orbital clocks. *Terra Nova* 15: 81–87.

Murphy JB, Fernandez-Suarez J, Keppie JD, and Jeffries TE (2004) Contiguous rather than discrete Paleozoic histories for the Avalon and Meguma terranes based on detrital zircon data. *Geology* 32: 585–588.

Myrow PM, Hughes NC, Searle MP, Fanning CM, Peng SC, and Parcha SK (2009) Stratigraphic correlation of Cambrian–Ordovician deposits along the Himalaya: Implications for the age and nature of rocks in the Mount Everest region. *Geological Society of America Bulletin* 121: 323–332.

Nasdala L, Pidgeon RT, and Wolf D (1996) Heterogeneous metamictization of zircon on a microscale. *Geochimica et Cosmochimica Acta* 60: 1091–1097.

Nasdala L, Pidgeon RT, Wolf D, and Irmer G (1998) Metamictization and U–Pb isotopic discordance in single zircons: A combined Raman microprobe and SHRIMP ion probe study. *Mineralogy and Petrology* 62: 1–27.

Nebel O, Scherer EE, and Mezger K (2011) Evaluation of the ^{87}Rb decay constant by age comparison against the U–Pb system. *Earth and Planetary Science Letters* 301: 1–8.

Nemchin AA and Pidgeon RT (1999) U–Pb ages on titanite and apatite from the Darling Range granite: Implications for Late Archean history of the southwestern Yilgarn Craton. *Precambrian Research* 96: 125–139.

Oberli F, Fischer H, and Meier M (1990) High-resolution ^{238}U–^{206}Pb zircon dating of Tertiary bentonites and the Fish Canyon Tuff: A test for age "concordance" by single-crystal analysis. Seventh International Conference on Geochronology, Cosmochronology and Isotope Geology, *Geological Society of Australia Special Publication*, vol. 27, p. 74 (Abstract). Canberra: Geological Society of Australia.

Oberli F, Meier M, Berger A, Rosenberg CL, and Gieré R (2004) U–Th–Pb and $^{230}Th/^{238}U$ disequilibrium isotope systematics: Precise accessory mineral chronology and melt evolution tracing in the Alpine Bergell intrusion. *Geochimica et Cosmochimica Acta* 68: 2543–2560.

Oosthuyzen EJ and Burger AJ (1973) The suitability of apatite as an age indicator by the uranium–lead isotope method. *Earth and Planetary Science Letters* 18: 29–36.

Ovtcharova M, Bucher H, Schaltegger U, Galfetti T, Brayard A, and Guex J (2006) New Early to Middle Triassic U–Pb ages from South China: Calibration with ammonoid biochronozones and implications for the timing of the Triassic biotic recovery. *Earth and Planetary Science Letters* 243: 463–475.

Paquette JL and Tiepolo M (2007) High resolution (5 μm) U–Th–Pb isotope dating of monazite with excimer laser ablation (ELA)-ICPMS. *Chemical Geology* 240: 222–237.

Parrish RR (1987) An improved micro-capsule for zircon dissolution in U–Pb geochronology. *Chemical Geology: Isotope Geoscience Section* 66: 99–102.

Parrish RR (1990) U–Pb dating of monazite and its application to geological problems. *Canadian Journal of Earth Sciences* 27: 1431–1450.

Parrish RR and Krogh TE (1987) Synthesis and purification of ^{205}Pb for U–Pb geochronology. *Chemical Geology: Isotope Geoscience Section* 66: 103–110.

Parrish RR and Noble SR (2003) Zircon U–Th–Pb geochronology by isotope dilution – Thermal ionization mass spectrometry (ID-TIMS). In: Hanchar JM and Hoskin PWO (eds.) *Zircon. Reviews in Mineralogy and Geochemistry*, vol. 53, pp. 183–213. Washington, DC: Mineralogical Society of America.

Paton C, Hellstrom J, Paul B, Woodhead J, and Hergt J (2011) Iolite: Freeware for the visualisation and processing of mass spectrometric data. *Journal of Analytical Atomic Spectrometry* 26: 2508–2518.

Paton C, Woodhead JD, Hellstrom JC, Hergt JM, Greig A, and Maas R (2010) Improved laser ablation U–Pb zircon geochronology through robust downhole fractionation correction. *Geochemistry, Geophysics, Geosystems* 11: Q0AA06.

Patterson C (1956) Age of meteorites and the Earth. *Geochimica et Cosmochimica Acta* 10: 230–237.

Peterman EM, Mattinson JM, and Hacker BR (2012) Multi-step TIMS and CA-TIMS monazite U-Pb geochronology. *Chemical Geology* 312–313: 58–73.

Petrus JA and Kamber BS (2012) VizualAge: A novel approach to laser ablation ICP-MS U–Pb geochronology data reduction. *Geostandards and Geoanalytical Research* 36: 247–270.

Pidgeon RT, O'Neil JR, and Silver LT (1966) Uranium and lead isotopic stability in a metamict zircon under experimental hydrothermal conditions. *Science* 154: 1538–1540.

Pisonero J, Fliegel D, and Günther D (2006) High efficiency aerosol dispersion cell for laser ablation-ICP-MS. *Journal of Analytical Atomic Spectrometry* 21. 922–931

Potts PJ (2012) Glossary of analytical and metrological terms from the International Vocabulary of Metrology (2008). *Geostandards and Geoanalytical Research*. 36: 231–246.

Poujol M, Boulvais P, and Kosler J (2010) Regional-scale Cretaceous albitization in the Pyrenees: Evidence from in situ U–Th–Pb dating of monazite, titanite and zircon. *Journal of the Geological Society* 167: 751–767.

Prowatke S and Klemme S (2005) Effect of melt composition on the partitioning of trace elements between titanite and silicate melt. *Geochimica et Cosmochimica Acta* 69: 695–709.

Prowatke S and Klemme S (2006a) Rare earth element partitioning between titanite and silicate melts: Henry's law revisited. *Geochimica et Cosmochimica Acta* 70: 4997–5012.

Prowatke S and Klemme S (2006b) Trace element partitioning between apatite and silicate melts. *Geochimica et Cosmochimica Acta* 70: 4513–4527.

Rainbird RH, Heaman LM, and Young G (1992) Sampling Laurentia: Detrital zircon geochronology offers evidence for an extensive Neoproterozoic river system originating from the Grenville orogen. *Geology* 20: 351–354.

Ramezani J, Schmitz MD, Davydov VI, Bowring SA, Snyder WS, and Northrup CJ (2007) High-precision U–Pb zircon age constraints on the Carboniferous–Permian boundary in the southern Urals stratotype. *Earth and Planetary Science Letters* 256: 244–257.

Rasbury ET and Cole JM (2009) Directly dating geologic events: U–Pb dating of carbonates. *Reviews of Geophysics* 47: RG3001.

Rasmussen B, Fletcher IR, and Sheppard S (2005) Isotopic dating of the migration of a low-grade metamorphic front during orogenesis. *Geology* 33: 773–776.

Rasmussen B, Sheppard S, and Fletcher IR (2006) Testing ore deposit models using in situ U–Pb geochronology of hydrothermal monazite: Paleoproterozoic gold mineralization in northern Australia. *Geology* 34: 77–80.

Reddy SM, Timms NE, Trimby P, Kinny PD, Buchan C, and Blake K (2006) Crystal-plastic deformation of zircon: A defect in the assumption of chemical robustness. *Geology* 34: 257–260.

Reid M, Vazquez J, and Schmitt A (2011) Zircon-scale insights into the history of a Supervolcano, Bishop Tuff, Long Valley, California, with implications for the Ti-in-zircon geothermometer. *Contributions to Mineralogy and Petrology* 161: 293–311.

Renne PR, Karner DB, and Ludwig KR (1998) Absolute ages aren't exactly. *Science* 282: 1840–1841.

Renne PR, Mundil R, Balco G, Min K, and Ludwig KR (2010) Joint determination of ^{40}K decay constants and $^{40}Ar^*/^{40}K$ for the Fish Canyon sanidine standard, and improved accuracy for $^{40}Ar/^{39}Ar$ geochronology. *Geochimica et Cosmochimica Acta* 74: 5349–5367.

Richter S, Alonso-Munoz A, Eykens R, et al. (2008) The isotopic composition of natural uranium samples – Measurements using the new $n(^{233}U)/n(^{236}U)$ double spike IRMM-3636. *International Journal of Mass Spectrometry* 269: 145–148.

Rioux M, Bowring S, Dudás F, and Hanson R (2010) Characterizing the U–Pb systematics of baddeleyite through chemical abrasion: Application of multi-step digestion methods to baddeleyite geochronology. *Contributions to Mineralogy and Petrology* 160: 777–801.

Robb LJ, Davis DW, and Kamo SL (1990) U–Pb ages on single detrital zircon grains from the Witwatersrand Basin, South Africa: Constraints on the age of sedimentation and on the evolution of granites adjacent to the basin. *Journal of Geology* 98: 311–328.

Roddick JC (1987) Generalized numerical error analysis with applications to geochronology and thermodynamics. *Geochimica et Cosmochimica Acta* 51: 2129–2135.

Roddick JC, Loveridge WD, and Parrish RR (1987) Precise U/Pb dating of zircon at the sub-nanogram Pb level. *Chemical Geology: Isotope Geoscience Section* 66: 111–121.

Romer R and Siegesmund S (2003) Why allanite may swindle about its true age. *Contributions to Mineralogy and Petrology* 146: 297–307.

Rubatto D (2002) Zircon trace element geochemistry: Partitioning with garnet and the link between U–Pb ages and metamorphism. *Chemical Geology* 184: 123–138.

Rubatto D and Hermann J (2007) Experimental zircon/melt and zircon/garnet trace element partitioning and implications for the geochronology of crustal rocks. *Chemical Geology* 241: 38–61.

Russell RD and Ahrens LH (1957) Additional regularities among dicordant lead–uranium ages. *Geochimica et Cosmochimica Acta* 11: 213–218.

Sano Y, Terada K, and Fukuoka T (2002) High mass resolution ion microprobe analysis of rare earth elements in silicate glass, apatite and zircon: Lack of matrix dependency. *Chemical Geology* 184: 217–230.

Schaltegger U (2007) Hydrothermal zircon. *Elements* 3: 51–79.

Schaltegger U, Brack P, Ovtcharova M, et al. (2009) Zircon and titanite recording 1.5 million years of magma accretion, crystallization and initial cooling in a composite pluton (southern Adamello batholith, northern Italy). *Earth and Planetary Science Letters* 286: 208–218.

Schaltegger U, Fanning CM, Günther D, Maurin JC, Schulmann K, and Gebauer D (1999) Growth, annealing and recrystallization of zircon and preservation of monazite in high-grade metamorphism: Conventional and in-situ U–Pb isotope, cathodoluminescence and microchemical evidence. *Contributions to Mineralogy and Petrology* 134: 186–201.

Schaltegger U, Guex J, Bartolini A, Schoene B, and Ovtcharova M (2008) Precise U–Pb age constraints for end-Triassic mass extinction, its correlation to volcanism and Hettangian post-extinction recovery. *Earth and Planetary Science Letters* 267: 266–275.

Schärer U (1984) The effect of initial ^{230}Th disequilibrium on young U–Pb ages: The Makalu case, Himalaya. *Earth and Planetary Science Letters* 67: 191–204.

Schärer U, Tapponnier P, Lacassin R, Leloup PH, Zhong D, and Ji S (1990) Intraplate tectonics in Asia: A precise age for large-scale Miocene movement along the Ailao Shan-Red River shear zone, China. *Earth and Planetary Science Letters* 97: 65–77.

Schenk V (1980) U–Pb and Rb–Sr radiometric dates and their correlation with metamorphic events in the granulite-facies basement of the serre, Southern Calabria (Italy). *Contributions to Mineralogy and Petrology* 73: 23–38.

Scherer E, Münker C, and Mezger K (2001) Calibration of the lutetium–hafnium clock. *Science* 293: 683–687.

Schmitt AK (2007) Ion microprobe analysis of $(^{231}Pa)/(^{235}U)$ and an appraisal of protactinium partitioning in igneous zircon. *American Mineralogist* 92: 691–694.

Schmitt AK, Danišík M, Evans NJ, et al. (2011) Acigöl rhyolite field, Central Anatolia (part 1): High-resolution dating of eruption episodes and zircon growth rates. *Contributions to Mineralogy and Petrology* 162: 1215–1231.

Schmitt AK, Stockli DF, Lindsay JM, Robertson R, Lovera OM, and Kislitsyn R (2010) Episodic growth and homogenization of plutonic roots in arc volcanoes from combined U–Th and (U–Th)/He zircon dating. *Earth and Planetary Science Letters* 295: 91–103.

Schmitz MD and Bowring SA (2001) U–Pb zircon and titanite sytematics of the Fish Canyon Tuff: An assessment of high-precision U–Pb geochronology and its

application to young volcanic rocks. *Geochimica et Cosmochimica Acta* 65: 2571–2587.
Schmitz MD and Bowring SA (2003a) Constraints on the thermal evolution of continental lithosphere from U–Pb accessory mineral thermochronometry of lower crustal xenoliths, southern Africa. *Contributions to Mineralogy and Petrology* 144: 592–618.
Schmitz MD and Bowring SA (2003b) Ultrahigh-temperature metamorphism in the lower crust during Neoarchean Ventersdorp rifting and magmatism, Kaapvaal Craton, southern Africa. *Geological Society of America Bulletin* 115: 533–548.
Schmitz MD and Bowring SA (2004) Lower crustal granulite formation during Mesoproterozoic Namaqua-Natal collisional orogenesis, southern Africa. *South African Journal of Geology* 107: 261–284.
Schmitz MD and Davydov VI (2012) Quantitative radiometric and biostratigraphic calibration of the Pennsylvanian–Early Permian (Cisuralian) time scale and pan-Euramerican chronostratigraphic correlation. *Geological Society of America Bulletin* 124: 549–577.
Schmitz MD and Schoene B (2007) Derivation of isotope ratios, errors, and error correlations for U–Pb geochronology using ^{205}Pb–^{235}U-(^{233}U)-spiked isotope dilution thermal ionization mass spectrometric data. *Geochemistry, Geophysics, Geosystems* 8: Q08006.
Schoene B and Bowring SA (2006) U–Pb systematics of the McClure Mountain syenite: Thermochronological constraints on the age of the ^{40}Ar/^{39}Ar standard MMhb. *Contributions to Mineralogy and Petrology* 151: 615–630.
Schoene B and Bowring SA (2007) Determining accurate temperature–time paths in U–Pb thermochronology: An example from the SE Kaapvaal craton, southern Africa. *Geochimica et Cosmochimica Acta* 71: 165–185.
Schoene B and Bowring SA (2010) Rates and mechanisms of Mesoarchean magmatic arc construction, eastern Kaapvaal craton, Swaziland. *Geological Society of America Bulletin* 122: 408–429.
Schoene B, Crowley JL, Condon DC, Schmitz MD, and Bowring SA (2006) Reassessing the uranium decay constants for geochronology using ID-TIMS U–Pb data. *Geochimica et Cosmochimica Acta* 70: 426–445.
Schoene B, de Wit MJ, and Bowring SA (2008) Mesoarochean assembly and stabilization of the eastern Kaapvaal craton: A structural–thermochronological perspective. *Tectonics* 27: TC5010.
Schoene B, Guex J, Bartolini A, Schaltegger U, and Blackburn TJ (2010a) Correlating the end-Triassic mass extinction and flood basalt volcanism at the 100,000-year level. *Geology* 38: 387–390.
Schoene B, Latkoczy C, Schaltegger U, and Günther D (2010b) A new method integrating high-precision U–Pb geochronology with zircon trace element analysis (U–Pb TIMS-TEA). *Geochimica et Cosmochimica Acta* 74: 7144–7159.
Schoene B, Schaltegger U, Brack P, Latkoczy C, Stracke A, and Günther D (2012) Rates of magma differentiation and emplacement in a ballooning pluton recorded by U–Pb TIMS-TEA, Adamello batholith, Italy. *Earth and Planetary Science Letters* 355–356: 162–173.
Searle MP, Noble SR, Cottle JM, et al. (2007) Tectonic evolution of the Mogok metamorphic belt, Burma (Myanmar) constrained by U–Th–Pb dating of metamorphic and magmatic rocks. *Tectonics* 26: TC3014.
Selby D, Creaser RA, Stein HJ, Markey RJ, and Hannah JL (2007) Assessment of the ^{187}Re decay constant by cross calibration of Re–Os molybdenite and U–Pb zircon chronometers in magmatic ore systems. *Geochimica et Cosmochimica Acta* 71: 1999–2013.
Shaw CA, Heizler M, and Karlstrom KE (2004) ^{40}Ar/^{39}Ar thermochronologic record of 1.45–1.35 Ga intracontinental tectonism in the southern Rocky Mountains: Interplay of conductive and advective heating with intracontinental deformation. In: Karlstrom KE and Keller GR (eds.) *The Rocky Mountain Region: An Evolving Lithosphere*. *Geophysical Monograph Series*, vol. 154, pp. 163–184. Washington, DC: American Geophysical Union.
Shen S-Z, Crowley JL, Wang Y, et al. (2011) Calibrating the end-Permian mass extinction. *Science* 334: 1367–1372.
Shimizu N, Semet MP, and Allègre CJ (1978) Geochemical applications of quantitative ion-microprobe analysis. *Geochimica et Cosmochimica Acta* 42: 1321–1334.
Silver LT and Deutsch S (1963) Uranium–lead isotopic variations in zircons: A case study. *Journal of Geology* 71: 721–758.
Simonetti A, Heaman LM, Hartlaub RP, Creaser RA, MacHattie TG, and Bohm C (2005) U–Pb zircon dating by laser ablation-MC-ICP-MS using a new multiple ion counting Faraday collector array. *Journal of Analytical Atomic Spectrometry* 20; 677–686.
Sinha AK, Wayne DM, and Hewitt DA (1992) The hydrothermal stability of zircon: Preliminary experimental and isotopic studies. *Geochimica et Cosmochimica Acta* 56: 3551–3560.
Slama J, Kosler J, Condon DJ, et al. (2008) Plesovice zircon – A new natural reference material for U–Pb and Hf isotopic microanalysis. *Chemical Geology* 249: 1–35.
Smith ME, Chamberlain KR, Singer BS, and Carroll AR (2010) Eocene clocks agree: Coeval ^{40}Ar/^{39}Ar, U–Pb, and astronomical ages from the Green River Formation. *Geology* 38: 527–530.
Soddy F (1913) Intra-atomic charge. *Nature* 92: 399–400.
Spear FS (2010) Monazite–allanite phase relations in metapelites. *Chemical Geology* 279: 55–62.
Spear FS and Pyle JM (2002) Apatite, monazite, and xenotime in metamorphic rocks. In: Kohn MJ, Rakovan J, and Hughes JM (eds.) *Phosphates: Geochemical, Geobiological, and Materials Importance*. *Reviews in Mineralogy and Geochemistry*, vol. 48. pp. 293–336. Washington, DC: Mineralogical Society of America.
Stacey JC and Kramers JD (1975) Approximation of terrestrial lead isotope evolution by a two-stage model. *Earth and Planetary Science Letters* 26: 207–221.
Steiger RH and Jäger E (1977) Subcommission on Geochronology: Convention on the use of decay constants in geo- and cosmochronology. *Earth and Planetary Science Letters* 36: 359–362.
Steiger RH and Wasserburg GJ (1966) Systematics in the Pb^{208}–Th^{232}, Pb^{207}–U^{235}, and Pb^{206}–U^{238} systems. *Journal of Geophysical Research* 71: 6065–6090.
Stern RA and Amelin Y (2003) Assessment of errors in SIMS zircon U–Pb gechronology using a natural zircon standard and NIST SRM 610 glass. *Chemical Geology* 197: 111–142.
Stewart JH, Gehrels GE, Barth AP, Link PK, Christie-Blick N, and Wrucke CT (2001) Detrital zircon provenance of Mesoproterozoic to Cambrian arenites in the western United States and northwestern Mexico. *Geological Society of America Bulletin* 113: 1343–1356.
Stirling CH, Andersen MB, Potter E-K, and Halliday AN (2007) Low-temperature isotopic fractionation of uranium. *Earth and Planetary Science Letters* 264: 208–225.
Storey CD, Smith MP, and Jeffries TE (2007) In situ LA-ICP-MS U–Pb dating of metavolcanics of Norrbotten, Sweden: Records of extended geological histories in complex titanite grains. *Chemical Geology* 240: 163–181.
Suzuki K and Adachi M (1994) Middle Precambrian detrital monazite and zircon from the Hida gneiss on Oki-Dogo Island, Japan: Their origin and implications for the correlation of basement gneiss of Southwest Japan and Korea. *Tectonophysics* 235: 277–292.
Sylvester PJ (2008) LA-(MC)-ICP-MS trends in 2006 and 2007 with particular emphasis on measurement uncertainties. *Geostandards and Geoanalytical Research* 32: 469–488.
Tera F and Wasserburg GJ (1972a) U–Th–Pb systematics in lunar highland samples from the Luna 20 and Apollo 16 missions. *Earth and Planetary Science Letters* 17: 36–51.
Tera F and Wasserburg GJ (1972b) U–Th–Pb systematics in three Apollo 14 basalts and the problem of initial Pb in lunar rocks. *Earth and Planetary Science Letters* 14: 281–304.
Thirlwall MF (2000) Inter-laboratory and other errors in Pb isotope analyses investigated using a ^{207}Pb–^{204}Pb double spike. *Chemical Geology* 163: 299–322.
Thomas JB, Bodnar RJ, Shimizu N, and Sinha AK (2002) Determination of zircon/melt trace element partition coefficients from SIMS analysis of melt inclusions in zircon. *Geochimica et Cosmochimica Acta* 66: 2887–2901.
Tilton GR (1960) Volume diffusion as a mechanism for discordant lead ages. *Journal of Geophysical Research* 65: 2933–2945.
Tilton GR and Grunenfelder MH (1968) Sphene: Uranium–lead ages. *Science* 159: 1458–1461.
Todt W, Cliff RA, Hanser A, and Hofmann AW (1996) Evaluation of a ^{202}Pb–^{205}Pb double spike for high-precision lead isotope analysis. In: Basu A and Hart S. (eds.) *Earth Processes: Reading the Isotopic Code*. *Geophysical Monograph Series*, vol. 95, pp. 429–437. Washington, DC: American Geophysical Union.
Toulkeridis T, Peucker-Ehrenbrink B, Clauer N, Kröner A, Schidlowski M, and Todt W (2010) Pb–Pb age, stable isotope and chemical composition of Archaean magnesite, Barberton Greenstone Belt, South Africa. *Journal of the Geological Society* 167: 943–952.
Tucker RD, Krogh TE, Ross RJ Jr., and Williams SH (1990) Time-scale calibration by high-precision U/Pb zircon dating of interstratified volcanic ashes in the Ordovician and Lower Silurian stratotypes of Britain. *Earth and Planetary Science Letters* 100: 51–58.
Tucker RD, Raheim A, Krogh TE, and Corfu F (1986) Uranium–lead zircon and titanite ages from the northern portion of the Western Gneiss Region, south-central Norway. *Earth and Planetary Science Letters* 81: 203–211.
van Achterbergh E, Ryan CG, Jackson SE, and Griffin WL (2001) Data reduction software for LA-ICPMS: Appendix. In: Sylvester PJ (ed.) *Laser Ablation ICP–MS in the Earth Sciences: Current Practices and Outstanding Issues*, *Mineralogical Association of Canada Short Course Series*, vol. 29, pp. 239–243. Ottawa: Mineralogical Association of Canada.
Vavra G, Gebauer D, Schmid R, and Compston W (1996) Multiple zircon growth and recrystallization during polyphase Late Carboniferous to Triassic metamorphism in

granulites of the Ivrea Zone (Southern Alps): An ion microprobe (SHRIMP) study. *Contributions to Mineralogy and Petrology* 122: 337–358.

Verts LA, Chamberlain KR, and Frost CD (1996) U–Pb sphene dating of metamorphism: The importance of sphene growth in the contact aureole of the Red Mountain pluton, Laramie Mountains, Wyoming. *Contributions to Mineralogy and Petrology* 125: 186–199.

Villeneuve M, Sandeman HA, and Davis WJ (2000) A method for intercalibration of U–Th–Pb and ^{40}Ar–^{39}Ar ages in the Phanerozoic. *Geochimica et Cosmochimica Acta* 64: 4017–4030.

VIM: Joint Committee for Guides in Metrology (2012) International vocabulary of metrology – basic and general concepts and associated terms (VIM). JCGM, vol. 200. http://www.bipm.org/vim.

Viskupic K and Hodges K (2001) Monazite–xenotime thermochronometry: Methodology and an example from the Nepalese Himalaya. *Contributions to Mineralogy and Petrology* 141: 233–247.

Voice PJ, Kowalewski M, and Eriksson KA (2011) Quantifying the timing and rate of crustal evolution: Global compilation of radiometrically dated detrital zircon grains. *Journal of Geology* 119: 109–126.

von Blanckenburg F (1992) Combined high-precision chronometry and geochemical tracing using accessory minerals: Applied to the Central-Alpine Bergell intrusion (central Europe). *Chemical Geology* 100: 19–40.

Vry JK and Baker JA (2006) LA-MC-ICPMS Pb–Pb dating of rutile from slowly cooled granulites: Confirmation of the high closure temperature for Pb diffusion in rutile. *Geochimica et Cosmochimica Acta* 70: 1807–1820.

Wadhwa M, Amelin Y, Bogdanovski O, Shukolyukov A, Lugmair GW, and Janney P (2009) Ancient relative and absolute ages for a basaltic meteorite: Implications for timescales of planetesimal accretion and differentiation. *Geochimica et Cosmochimica Acta* 73: 5189–5201.

Wasserburg GJ (1963) Diffusion processes in lead–uranium systems. *Journal of Geophysical Research* 68: 4823–4846.

Wasserburg GJ, Jacousen SB, DePaolo DJ, McCulloch MT, and Wen T (1981) Precise determinations of Sm/Nd ratios. Sm and Nd isotopic abundances in standard solutions. *Geochimica et Cosmochimica Acta* 45: 2311–2323.

Watson EB and Harrison TM (2005) Zircon thermometer reveals minimum melting conditions on earliest Earth. *Science* 308: 841–844.

Watson E, Wark D, and Thomas J (2006) Crystallization thermometers for zircon and rutile. *Contributions to Mineralogy and Petrology* 151: 413–433.

Wayne DM and Sinha AK (1988) Physical and chemical response of zircons to deformation. *Contributions to Mineralogy and Petrology* 98: 109–121.

Wayne D, Sinha A, and Hewitt D (1992) Differential response of zircon U—Pb isotopic systematics to metamorphism across a lithologic boundary: An example from the Hope Valley Shear Zone, southeastern Massachusetts, USA. *Contributions to Mineralogy and Petrology* 109: 408–420.

Wendt I (1984) A three-dimensional U/Pb discordia plane to evaluate samples with common lead of unknown isotopic composition. *Chemical Geology* 46: 1–12.

Wendt I and Carl C (1991) The statistical distribution of the mean squared weighted deviation. *Chemical Geology* 86: 275–285.

Wetherill GW (1956) Discordant uranium–lead ages. *Transactions of the American Geophysical Union* 37: 320–326.

Weyer S, Anbar AD, Gerdes A, Gordon GW, Algeo TJ, and Boyle EA (2008) Natural fractionation of $^{238}U/^{235}U$. *Geochimica et Cosmochimica Acta* 72: 345–359.

White LT and Ireland TR (2012) High-uranium matrix effect in zircon and its implications for SHRIMP U-Pb age determinations. *Chemical Geology* 306–307: 78–91.

White NM, Parrish RR, Bickle MJ, Najman YMR, Burbank D, and Maithani A (2001) Metamorphism and exhumation of the NW Himalaya constrained by U–Th–Pb analyses of detrital monazite grains from early foreland basin sediments. *Journal of the Geological Society* 158: 625–635.

Whitehouse MJ and Platt JP (2003) Dating high-grade metamorphism – Constraints from rare-earth elements in zircon and garnet. *Contributions to Mineralogy and Petrology* 145: 61–74.

Wiedenbeck M, Allé P, Corfu F, et al. (1995) Three natural zircon standards for U–Th–Pb, Lu–Hf, trace element and REE analyses. *Geostandards Newsletter* 19: 1–23.

Williams IS (1998) U–Th–Pb geochronology by ion microprobe. In: McKibben MA, Shanks WC III, and Ridley WI (eds.) *Applications of Microanalytical Techniques to Understanding Mineralizing Porcesses*. *Reviews in Economic Geology*, vol. 7, pp. 1–35. Littleton, CO: Society of Economic Geologists.

Williams IS, Compston W, Black LP, Ireland TR, and Foster JJ (1984) Unsupported radiogenic Pb in zircon: A cause of anomalously high Pb–Pb, U–Pb and Th–Pb ages. *Contributions to Mineralogy and Petrology* 88: 322–327.

Williams ML and Jercinovic MJ (2002) Microprobe monazite geochronology: Putting absolute time into microstructural analysis. *Journal of Structural Geology* 24: 1013–1028.

Williams ML, Jercinovic MJ, and Hetherington CJ (2007) Microprobe monazite geochronology: Understanding geologic processes by integrating composition and chronology. *Annual Review of Earth and Planetary Sciences* 35: 137–175.

Willigers BJA, Baker JA, Krogstad EJ, and Peate DW (2002) Precise and accurate in situ Pb–Pb dating of apatite, monazite, and sphene by laser ablation multiple-collector ICP-MS. *Geochimica et Cosmochimica Acta* 66: 1051–1066.

Wing BA, Ferry JM, and Harrison TM (2003) Prograde destruction and formation of monazite and allanite during contact and regional metamorphism of pelites: Petrology and geochronology. *Contributions to Mineralogy and Petrology* 145: 228–250.

York D (1967) The best isochron. *Earth and Planetary Science Letters* 2: 479–482.

York D (1968) Least-squares fitting of a straight line with correlated errors. *Earth and Planetary Science Letters* 5: 320–324.

York D, Evensen NM, Lopez Martinez M, and De Basabe Delgado J (2004) Unified equations for the slope, intercept, and standard errors of the best straight line. *American Journal of Physics* 72: 367–375.

Yuan H-L, Gao S, Dai M-N, et al. (2008) Simultaneous determinations of U–Pb age, Hf isotopes and trace element compositions of zircon by excimer laser-ablation quadrupole and multiple-collector ICP-MS. *Chemical Geology* 247: 100–118.

Zack T, Moraes R, and Kronz A (2004) Temperature dependence of Zr in rutile: Empirical calibration of a rutile thermometer. *Contributions to Mineralogy and Petrology* 148: 471–488.

Zhang S, Jiang G, Zhang J, Song B, Kennedy MJ, and Christie-Blick N (2005) U–Pb sensitive high-resolution on microprobe ages from the Duoshantuo Formation in south China: Constraints on late Neopproterozoic glaciations. *Geology* 33: 473–476.

Zheng Y-F (1992) The three-dimensional U/Pb method: Generalized models and implications for U–Pb two-stage systematics. *Chemical Geology* 100: 3–18.

Zhu XK, O'Nions RK, Belshaw NS, and Gibb AJ (1997) Significance of in situ SIMS chronometry of zoned monazite from the Lewisian granulites, northwest Scotland. *Chemical Geology* 135: 35–53.